(12)

POR-2038(EX)
(WT-2038)(EX)
EXTRACTED VERSION

OPERATION DOMINIC, FISH BOWL SERIES

Project Officer's Report—Project 8B
Nuclear Weapon X-ray Effects as Measured by Passive Instruments

C. M. Gillespie, Project Officer
Air Force Weapons Laboratory
Kirtland Air Force Base, NM

P. G. Wing, Project Scientist
Allied Research Associates, Inc.
Concord, MA

15 December 1965

NOTICE:
This is an extracted version of POR-2038 (WT-2038), OPERATION DOMINIC, Fish Bowl Series, Project 8B.

Extracted version prepared for
Director
DEFENSE NUCLEAR AGENCY
Washington, DC 20305-1000

1 September 1985

Destroy this report when it is no longer needed. Do not return to sender.

PLEASE NOTIFY THE DEFENSE NUCLEAR AGENCY ATTN: TITL, WASHINGTON, DC 20305 1000, IF YOUR ADDRESS IS INCORRECT, IF YOU WISH IT DELETED FROM THE DISTRIBUTION LIST, OR IF THE ADDRESSEE IS NO LONGER EMPLOYED BY YOUR ORGANIZATION.

UNCLASSIFIED
SECURITY CLASSIFICATION OF THIS PAGE

AD-A995 495

REPORT DOCUMENTATION PAGE

1a. REPORT SECURITY CLASSIFICATION UNCLASSIFIED	1b. RESTRICTIVE MARKINGS
2a. SECURITY CLASSIFICATION AUTHORITY	3. DISTRIBUTION / AVAILABILITY OF REPORT Approved for public release; distribution is unlimited.
2b. DECLASSIFICATION / DOWNGRADING SCHEDULE	
4. PERFORMING ORGANIZATION REPORT NUMBER(S)	5. MONITORING ORGANIZATION REPORT NUMBER(S) POR-2038 (EX) (WT-2038) (EX)
6a. NAME OF PERFORMING ORGANIZATION 1-Air Force Weapons Lab. 2-Allied Research Associates, Inc.	6b. OFFICE SYMBOL (If applicable)
7a. NAME OF MONITORING ORGANIZATION Defense Atomic Support Agency	
6c. ADDRESS (City, State, and ZIP Code) 1-Kirtland AFB, New Mexico 2-Concord, Massachusetts	7b. ADDRESS (City, State, and ZIP Code) Washington, DC
8a. NAME OF FUNDING / SPONSORING ORGANIZATION	8b. OFFICE SYMBOL (If applicable)
9. PROCUREMENT INSTRUMENT IDENTIFICATION NUMBER	
8c. ADDRESS (City, State, and ZIP Code)	10. SOURCE OF FUNDING NUMBERS

PROGRAM ELEMENT NO	PROJECT NO	TASK NO	WORK UNIT ACCESSION NO

11. TITLE (Include Security Classification)
OPERATION DOMINIC, FISH BOWL SERIES, PROJECT OFFICER'S REPORT - PROJECT 8B - Nuclear Weapon X-ray Effects as Measured by Passive Instruments, Extracted Version

12. PERSONAL AUTHOR(S)
C. M. Gillespie and P. G. Wing

13a. TYPE OF REPORT	13b. TIME COVERED FROM ____ TO ____	14. DATE OF REPORT (Year, Month, Day)	15. PAGE COUNT
		651215	212

16. SUPPLEMENTARY NOTATION This report has had sensitive military information removed in order to provide an unclassified version for unlimited distribution. The work was performed by the Defense Nuclear Agency in support of the DoD Nuclear Test Personnel Review Program.

17. COSATI CODES		
FIELD	GROUP	SUB-GROUP
18	3	
20	8	

18. SUBJECT TERMS (Continue on reverse if necessary and identify by block number)
Dominic, Fish Bowl, King Fish, Spalling, Passive Indicators, X-rays, Radiation Measurements

19. ABSTRACT (Continue on reverse if necessary and identify by block number)

The objectives of this project were to measure X-ray characteristics, that is, total energy and spectral shape, and to measure certain effects fo the induced X-ray blowoff and impulse in various materials.

Accordingly, suitable instruments designed for the conditions of Shots Star Fish Prime and King Fish were carried aloft by pods parasitic to the Thor missiles. These pods were released prior to vernier engine cutoff such that at burst time each intercepted the X-rays at a different range.

The three Star Fish Prime pods were recovered. For all pods the misorientation and ranges from burst were greater than expected, and one pod was side on to the burst. Despite the 40-percent loss of instruments and the functional impairment from misorientations and low fluxes of those remaining, it was possible to achieve a substantial part of the experimental (Continued)

20. DISTRIBUTION / AVAILABILITY OF ABSTRACT	21. ABSTRACT SECURITY CLASSIFICATION
☒ UNCLASSIFIED/UNLIMITED ☐ SAME AS RPT ☐ DTIC USERS	UNCLASSIFIED

22a. NAME OF RESPONSIBLE INDIVIDUAL	22b. TELEPHONE (Include Area Code)	22c. OFFICE SYMBOL
Mark D. Flohr	(202) 325-7559	DNA/ISCM

DD FORM 1473, 84 MAR 83 APR edition may be used until exhausted.
All other editions are obsolete.

SECURITY CLASSIFICATION OF THIS PAGE
UNCLASSIFIED

19. ABSTRACT (Continued).

objectives.

In the subsequent shot, King Fish, water impact was apparently unchecked, and although one pod was recovered, both instrument bulkheads were lost. Important and consistent X-ray impulse data from metals, plastics, and reentry vehicle materials were obtained from two Star Fish Prime pods.

Samples of actual reentry vehicle material cross sections were exposed. The flux levels were such that most materials on the closer pod were damaged, and those on the farther pod were largely undamaged.

FOREWORD

Classified material has been removed in order to make the information available on an unclassified, open publication basis, to any interested parties. The effort to declassify this report has been accomplished specifically to support the Department of Defense Nuclear Test Personnel Review (NTPR) Program. The objective is to facilitate studies of the low levels of radiation received by some individuals during the atmospheric nuclear test program by making as much information as possible available to all interested parties.

The material which has been deleted is either currently classified as Restricted Data or Formerly Restricted Data under the provisions of the Atomic Energy Act of 1954 (as amended), or is National Security Information, or has been determined to be critical military information which could reveal system or equipment vulnerabilities and is, therefore, not appropriate for open publication.

The Defense Nuclear Agency (DNA) believes that though all classified material has been deleted, the report accurately portrays the contents of the original. DNA also believes that the deleted material is of little or no significance to studies into the amounts, or types, of radiation received by any individuals during the atmospheric nuclear test program.

ABSTRACT

The objectives were to measure X-ray characteristics, that is, total energy and spectral shape, and to measure certain effects of the induced X-ray blowoff and impulse in various materials.

Accordingly, suitable instruments designed for the conditions of Shots Star Fish Prime and King Fish were carried aloft by pods parasitic to the Thor missiles. These pods were released prior to vernier engine cutoff such that at burst time each intercepted the X-rays at a different range.

The three Star Fish Prime pods were recovered. For all pods the misorientation and ranges from burst were greater than expected, and one pod was side on to the burst. Despite the 40-percent loss of instruments and the functional impairment from misorientations and low fluxes of those remaining, it was possible to achieve a substantial part of the experimental objectives.

In the subsequent shot, King Fish, water impact was apparently unchecked, and although one pod was recovered, both instrument bulkheads were lost.

Important and consistent X-ray impulse data from metals, plastics, and reentry vehicle materials were obtained from two Star Fish Prime pods.

Samples of actual reentry vehicle material cross sections were exposed. The flux levels were such that most materials on the closer pod were damaged, and those on the farther pod were largely undamaged.

PREFACE

The work reported here was performed by Allied Research Associates, Inc., of Concord, Massachusetts, for the Research Directorate, Air Force Special Weapons Center (now the Air Force Weapons Laboratory), Kirtland Air Force Base, New Mexico, and the Defense Atomic Support Agency. The Star Fish Prime experiment was carried out under Contract No. AF 29(601)-5150 with the Air Force Special Weapons Center, and the King Fish experiment under Contract No. DA 49-146-X2-168 with the Defense Atomic Support Agency.

Special appreciation is due many associates at Allied Research, in particular Mr. David Knodel, Project Supervisor, for his unflagging help, encouragement, and criticism. Also, Mr. John Stewart as Project Engineer during both Star Fish Prime and King Fish events deserves highest praise for inventiveness and conscientiousness. Other personnel whose help was indespensable were Messrs. R. Papirno, T.E. Pascoe, H. Hamilton, C. Jamieson, R. Johnson, P.O. Koch, and Dr. H. Meyer. For obtaining the radioactivity data essential to the evaluation of certain impulse data we wish to thank Col. Irving Russell of AFSWC.

CONTENTS

TABLES

FIGURES

CHAPTER 1

INTRODUCTION

1.1 OBJECTIVES

The objectives of both the King Fish and Star Fish experiments were the measurement, in essentially extra-atmospheric conditions, of the nature of the X-ray emission from a nuclear device, the characteristics of the induced impulse from X-ray blowoff, and the effects on various materials. The specific experimental objectives were to determine: (1) total X-ray energy emitted by the weapon, (2) X-ray spectrum, and (3) X-ray-induced total momentum.

A number of other relevant measurements concerned with X-ray phenomena were attempted. These were: (1) to determine peak pressure profiles, as well as time durations of blowoff impulses; (2) to determine the initial temperature gradients established in materials by the X-ray flux; (3) to observe X-ray effects on samples of reentry vehicle (R/V) composite materials; and (4) to observe the X-ray effects on the hardened structure of the instrument pod.

Measurement of X-ray blowoff impulse as a function of material and flux was the most important test objective. The weapon X-ray diagnostic data were also an important objective, not only because they are necessary for data reduction of other parts of the experiment, but also because few such measurements have ever been made.

1.2 BACKGROUND AND THEORY

At altitudes above 90 km (300,000 feet) the nature of weapon phenomenology is qualitatively different from that encountered at sea level. The energy of the weapon, which at lower altitudes is converted into blast and thermal radiation, must now appear as kinetic energy of the bomb materials and as X-radiation characteristic of a very high temperature source. Present theory and experiments indicate that for many weapons

This soft X-radiation represents an important area of weapon phenomenology, since at high altitudes (and rarefied atmosphere) X-rays will propagate to distances of many kilometers with essentially only a geometric decrease of the flux.

For various sound reasons, the idea of killing hostile ICBM's at such extra-atmospheric altitudes has become highly attractive in recent years. Because the predominant weapon output there is X-rays, the associated kill mechanism, impulsive blowoff, has been given much attention. Several field tests were conducted prior to the 1958 Moratorium that were designed to give some data on this phenomenon.

However, in these prior high-altitude field tests (Reference 1), meager X-ray and/or thermal effects data were obtained. In Shot Orange the instrumentation pod was not recovered, and although the Shot Teak pod was recovered, only limited X-ray effects data could be extracted.

Unfortunately however, little X-ray effects data were obtained.

During the three-year moratorium from 1958 to 1962, a large-scale theoretical as well as experimental simulation program was carried out to determine the exact nature of the X-ray effects and their kill radii on operational systems. The various simulation techniques have included high-explosive loading of entire R/V's, exploding foil methods for applying fractional microsecond pulses to sections of materials, and air guns. The experimental simulation program indicated that lethal structural damage might be produced in targets at militarily significant distances, i.e., several kilometers from Mt weapons. The following damage mechanisms have been deemed significant to reentry vehicles: (1) crushing, delamination, and fracture of ablative material; (2) crushing, deformation, or shock damage to internal components such as arming and fusing equipment; (3) spall damage to frangible impact fuzes; (4) thermal fracture of surface materials; (5) gross structural damage; and to space vehicles: (1) changes in thermal control surfaces which then upset the thermal balance of sensitive components; (2) damage or removal of reflective and optical coatings on IR, UV or visible windows and lens systems; and (3) low-impulse damage to supporting structures of large solar collecting surfaces.

However, present laboratory methods do not adequately simulate the X-ray deposition and early shock. This is due to the inherent difficulty of simulating the X-ray energy density absorbed as a function of depth and time

in the target material. It was anticipated that data would remove most of the uncertainties and sources of possible error in present theoretical-simulation programs. That experiment was conducted under controlled conditions where individual X-ray effects measurements could be made. However, in some respects the while an excellent check on current theories and simulation techniques, did not simulate the situation of immediate military interest.

The Fish Bowl experiments provided the opportunity to make some of the same measurements that attempted but with the environment associated with the real vulnerability problem. An equally important consideration was that the success of could not be guaranteed and the Fish Bowl experiment provided a backup.

Paralleling the above-mentioned experimental studies of weapon effects, there have been continuing theoretical programs concerned with the physical mechanism of X-ray-induced impulses. Theoretical effort has produced two compatible methods of vastly disparate sophistication: the conservation of momentum description and the hydrodynamic model.

In the conservation of momentum method the absorption of X-ray energy in the surface layer is calculated as a function of depth, using known X-ray absorption coefficients (Reference 6). Knowledge of specific heats and heats of vaporization of materials involved is then used to calculate the depth of vaporized material and the energy of vaporized molecules as a function of depth. It is usually assumed that the molecules leave the surface

normally and that X-ray deposition is instantaneous. Having calculated the energy of the molecules leaving the surface, it is possible to calculate the momentum carried away from the surface by the molecules. Conservation of momentum requires that the surface receive an impulse equal in magnitude but opposite in direction.

The conservation of momentum method is admittedly an approximation, but it permits a quick estimate of the time-integrated impulse; time dependence of the impulse cannot be caluclated nor can information about peak pressures or pulse durations. Yet,for a first estimate of total impulse, this technique appears to be suitable, particularly in view of the fact that the values calculated do not vary inordinately from those of other more sophisticated methods.

In the more detailed hydrodynamic analysis of impulse, the deposition of X-ray energy in the surface layer yields the pressure and temperature conditions in the resulting vapor. The vapor is assumed to have a particular equation of state and to obey the hydrodynamic differential equations. The equations are solved using appropriate boundary and initial conditions. One output of the calculations is the pressure as a function of time at the interface between the gaseous layer and the solid material. This yields directly the pressure transmitted to the solid material as a function of time.

In practice the hydrodynamic problem is far from trivial. Analytic solutions which have been obtained are approximate, and machine computations are required to obtain more nearly exact solutions.

Bethe, for example, has derived an approximate analytical expression

for the deposition of X-ray energy in the surface layer (References 7 and 8). This expression is apparently quite satisfactory except very near the surface. Bethe was also able to solve analytically, to a good approximation, the hydrodynamic differential equations.

The alternative approach to the solution of the hydrodynamic problem has been to calculate energy deposition as a function of depth and to obtain the required solutions of the differential equations of hydrodynamic motion using numerical methods. The complexity of the problem requires the use of computers. A machine code used for this at Lawrence Radiation Laboratory was known as SHARP (Reference 9); a later version developed at AFSWC is called PUFF (Reference 8). The PUFF Code uses empirical equations of state instead of the perfect gas law.

The Bethe analytical solution and the PUFF numerical solution agree well for the integrated X-ray impulses in a number of cases which have been studied. Differences in the results of the two methods are obtained in computing the time and depth dependence of pressure and other dynamic variables.

Regardless of the description used in predicting impulses, however, the success any one theory achieved in describing the hydrodynamics was unknown until and Fish Bowl, since virtually no experimental data existed from which an evaluation could have been made.

1.3 OPERATIONS

Allied Research, in the period from January to May 1962, designed, fabricated, and delivered to Johnston Island several complete sets of passive X-ray instruments for the Star Fish shot in the Fish Bowl Series of Operation Dominic. Originally, the operation had been conceived to incorporate

three instrumented recoverable pods. These pods and their instrumentation were to be carried aloft by the Thor missile and, through selective release, to be positioned at slant ranges of 7.5, 10, and 14 km from the burst. In May, however, a decision was rendered by HQ, Defense Atomic Support Agency (DASA) to substitute Mk V reentry vehicles for the 7.5- and 14-km pods. This was the configuration which was flown in the first Star Fish shot, 19 June 1962, in which the Thor malfunctioned and was destroyed as a result of aerodynamic problems caused by the smaller size of the substituted R/V's. The repeat experiment was then revised to the initial concept of three Project 8B pods and took place 9 July 1962 (Star Fish Prime, hereafter abbreviated SF').

The survey of the X-ray source characteristics and X-ray effects attempted in SF' met with mixed success. One of the three instrument carriers (pods) was unstabilized and produced no data, since the contained instruments did not view the burst. With regard to the remaining two pods, the pod axis-line of sight angles were considerably greater than anticipated, with the consequence that the diagnostic instruments either failed to view the burst or were impaired beyond usefulness. Hence, none of the originally anticipated information about the X-ray source characteristics could be extracted from the SF' instruments (limited X-ray data were ultimately extracted from certain unpremediated physical effects, however). On the other hand, it appeared that the effects instruments had operated with some degree of success, despite the large incidence angles. In particular the limited impulse data retrieved represented an important breakthrough, since there was essentially none prior to SF' Nevertheless, because of the limited source and flux characteristics information and the

limited amount of the valid impulse data, it was decided by DASA that additional X-ray input and effects measurements should be made under similar high-yield, high-altitude conditions with essentially the same instruments used in SF'. As a result, more instruments were fabricated, added to those remaining from SF', and sent back to Johnston Island for inclusion in Shot King Fish. In certain ways, notably the weapon characteristics and environment, the conditions of King Fish were changed from SF', however. Thus, minor modifications of certain instruments were accomplished on the basis of experiences gathered from the SF' event.

King Fish took place on 1 November 1962. Two pods instrumented for X-ray measurements were carried aloft by the Thor missile and released subsequent to main engine cutoff and prior to vernier engine cutoff such that at burst time their slant ranges from the burst were intended to be 2.4 and 3.3 km. The burst occurred as planned but because of the apparent failure of the pod recovery systems, none of the X-ray instrumentation was recovered.

Simultaneously with these activities, a very small program was carried out to complement the Fish Bowl effects data with comparable data. Several slightly modified SF'-type instruments were built and supplied to Air Force Special Weapons Center (AFSWC) for inclusion in the experiment. No Allied Research personnel were involved in the field program. Subsequently, the gages were returned to Allied Research for data reduction and correlation.

PART 1 STAR FISH PRIME

CHAPTER 2

PROCEDURE

2.1 INSTRUMENT PODS

The instrument pods were designed and fabricated by General Dynamics/ Astronautics (GD/A). The design used was a modification of GD/A's existing scientific passenger pod. As illustrated in Figure 2.1, the pod configuration consists of a hemispherical nose, a cylindrical body section 31 inches in diameter, and a base flare with a diameter of 46 inches. Overall length was approximately 80 inches, and total weight about 1200 pounds. The instruments were positioned on the rear bulkhead of the pod, in an annular area surrounding the recovery equipment. The flywheel, required to stabilize the pod during the free-fall period before burst time, was mounted in the nose of the pod. Also included in the pods were tracking transponders. Empty spaces in the pod were filled with foam to provide bouyancy.

The recovery sequence began with the deployment of a drogue parachute which was required for stability after the pod decelerated to a subsonic velocity. This occurred at about 29,000 feet. The drogue parachute, upon signal from the recovery sequence timer, deployed the main recovery parachute at approximately 14,000 feet. After water impact, recovery was aided by dye marker, radio beacon, and a flotation balloon with a lifting strap and loop to facilitate hooking by the retrieval vehicle. For instrumentation design purposes the acceleration environment during powered flight was assumed to consist of a peak steady-state acceleration of 20 g's and a superimposed vibratory load of a flat 20-g spectrum from 2000 to 30 cps and 0.44-inch amplitude spectrum from 30 cps to 5 cps. Assumed re-entry decelerations consisted of inputs from several effects. Aerodynamic drag during re-entry was assumed to be 60 g's, drogue chute deployment was estimated at 6-1/2 g's, and main chute deployment at 8-1/3 g's. These design values were reasonably close to the levels recorded during certification tests which were 40 g's, 10 g's, and 6 g's, respectively. Water impact, estimated to occur at 80 ft/sec, was assumed to produce a 35-g, 3.6-millisecond impulse. Axial and transverse vibrations, produced by aerodynamic oscillations and buffeting, were also considered during reentry and subsequent deceleration.

A comprehensive series of proof tests was conducted on the pod and associated components to insure satisfactory recovery. Structural integrity was tested and verified at Stanford Research Institute by subjecting the pod

to a series of impulse loadings produced by gas bag and sheet high explosive. The magnitude of the loadings far exceeded the X-ray inputs anticipated in SF'. Airdrops were accomplished to test the drogue and recovery systems. Water recovery procedures were developed using a dummy pod. Culminating these tests was Tiger Fish, a complete certification test duplicating the entire mission with the exception of the nuclear detonation (see Appendix A). Successful flight recovery of the certification pods gave added confidence for a successful experiment.

2.2 FLIGHT SEQUENCES

The following sequence of events was programmed. The three instrument pods were affixed to a Thor missile in a nosedown attitude. A streamlined shield, attached to the Thor, was placed snugly around the rear of the pods to reduce aerodynamic pressures and heating of the pod instruments (see Figure 2.2). The pods were released (not ejected) from the missile at different times after the main engine cutoff. This occurred at altitudes above 125 km. Shortly after vernier engine cutoff, the warhead was separated and the booster retro rockets fired. Warhead apogee was about 700 km. Stabilization of the pods was to be accomplished by use of a flywheel. After descent of the to 400-km altitude, the burst occurred (Figure 2.3). Total yield was about 1.3 Mt (Reference 10). The pods then dropped to a much lower altitude where the main parachute opened, reducing the water impact velocity to an estimated 80 ft/sec.

Since it was desired to know the range from burst to pods to an accuracy of $\pm$ 5 percent, each pod carried a Cubic Corporation (CC) transponder. In addition Pod S3 and the warhead carried Sandia Corporation (SC) transponders. The dual tracking systems in this pod were included to provide burst to pod separation distances and a determination of SC and CC system bias errors.

2.3 INSTRUMENTATION

The Star Fish experiment was concerned primarily with two aspects of the weapon's X-ray emission. Of foremost interest was the investigation of the induced blowoff and consequent impulse. In this category, experiments were designed to observe the following: (1) blowoff behavior of metals with widely ranging thermal and X-ray properties, (2) blowoff behavior of a variety of R/V materials and plastics, (3) time duration of the induced pressure pulse and peak pressure, (4) induced temperature gradients in several materials, and (5) induced spalling in laminated structures.

The second important investigation was of the incident X-ray characteristics themselves. The two experiments attempted were: (1) time-integrated spectrum, (2) total incident X-ray energy.

A major consideration governing the choice of instruments was the established time schedule. The limited time available dictated that only those instruments which were already available or designed could be used. In this respect the instrumentation development work performed for proved invaluable (Reference 3). Active experiments requiring telemetry or data storage were considered but were rejected for this experiment. This was for two reasons. First, no active experiments were in a sufficiently advanced state of development to have been adapted to the pod. Second, there was insufficient time to develop electronics which could be expected to function in the nuclear environment.

Following is a list of the Project 8B SF' instruments carried on the rear bulkhead of the pods. Detailed information on each of these instruments is presented in Sections 2. 3. 1 and 2. 3. 2. Figures 2. 4 to 2. 9 show the gage arrays in the three pods; in addition, certain devices from other agencies were included.

Instrument	Number per pod
MK 1 Indenter	4
MK 2 Indenter	4
MK 3 Indenter	7
K-Edge Detector	2
R/V Composite	7
Plated Hole	2 to 3
Calorimeter	2 to 3
Metallurgy	10
Fracture	2

Each instrument was designed to have a minimum acceptance angle of $\pm$ 15° because this was believed to be the largest orientation error possible if the pod gyros operated properly. This criterion turned out to be unfortunate.

For instrument design purposes the following fluxes and conditions were assumed:

2.3.1 X-Ray Effects Instruments.

Impulse Recorders. Three variations on one basic type of impulse recording gage were included in Star Fish. These are discussed separately in the following sections. The basic gage consisted of four pistons resting in cylindrical barrels with conical ends pointing toward an anvil. The pistons were held by restraining springs to prevent premature release due to vehicle-induced accelerations or vibrations. Upon X-ray blowoff, an impulse was transmitted to the front face of each piston. In the instances where this impulse was sufficient to overcome the small retention force, the piston flew forward striking the anvil. The volume of the indent which was formed in the anvil is a function of impact energy. This in turn is a function of impulse, and therefore, the indent is a measure of the impulse imparted to the sample.

The relationship between indent diameter in a lead anvil and the kinetic energy of the indenter has been established by a series of calibrating experiments at Allied Research. Figure B. 2 in Appendix B presents the results of the calibration for the particular gages used in Star Fish. The range of energies covered includes those associated with the experiment. Additional data gathered at the AFSWC Pulse Power Laboratory corroborates the data shown in Figure B. 2.

Mark 1 Indenter Gage. The Mark 1 gage was designed to record the impulse induced by metal blowoff. In general, impulses from the metals were anticipated to be higher than for the non-metallic samples included in Star Fish (except for beryllium), on the order of

Because of the X-ray opacity of these sample materials, the indenter piston and gage design shown in Figure 2.11 was possible; piston parameters are given in Table 2.1. A thin cap of the sample material was affixed

weakly to the face of the piston's aluminum shank, except in the case of aluminum and magnesium where the entire piston-cap assembly was one piece. Upon X-ray vaporization, the compressive wave generated within the cap passed into the piston proper as a compressive wave. Multiple reflections occur at the cap-piston boundary, but it is easily shown (Section 3. 3. 1) that regardless of whether or not the cap remained on, the piston would move forward with virtually all the blowoff momentum.

The cap thickness was kept thick enough to prevent transmitted X-rays from heating the piston face above 100°C under the anticipated conditions, yet as thin as was consistent with the foregoing criterion in order to maximize momentum transfer. It was felt that the piston might deform and bind in the hole if allowed to heat appreciably higher than 100°C. The cap thicknesses used are shown in Table 2. 1 for the three pods of Star Fish Prime. The retarding action of the restraining springs was corrected for during data reduction and represented essentially no error in impulse analysis.

One piston was solid magnesium rather than aluminum. This was done rather than cap magnesium onto aluminum. The acoustic impedances were such that momentum transfer characteristics would have been uncertain. Although aluminum pistons were somewhat more desirable because of the greater tensile strength involved, tests conducted at the AFSWC pulse facilities indicated no problems would result by substituting magnesium.

Every sample metal in the Mark 1 gages was capped on two pistons. The redundancy thus introduced lead to greater confidence in the data obtained. Consequently, four Mark 1 gages were aboard each pod.

Because of the highly corrosive action of the salt air at Johnston, it was believed imperative to surface-treat the magnesium and aluminum pistons against this corrosion. Accordingly, a surface treatment was given all pistons; the magnesium was coated with a Dow 17 dip, and the aluminum was anodized. The effect of the treatments was to increase the sliding friction of the shanks in the holes, but the retardation effect was estimated still to be virtually nil, primarily because of the large clearance between piston and wall (about 2. 006 inch on the diameter). Regardless, the deleterious consequences of not treating the pistons would probably have been serious. Both magnesium and aluminum form very rough binding surfaces quickly in the kind of environment found at Johnston.

An important feature of the gage was the floating anvil. That is, the anvil was essentially isolated mechanically from the case in the axial direction. Had the pod itself received no impulse, then this sophistication would have been unnecessary. However, any impulse-derived shock in the pod might have obscured the recorded impulse to an unknown degree if the anvil had been rigidly attached to the case, since the case was rigidly attached to the pod. A very conservative calculation indicated that a rigidly attached anvil might have reduced the relative piston-anvil velocity by 100 cm/sec under extreme conditions. At the lower flux station this was an appreciable fraction of the piston velocity. By allowing the anvil to float, this problem was avoided. The various distances, times, and spring constants involved were such that the piston impacted while the anvil was free floating, yet the relative case-anvil motion was stopped mechanically before trapping the piston.

Mark 2 Indenter Gage. It was found that for a number of sample materials a modified indenter gage and piston design was preferable to the Mark 1 design. The principal reason was that, for certain non-metals, the anticipated impulses would have been too low with the Mark 1 piston design to result in adequate piston velocities. In addition, the arrangement of a weakly affixed cap on a piston introduced unacceptable uncertainties into subsequent analysis, simply because of the low acoustic impedances of these non-metals. The momentum transfer from cap to piston would be a highly uncertain function of pulse characteristics and dimensions. Also, these samples were comparatively transparent to the X-rays and would have required cap thicknesses on the order of the piston shank length.

Hence the Mark 2 design evolved from the Mark 1 to accommodate the various requirements of six R/V and two plastic samples. Figure 2.12 illustrates the Mark 2 design. The piston diameter was increased to increase the total impulse while the total piston mass in most cases was less than the Mark 1 design. The piston was not solid, but relieved to a depth of 0.200 or 0.040 inch depending on the sample material. The samples were then inserted and glued into place as indicated by Figure 2.12. Table 2.2 gives certain Mk 2 piston parameters.

There were several compelling reasons for this arrangement. First, appreciable sample lengths were necessary to prevent the piston shank from heating excessively or even melting. Second, as already mentioned, it was not advisable to affix the samples as caps. Hence, the obvious arrangement was to insert the samples into the hollowed piston, thereby

gaining sample depth and avoiding other capping problems. A bonus feature in several cases was the lightening of the piston weight, since some sample densities were lower than those of the piston material.

The X-ray-induced temperature at the piston shell-sample interface was calculated for each sample type using the anticipated X-ray characteristics mentioned earlier, and in no instance was it greater than 20°C (see Table 2.2). Thus, problems associated with pistons exploding from internal vaporization were avoided. There was some question about the peak blowoff pressure effect on the piston shell walls. The possibility of sufficient radial deformation resulting in binding of the piston in its hole existed. Extensive high-impulse tests at the AFSWC Pulse Power Laboratory indicated that no appreciable effect occurred. To reduce this possibility further, and to avoid unwarranted blowoff effects from the piston shell, an aperture smaller than the inside shell diameter was placed over the pistons. In this manner, the cold strength of the shell material was preserved and inside wall heating minimized.

Again, all piston shells were treated to prevent corrosion. Magnesium shells were used at the two low flux stations because minimal piston weights were very important there. Aluminum was preferable for strength reasons, however, and was used at the high flux location.

Each material was repeated once except for the unpainted and the painted samples which were each on three pistons. Despite favorable design characteristics of the Mark 2 piston, the induced impulses were anticipated to be consistently below those of the metal-capped pistons. Again the retarding action of the restraining springs could be corrected for during data analysis.

The free-floating nature of the anvil was believed even more important in the Mark 2 gage, since a number of piston velocities were expected to be quite low, potentially on the order of the case velocity. It was necessary to shift the anvil spring from inside the gage to outside because of the greater diameter of the pistons.

A carbon disk was attached covering the front face of both the Mark 1 and Mark 2 indenter gages. This 1/4-inch shield was sufficiently thick to prevent vaporization of the steel gage face at all three stations. The carbon itself, on a theoretical basis, was calculated not to blowoff, so that no impulse at all was expected to reach the case. Flared holes through the carbon permitted the pistons to view the X-rays.

Mark 3 Indenter Gage. A third variation in the basic indenter design was included in Star Fish. It was necessitated because a certain few materials—R/V, plastic, and metal—were so transparent to X-rays that even the Mark 2 piston design was unsatisfactory. Had these materials been used in Mark 2 pistons, the shell-sample interface would have become dangerously hot. The thicknesses of these transparent materials had to be, in general, over 3/8 inch at the Pod S1 range to keep the aluminum behind it below 100°C; in some instances the sample thickness required was as great as an inch. In Table 2. 3 these materials are listed together with the thicknesses necessary to keep the aluminum behind it below about 100°C under the X-ray conditions anticipated.

The design of the Mark 3 is shown in Figure 2. 13. The case design is essentially the same as the Mark 2 except that a solid slab or disk of the sample material, called the striker, completely covered the front face of the gage and pistons. The pistons were solid aluminum. Their shanks were slightly longer than the face thickness so that each piston pressed against the striker with a small pressure. In Table 2.3 the striker thicknesses used are shown, and it is evident that none of the piston faces were heated much above 100°C by the transmitted X-ray flux. Because each striker sample covered all four pistons, one entire gage was assigned to each material. Hence, there were seven Mark 3 gages in each pod.

The action of the striker plate arrangement is straightforward and has been analyzed in numerous texts. The impulse was generated at the outside surface, and the short pulsed compressive wave traveled through the plate to the sample-piston interface. Table 3.20 indicates that the acoustic impedance of all the striker samples except beryllium is lower than that for aluminum. As a result, it can be shown that the incident pulsed wave crossed the interface only once before separation of the piston from the striker. Also, from conservation of momentum considerations, it can be shown that the momentum carried by the piston was greater than the initial momentum imparted to the striker by the blowoff process (the striker attained a reverse velocity). Or, the initial impulsive momentum was enhanced by a factor which depends on the acoustic impedances. The relation defining this enhancement factor, is:

$$\text{Momentum Enhancement Factor} = \frac{2 Z_2}{Z_1 + Z_2}$$

where Z_2 = acoustic impedance of aluminum piston

Z_1 = acoustic impedance of striker sample

The impulses anticipated for the Mk3 materials ranged from zero to 10^4 dyne-sec/cm^2. A very low impulse was anticipated on a theoretical basis for either carbon or beryllium at any of the three pod ranges.

Although the impulse was enhanced in most instances, such was not the case for the beryllium or aluminum strikers. The acoustic impedance of beryllium is slightly more than aluminum. No complication in analysis was introduced thereby.

The aluminum pistons were all anodized to limit corrosion. No magnesium pistons were used, because its acoustic impedance is only half that of aluminum.

The anvil arrangement in the Mark 3 design was identical to the Mark 2, so that the anvil was free floating and unaffected by extraneous shocks. The restraining springs pressing the pistons against the striker plate were studied, and their effect on the piston velocity could be corrected for. One piston was not in contact with the striker, being shorter than the front case face. This piston served as a control.

A brief summary of the design differences between the three types of indenters is given below:

Indenter Design Differences

Mk1

1. Sample is a thin cap glued to piston
2. Anvil spring inside case
3. All pistons Al (except 2 solid Mg pistons per pod)

Mk2

1. Sample is a plug inserted into recessed piston
2. An aperture is in front of each sample
3. Anvil spring outside case
4. Piston shape different from Mk1
5. All S2 and S3 pistons Mg, all S1 pistons Al

Mk3

1. Sample is large plate covering all pistons (striker)
2. All pistons solid Al
3. One piston in each case not in contact with striker
4. Anvil spring outside case

Indenter Design Verification. In checking the ability of the restraining springs to retain the pistons under the missile acceleration and vibration environment, the following test was performed. A spring arrangement was devised which exerted a 20-g force on the piston to simulate a constant acceleration.- With this spring in place, the instrument was subjected to vibration inputs covering the following range; 20 g at 2000 to 30 cps, 0.44-inch amplitude at 30 to 5 cps. In order to minimize the piston velocity reduction due to work done in deflecting the restraining spring, it was desirable to choose the minimum size spring which just met the above requirements. The spring dimensions were experimentally determined through a series of vibration tests.

In addition, extensive testing of the indenter gages was performed at the AFSWC Pulse Power Facility which simulated impulses with the characteristics expected in order to ascertain: (1) that neither the Mark 1 nor Mark 2 pistons would tumble in flight, (2) the proper piston clearance to preclude binding in the hole, (3) the feasibility of the Mk2 sample-hollowed piston configuration, and (4) the lower limit on velocity for reliable indents. Satisfactory operation of the gages over a piston velocity range exceeding that anticipated in Star Fish verified the gage designs.

Metallurgy Gage. The metallurgy experiment in Project 8B was designed to utilize the known metallurgical characteristics of selected metals as indicators of radiation-induced presure and temperature histories in the exposed specimens. The experiment was designed in a joint effort of the Physics Division of the Air Force Special Weapons Center and Allied Research Associates.

In experiencing an X-ray-induced impulse, a given material is subjected to pressure and temperature transients. The structure of all known metals is altered to some degree by changes in temperature and stress, and some of these alterations are stable or at least metastable when the sample is returned to a standard environment. Such alterations are phase changes, order-disorder reactions, crystallographic changes, microstructure changes, hardness changes, and composition changes. Changes metastable over a considerable period should permit analysis of the material some time after exposure to the nuclear environment. The changes that were anticipated in Star Fish fell in the category of metastable states with reasonably long lifetimes.

A detailed discussion correlating these observable microstructural transformations to the X-ray-induced thermal and peak pressure gradients

can be found in Reference 12. It has been shown in that reference that under the proper conditions the following data can be deduced from materials exposed to a nuclear burst: (1) maximum temperatures and pressures, (2) temperature and pressure gradients, (3) duration of high-temperature conditions and pressure pulses, and (4) interaction of temperature and pressure effects.

The Star Fish metallurgy instrument was designed to capitalize on these potential effects and is presented in Figure 2. 14. The instrument consists of a 2024-T4 aluminum housing with a 2-3/4-inch flange to attach the instrument to the pod bulkhead. The metallurgy specimen, mounted in an aperture in the instrument face, was exposed to the nuclear detonation. In order to reduce extraneous effects derived from reflection of the pressure pulse from the sides and back of the metallurgy samples, these surfaces were protected by machined and lapped mating surfaces of the same material. This permitted the shock wave to travel through the mating edges into the surrounding material. The edge of the sample was protected by a spall ring, the rear of the sample by a spall plate. The assembly of sample and spall units was held in place in the face of the instrument, with only the sample exposed to the nuclear detonation, by the stafoam shock absorber. A spall ring shield prevented impingement of X-radiation on the spall ring. The expected mechanical operation of the instrument was as follows. The impulse derived from the X-ray blowoff imparts a velocity to the metallurgy sample and spall plate, causing them to move toward the rear of the instrument. These pieces are gently decelerated by the gradual crushing of the stafoam shock-absorber, thus preventing any damage to the sample by impact with the rear of the case. The sample is then retained in the instrument housing, because the base diameter of the sample is greater than the hole diameter of the spall ring shield.

During the month of March 1962, representatives of AFSWC and Allied Research met with several authorities in the metallurgical field in order to discuss aspects of the experiment design, calibration, and post-shot analysis, in order to maximize the amount of usable data to be obtained from the Fish Bowl experiment. In support of these experiments a series of calibration tests using HE charges to simulate the environmental pressure loadings were scheduled at the Colorado School of Mines by Dr. John Reinhart.

Because of their particularly desirable characteristics, the following materials were selected for metallurgical specimens; (1) naval brass, (2) 550°C brass, (3) 750°C brass, (4) 1095 steel, martensitic structure, (5) fine-grained molybdenum, (6) austenitic (321) stainless steel, (7) LASL

FeNi alloy, (8) Armco iron, and (9) Alnico. In addition, in order to protect the original substrate of material from being blown off, an additional 1095 sample coated with a thin film of lead (Pb-1095) was included. Hence, there was a total of 10 metallurgy instruments per pod.

To insure that the proper references were retained from which metallurgical changes could later be measured, AFSWC provided control samples of each metallurgy sample which was machined in their shop. In addition, AFSWC controlled the chemistry of these materials via special heats and subsequent analysis of these heats prior to accepting the materials.

The metallurgy instrument, like the other instruments intended for the Fish Bowl experiment, was subjected to a thorough series of laboratory tests to prove its mechanical integrity. The stafoam shock absorber was selected as a result of a series of drop tests in which the heights of fall and the mass of the weight were chosen to simulate the kinetic energy predicted from the X-ray-induced impulse. The entire instrument was subjected to a series of vibration tests, in which a vibration input of 20 g's from 2000 to 30 cps and 0.44-inch amplitude from 30 to 5 cps was applied both axially and transversely to the instrument, with no mechanical difficulties being observed.

Reentry Vehicle (R/V) Material Gage. The purpose of the R/V experiment was to obtain information from which the effect of X-ray-induced impulses on various reentry vehicle structures could be evaluated.

In the Project 8B R/V experiments, flat plate samples of actual reentry vehicle structures were used. In order that the effects of the nuclear detonation on the specimen be the same as on the actual reentry vehicle structure, it was necessary that the propagation of the wave simulate the 2-dimensional case as closely as possible. This was achieved where possible by utilizing a specimen having a relatively large diameter to thickness ratio (see Figure 2.15). Also, the specimen was mounted as freely as possible, using spring-loaded detents, in order to preclude shock wave distortions caused by supporting structures. Following the impulse, the R/V sample was driven free of the detents. In the short duration of free flight which followed, the shock wave was able to complete many traversals of the sample. The sample then impacted into a crushable foam which absorbed the kinetic energy of the sample.

Table 2.4 presents the R/V samples included in the SF' experiment. One of each sample was tested at each station, yielding a total of seven R/V instruments per pod. All samples were 1.50 inches in diameter.

The R/V sample was held centered in the face of the instrument by a thin flange on the case which contacted the front shoulder of the sample. A 1/4-inch carbon shield protected the front face of the case and prevented any X-ray blowoff.

Laboratory tests of the R/V instrument were conducted in order to prove the feasibility of the spring-loaded detents. A replica of the instrument was constructed and a representative R/V sample fitted. This instrument was subjected to an impact scaled to simulate the X-ray-induced impulse. The action of the detents was observed and adjusted until the desired behavior was obtained. Vibration tests of the instrument, using an auxiliary spring pressing on the R/V sample to simulate a steady 20-g acceleration, were also conducted. The vibration spectrum chosen consisted of a 20-g intensity from 2000 cps to 30 cps, and 0.44 amplitude from 30 cps to 5 cps. Both axial and transverse acceleration inputs were checked. Successful completion of these laboratory tests helped insure proper functioning of the R/V composite instrument in the Star Fish experiment. In addition the capability of the

stafoam to absorb the anticipated kinetic energy of the sample was confirmed.

Fracture Gage. The fracture gage was designed to give information about the shape of the blowoff pulse: in particular, its duration and peak amplitude. Thus, it was different from the other gages used in the experiment, for they were designed to measure quantities integrated over the entire pulse. A gage of this kind was used in Operation Hardtack and was later analyzed to give data consistent with other results of that experiment (Reference 1).

The gage, in brief, consists of a lucite cylinder, on one end of which was glued a small metallic button (see Figure 2. 16). The button is designed to blow off upon exposure to the X-ray flux, thus creating a compressive stress pulse which is transmitted through the metal and into the lucite cylinder. Since the diameter of the button is small by comparison with the diameter of the lucite, one can idealize the loading of the cylinder by considering it a point impulsive load applied at the center of the end of the cylinder. As a result of this load, a spherical stress pulse propagates into the lucite. This compressive stress gives rise on reflection to a tensile wave and a shear wave. Subsequently, the stress pattern in the cylinder becomes more and more complicated because of the cascading reflections. However, the gage is designed so that only the tensile waves produced during the initial reflection need be treated.

When the tensile stress at some point in the lucite exceeds the fracture strength of the material then a crack is initiated. This crack should grow at a known rate until the stress drops below a certain value By studying the fracture pattern in the lucite, an estimate of the duration and peak of the initial blowoff pulse can be made. The details of this subject are given in Reference 13, and it will suffice here to mention the simplest kinds of fracture one can observe. The simplest fracture is the disk-like fracture, parallel to the end of the cylinder, which is caused by the tensile wave produced when the incident compression reaches the end of the cylinder. It is this fracture which, if it extends to the boundary of the cylinder, causes the end to spall. Another possible fracture has the form of a roughly cylindrical surface coaxial with the cylinder and near the front face. This is due to tensile waves reflected from the sides of the cylinder. Also, at the end of the cylinder, a conical fracture may be observed which is due to the superposition of waves from the sides and the end. In order for these effects to occur as described,

it is necessary that the cylinder be shock isolated. To this end the gage was supported by O-rings in an aluminum housing.

The gages used in this experiment were designed to satisfy the criterion that a fracture would be produced when the stress wave is reflected from the end of the cylinder. With a given impulse, this criterion establishes a maximum length for the lucite cylinder. In each case, there was a second cylinder whose length was arbitrarily chosen to be twice this length. This, of course, extended the dynamic range of the instrumentation.

At each of the three pod ranges, anticipated impulses and melt depths were calculated for a variety of materials. In every case, it was desirable to have the button as thin as possible, for this reduces the distortion of the stress pulse as it passes from the button into the lucite. As an arbitrary safety criterion, it was assumed that each button would have a thickness three times the depth of melt. Button materials were chosen such that the predicted peak stress transmitted to the lucite cylinder would be roughly the same at each pod. The buttons all had a radius of 0.140 inch. The cylinder length which would just produce an end fracture was then computed, taking into account the inverse variation of the stress amplitude with distance in a spherical wave. This length was 0.445 in. On each pod, there was a second cylinder whose length was 0.890 inch. A summary of pertinent gage parameters is given in Table 2.5.

2.3.2 Source Parameter Instruments. The three instruments discussed below were intended to function diagnostically, that is, the characteristics of the X-ray flux incident on the pods at each location were to be observed and recorded. One instrument was designed to measure the time and spectral integrated X-ray flux at each pod. The two other instruments were concerned with resolving the spectral shape of the flux.

Carbon Calorimeter. This instrument was based on the calorimetric principle of measuring a final equilibrium temperature of a heated material and therefrom deducing the absorbed energy. Because of the environmental and experimental difficulties associated with nuclear bursts, however, interpretation of the gage would depend upon the successful application of certain corrections. Nevertheless, this gage represented the only approach developed that could have directly measured the total X-ray energy with a passive detector. (It was possible to determine part of the total flux by other methods, however.)

The device was simply a carbon disk sufficiently thick to absorb most of the incident X-ray energy, yet thin enough to permit an appreciable final equilibrium temperature. A drawing of the device is given in Figure 2.17.

The carbon block was thermally insulated on all sides but that exposed to the X-rays. If no material were to evaporate after exposure, and there were no reradiation losses, then all the energy absorbed would go into determining the final equilibrium temperature. In fact, however, a significant fraction of the X-ray energy may be reradiated, and a certain amount of carbon may evaporate, thus physically removing some absorbed energy. As a result, the two energy-removing processes would have to be corrected for during data analysis to properly interpret the data.

Referring to the drawing, Figure 2.17, a few points should be explained. The disk closest to the aperture is the calorimeter; the other two immediately behind are combination X-ray attenuators and insulators. The insulating mitten around the first two disks served a double purpose: to reduce radial conduction losses and to keep the rear of the calorimeter watertight. A novel modification of the original design (see Reference 1) was in using pyrolytic graphite instead of conventional graphite for the calorimetric disk (as well as the others). The pyrographite, which is highly conductive in two directions, was cut into disk form such that one of the highly conductive axes was through the disk. This orientation meant that axial temperature equilibrium would be approached at a much greater rate than would have been the case with conventional graphite. The benefit of this rate enhancement is that reradiation losses are abbreviated somewhat because the heat is conducted rearward quickly. The conduction in the "a" axis direction is as high as that of copper.

The second disk, which was pressed against the rear of the calorimetric disk was also pyrographite but cut such that the highly insulating "c" axis was parallel to the center axis. Thus, this disk acts as an insulator in that direction, and little conduction through the back of the calorimeter occurs. More conventional insulation was not used, because it was feared that the X-ray transparency of the first disk would be high enough to allow most insulators to melt.

The temperature-recording elements consisted of eighteen small holes drilled into the rear of the calorimetric disk and partially filled with temperature-sensitive crayons. These crayons undergo permanent color changes when their temperatures reach certain critical points. The holes were not uniformly spaced around the perimeter of the disk, but rather were clustered at opposite ends of a diameter corresponding to the second "a" axis (highly conducting direction). Also, the holes were positioned to avoid the X-ray flux up to an incidence angle of 15°.

Tests conducted at Allied Research demonstrated that the colors of the paints were not affected by salt water attack. This result applied equally to changed and unchanged paints. The paints used allowed temperature interval of 10 to 20 percent between color change points. The estimated equilibrium temperatures associated with the design illustrated indicated that coverage from 65° to 600°C would provide sufficient dynamic range. Careful coding of the paints was accomplished and color photographs of their initial state taken.

Two of these calorimeters were flown in each of the two outer pods, S2 and S3. It was expected that the lowest flux station would require the least subsequent data correction, because the temperatures involved would be lower, and consequently, would be re-radiation and evaporation effects. Although the interpretability of this gage in Pod S1 was considered extrem poor, nevertheless it was decided to include the gage there with the thought that it might give additional quantitative information on the corrections to be applied to the other calorimeters. An additional calorimeter was flown on Pod S3 but was shielded against X-rays to provide a check on any non-X-ray, thermal background.

Careful measurements on each calorimetric disk thickness and weight were made beforehand to allow determination of the evaporation of the front surface.

A carbon (conventional graphite) shield covered the face of the gage case. This was designed to prevent the aluminum case from vaporizing and perhaps diffusing in front of the aperture, thus attenuating the total X-radiation reaching the calorimeter.

K-Edge Gage. The K-edge instruments were designed to provide data on the X-ray spectrum of a nuclear detonation. These instruments originally were designed and used by Stanford Research Institute (SRI) in Th similar designs for the Project 8B K-edge instruments evolved through consultation between SRI and Allied Research based on the previous designs for (Reference 14).

This instrument attempts to measure the time integrated intensity of the incident X-ray flux as a function of wavelength. It consists of an aggegrate of filter-detector pairs which all view the X-rays simultaneously. The filters are all different from one another, consisting of materials with K-edges progressing from Consequently, the transmitted spectrur through a given filter is greatly modified according to the position of the K-edge (Figure 2.18) and is unlike that transmitted through any other filter.

The other component of this device is the detector on which a record of the energy passed by the filter is made. The detector itself has an inherent wavelength sensitivity which influences the resolution of the instrument. The detector component consists of a stack of foils which are alternately plastic, "metal", plastic, etc. The "metal" foil is one of several materials, which depends upon anticipated source characteristics. The energy density within a given metal-plastic pair required to cause physical sticking of that pair has been determined (about 100 cal/gm). It is this effect that is used to determine the energy transmitted by the filter.

The analysis of the gage depends on the fact that each filter-detector channel represents an independent view of the spectrum within the kev region. Since there are essentially seven independent channels, values of the spectral intensity of seven different wavelengths can be obtained. A complete discussion of the techniques used can be found in Reference 14.

Figure 2.19 is a detailed drawing of the detector channels mounted in the gage cylindrical container which was designed to be bolted to the face plate of the pod. One channel position is empty for purposes of illustration.

Each detector stack was mounted in a cartridge and backed by a carbon plug and metal spacers. The rear end of each cartridge had short slots permitting the edge to be bent, holding the stack, carbon plug, and metal spacers in place in the cartridge. The front end of each cartridge had a circular window to permit X-radiation to fall on the detector stack. An air escape slot in the side of each cartridge permitted equalization of air pressure. Each detector cartridge was a self-contained, interchangeable unit.

Each filter was held in place by a carbon insert and a channel cylinder. After the filter, carbon insert, channel cylinder, and detector cartridge were placed in the hole provided in the gage cylinder container, the whole channel assembly was fixed in position by a metal plug. The carbon insert was included to prevent excessive vaporization of metallic material by X-ray absorption. The carbon in the detector cartridges was to prevent similar undesired blowoff effects.

The X-ray flux produces heat in the metal foil of the detector which has two components, Q_s, the heat generated by absorption of X-radiation whose photon energy is slightly below the K-edge, and Q_n, the heat generated by X-radiation with photon energy above the K-edge. The channels were designed to have $Q_s \gg Q_n$ and also the parameters are such that $Q_s + Q_n$ exceeds the heat required for sticking at the entrance end of the detector stack.

Some of the channel parameters used are given in Tables 2.6, 2.7, and 2.8. Fourteen channels were in each pod, seven in each of two gages. The filter element and thickness are listed for each channel. The quantities Q_s and Q_n at the entrance end of the detector were calculated for possible device temperatures of assuming a Planck spectrum. For optimal operation of a channel it was necessary that $Q_s > 100$ cal/gm and $Q_n < 100$ cal/gm.

Channel 14 in each pod was designed to have $Q_s + Q_n$ less than the sticking value. This provided a check against spurious heating effects.

Channels 8, 9, and 10 in each pod used carbon filters. These were not K-edge channels but operated on much the same principle as the plated hole gage discussed below. The reasons for this inclusion among the K-edge channels were the expectation of greater structural strength in the filter and the useful redundancy in data provided by the similarity to the plated hole gage.

Plated Hole Instrument. The plated hole gage evolved from an instrument first designed for the experiment and discussed in detail in Reference 3. The design utilized for SF' was in principle the same as its predecessor, but somewhat modified physically. A working drawing of the SF' plated hole gage is shown in Figure 2.20. Its purpose was to determine the spectral characteristics of the incident X-ray flux.

The inside cavity was vacuum plated with one of three metals—chromium, lead, or gold. The plating thickness was not critical and did not have to be known in view of the thicknesses involved, that is, the X-ray-induced energy density drop across the plating is negligible because the plating is so thin.

The explanation of the theoretical aspects of this instrument has been given in Reference 3 and need not be repeated in detail here. Qualitatively, what was expected to occur is the following. X-rays penetrate the carbon and are attenuated selectively with respect to wavelength. Having traveled a given distance through the carbon, the flux impinging on the metal layer is modified both in intensity and spectral shape. The degree of modification depends not only on wavelength but also on depth traversed through the carbon. It is obvious that the energy density within the metal plating should diminish monotonically as one travels toward the rear. Consequently, at the flux

levels anticipated in SF', the metal should vaporize to a certain distance (going in a rearward direction), melt to a greater distance, and be simply heated beyond the melt-solid boundary. In addition, because chrome plating was used, another transition depth due to a crystalline change could occur in the plating. Hence, at least two, and perhaps more, observable phenomena might be related to linear distance on this device—vapor-melt boundary, melt-solid boundary, and heat-induced crystalline transition boundaries.

The different boundary positions are determined by appropriate visual or metallurgical techniques. From these, two or possibly more points on an energy density against linear depth diagram can be uniquely determined. The energy densities associated with each thermal transition are known with good accuracy for the metals under consideration. By a process similar to that outlined in Section 3.2.4, the X-ray source spectrum and energy best predicting the observed phase transition depths can be determined.

Clearly, the greater the number of independent phase transition depths obtained, the more definitively the spectral shape is determined. Hence, three metals were used in two of the three pods. Nevertheless, information on the spectral shape below about 5 kev is essentially unobtainable from this gage. Sulfur, which has a K-edge absorption coefficient discontinuity below that of chromium, was plated on the rear carbon disk in an attempt to extend the working limit of the gage below 5 kev.

A variety of metals were tested for salt water corrosion during the developmental phase of Project 8B. Salt water immersion of the plating was unavoidable with this instrument, thus making it necessary to use metals highly corrosion resistant.

Gold, lead, and chrome platings were among the very few that survived salt water attack. Sulfur, too, was satisfactory.

Pyrolytic carbon was used as the X-ray-absorbing material because of its high conductivity radially (the "a" axes were parallel to the disk surface). This feature permits more rapid cooling of the metal film than would occur with conventional graphite. The advantage of this lies in the reduction of: (1) diffusion of the plating into the carbon, (2) carbide-producing reactions, and (3) evaporation. Because of the differences in the thermal characteristics and X-ray absorption coefficients, the carbon at the carbon-metal interface is considerably cooler than the metal, as much as an order of magnitude cooler in places. Thus, extremely rapid conductive cooling of the very thin metal plate could be expected. Carbon was selected over other

materials, because blowoff of carbon was estimated to be nil. Plastics, under Star Fish conditions, would have vaporized badly.

Visual examination of the type of pyrographite supplied for use in the gages indicated what appeared to be strong density variations across the plane of the sample. A density mapping of large areas using high-resolution X-ray techniques showed, however, that the maximum local variations in density across the area was considerably less than 1 percent (Reference 15).

As with other instruments, the face of this gage was protected from induced blowoff by a carbon shield. Similarly, the rear internal carbon disks protected the metal case from the transmitted X-rays.

2.3.3 Correlation Instruments. It was believed that data correlating the SF' phenomena with those occuring under the would be extremely valuable. Accordingly the decision was made by AFSWC to include several of the X-ray-effects-measuring instruments designed for the SF' event in the No SF' diagnostic gages were used, inasmuch as this aspect of the experiment had extensive coverage already.

Three fracture gages and three indenter gages were fabricated and delivered to AFSWC in April 1962. The designs were essentially those discussed for SF' in Section 2.3.1, the modifications being in the cases and certain dimensions in order to accommodate the design to the catchers and the somewhat different flux levels.

Fracture Gage. A discussion of the theory and design of this gage has been presented in Section 2.3.1. Three of these gages were packaged in one cylindrical container and were identical except that the lucite cylinder lengths ranged from .445 to .890 inch. Each cylinder had a zinc button .007 inch thick exposed to the X-rays. The package of 3 gages was positioned at Station B3, a high-temperature, low-flux-level station.

The entire assembly is shown broken down in Figure 2.21.

MK 1 Indenter Gage An extensive discussion of this gage can be found in Section 2.3.1. The version remained virtually identical to the SF' design except that the flange was removed from the case and skates submitted (see Figures 2.22 and 2.25) so that the entire gage could slide inside the catcher. This indenter was stationed at B3 and the sample caps were: (1) aluminum, (2) 321 stainless steel, (3) gold, (4) ARMCO iron.

Mk 2 Indenter Gage. Similarly, this instrument has been treated in Section 2. 3. 1. Two changes were introduced into the design; (1) the case flange was removed and skates substituted (Figures 2. 23 and 2. 25) enabling the gage to slide in its catcher, and (2) the anvil spring was moved inside as in the Mk 1 arrangement. This gage was stationed at T2 and the sample slugs were:

Mk 3 Indenter Gage. This gage was virtually identical with its SF' counterpart, which has been discussed in Section 2. 3. 1. The changes were the removal of the mounting flange and the addition of skates (Figures 2. 24 and 2. 25) and the placing of the anvil spring inside the housing. It was stationed at T?' The aluminum striker was 0.032 inch thick. Unlike the corresponding SF' gage, there was no control piston.

TABLE 2.1 MK 1 PISTON DESIGN PARAMETERS

Pod No.	Cap Material	Cap Density	Cap Thickness	Piston Material	Shank Length
		gm/cm^3	inch		inch
S1	Mg	1.74	-	Mg	0.25
	Al	2.70	-	Al	0.25
	Fe	7.87	0.01	Al	0.24
	Cu	8.96	0.01	Al	0.24
	Zn	7.14	0.01	Al	0.24
	Sn	7.30	0.01	Al	0.24
	Au	19.30	0.01	Al	0.24
S2	Mg	1.74	-	Mg	0.25
	Al	2.70	-	Al	0.25
	Fe	7.87	0.01	Al	0.24
	Cu	8.96	0.01	Al	0.24
	Zn	7.14	0.01	Al	0.24
	Sn	7.30	0.01	Al	0.24
	Au	19.30	0.01	Al	0.24
S3	Mg	1.74	-	Mg	0.25
	Al	2.70	-	Al	0.25
	Fe	7.87	0.01	Al	0.24
	Cu	8.96	0.01	Al	0.24
	Zn	7.14	0.01	Al	0.24
	Sn	7.30	0.01	Al	0.24
	Au	19.30	0.01	Al	0.24

Pages 41 thru 43 deleted.

TABLE 2.5 FRACTURE GAGE PARAMETERS

	Pod S1	Pod S2	Pod S3
Button material	Aluminum	Magnesium	Zinc
Button thickness(cm)	6.6×10^{-2}	7.2×10^{-2}	1.7×10^{-2}
Button radius (cm)	0.36	0.36	0.36
Anticipated peak transmitted stress (dynes/cm^2)			
Lucite cylinder length (inch)	(a) .445 (b) .890	(a) .445 (b) .890	(a) .445 (b) .890

TABLE 2.6 K-EDGE DETECTOR PARAMETERS, POD S3

pages 45 & 46 deleted.

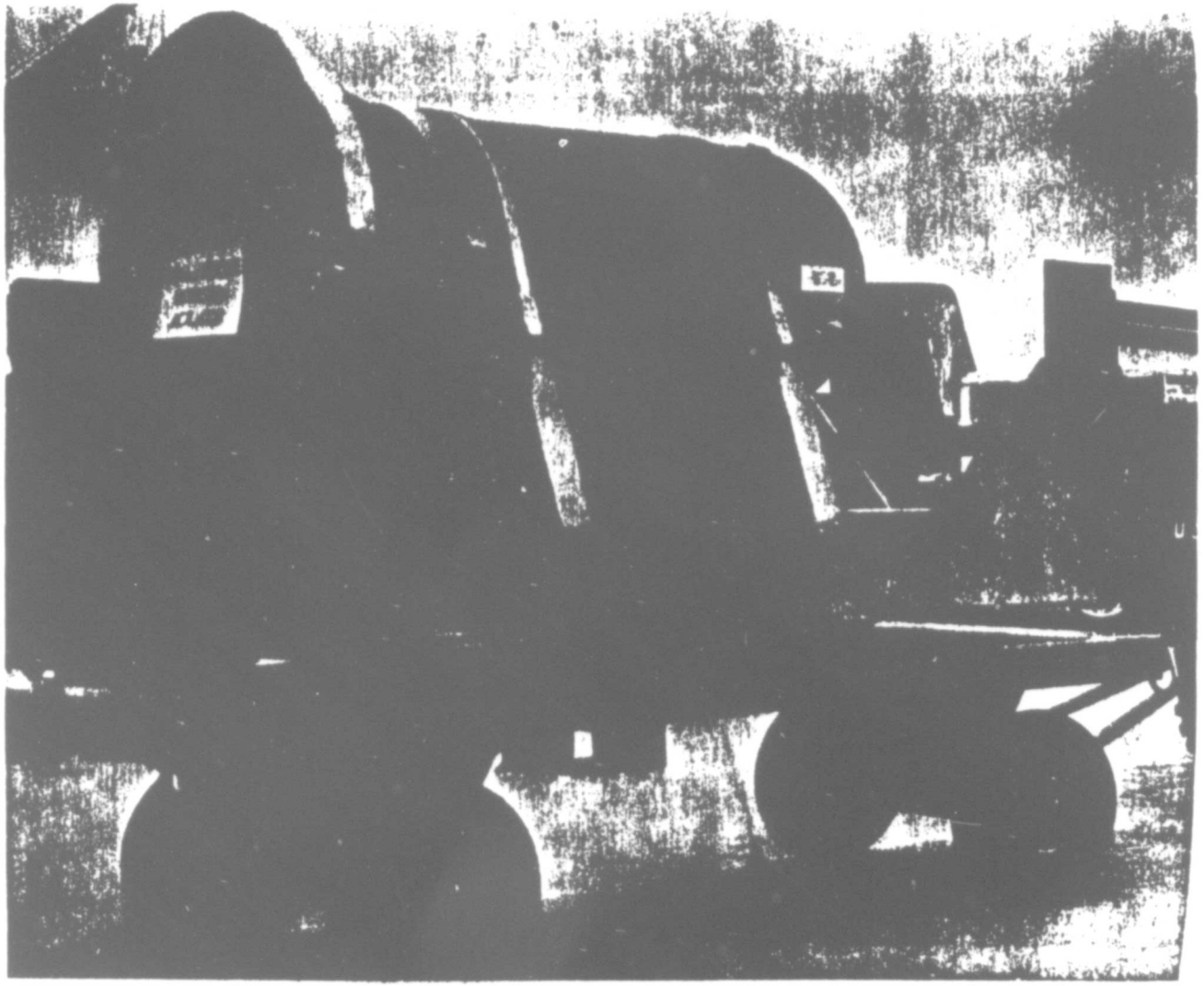

Figure 2.1 Instrument pod, Shot Star Fish Prime. (ARA photo)

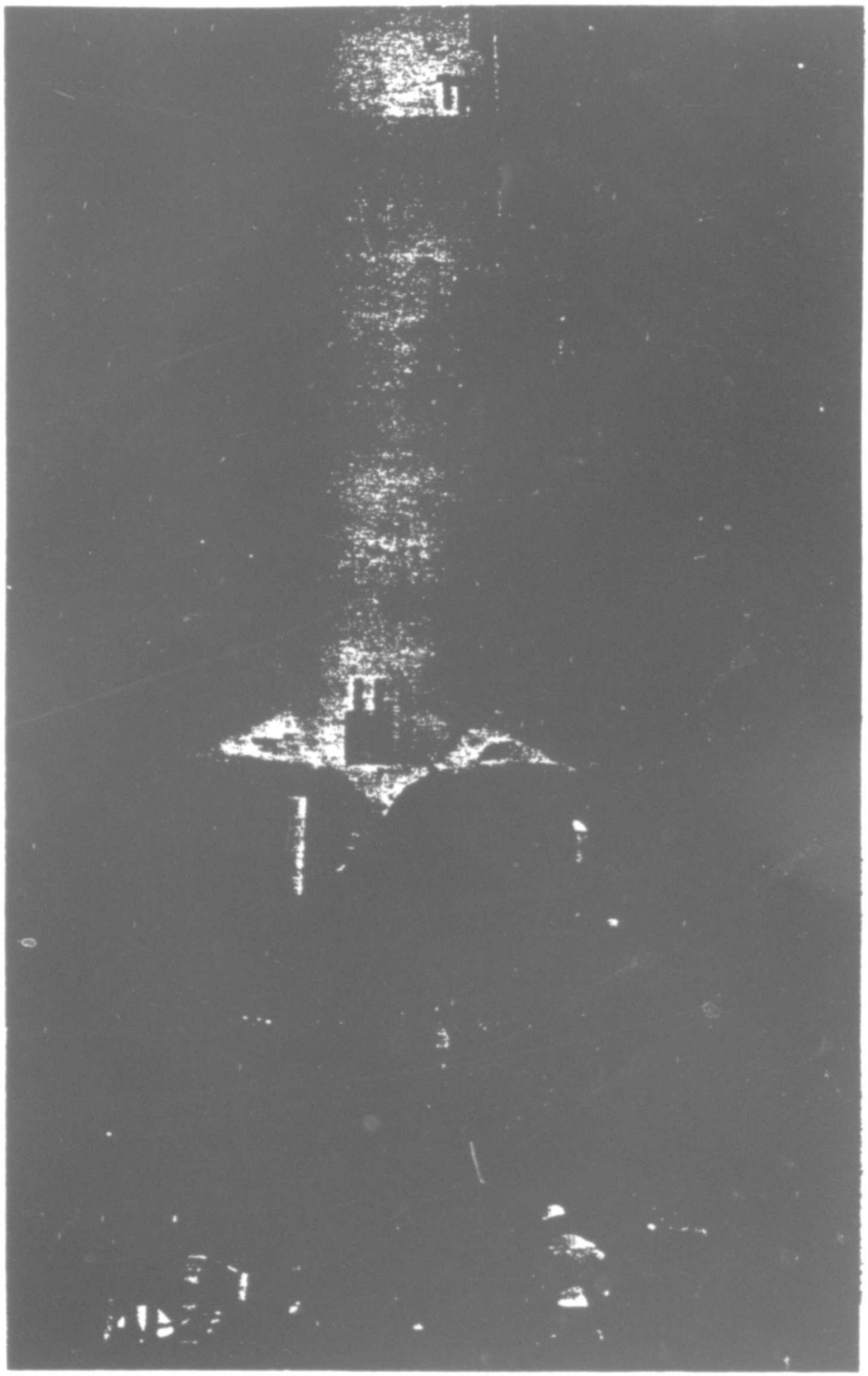

Figure 2.2 Two pods mounted on Thor, Shot Star Fish Prime. (ARA photo)

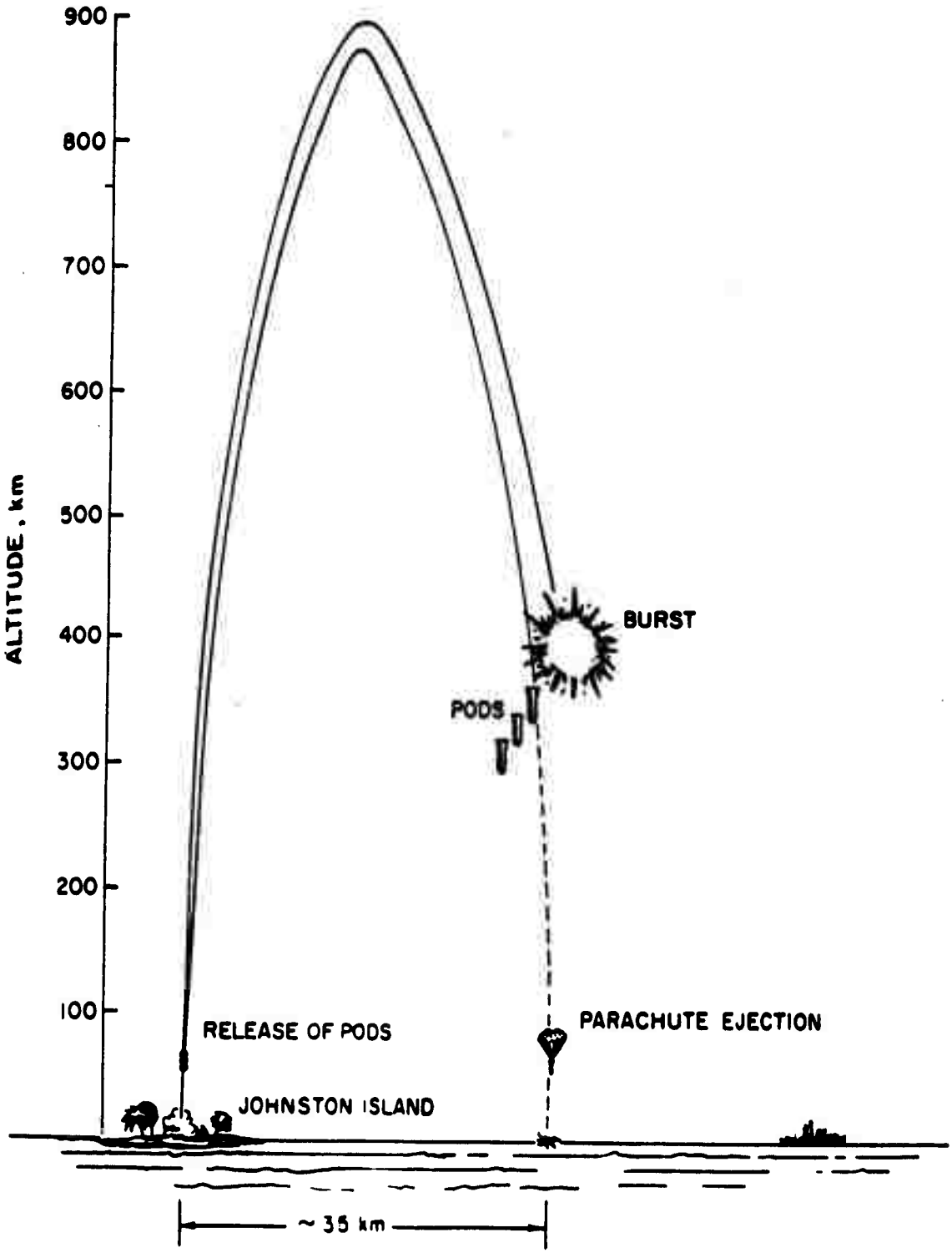

Figure 2.3 Trajectory sequences, Shot Star Fish Prime.

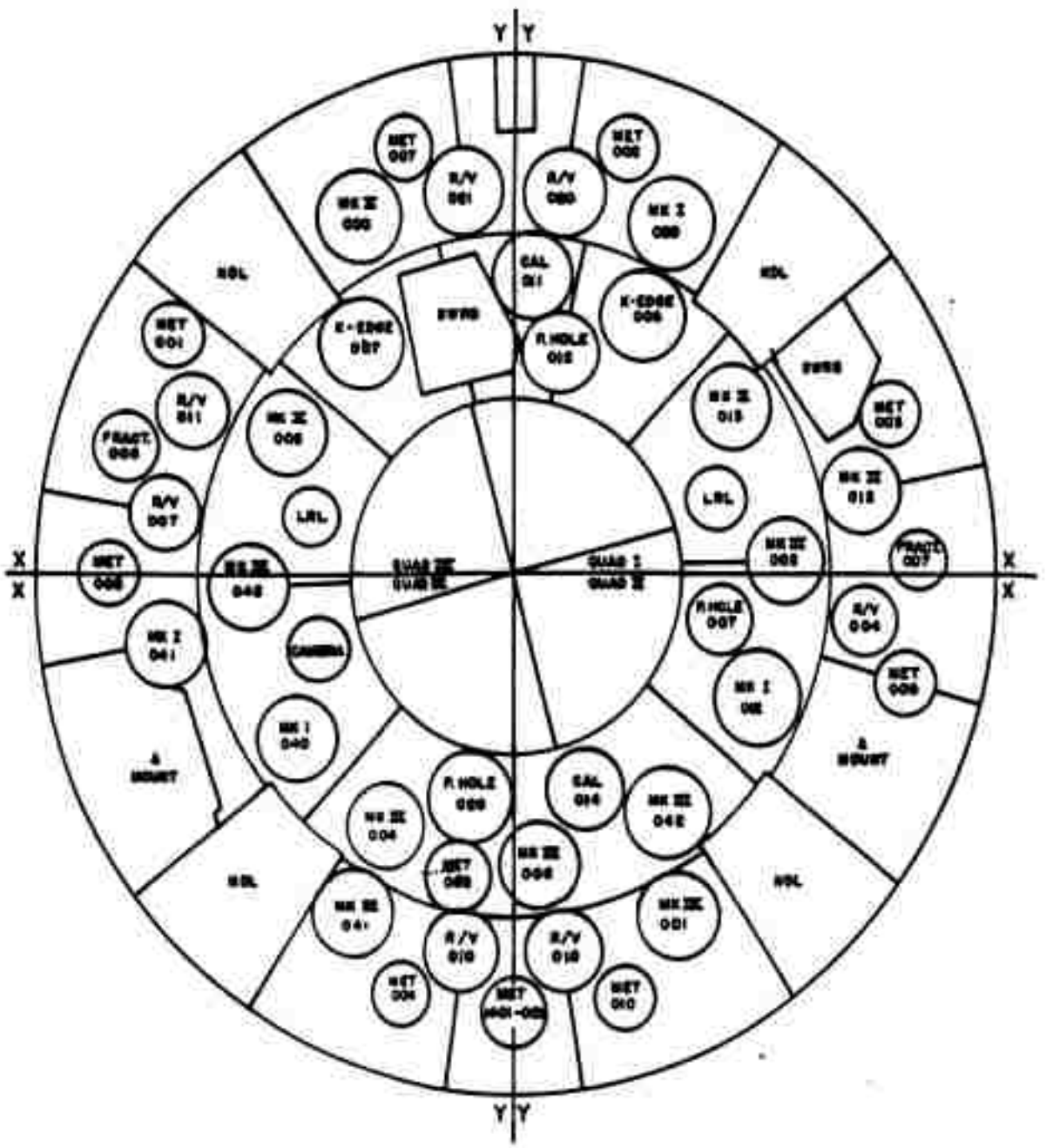

Figure 2.4 Pedestal instrument layout, Shot Star Fish Prime.

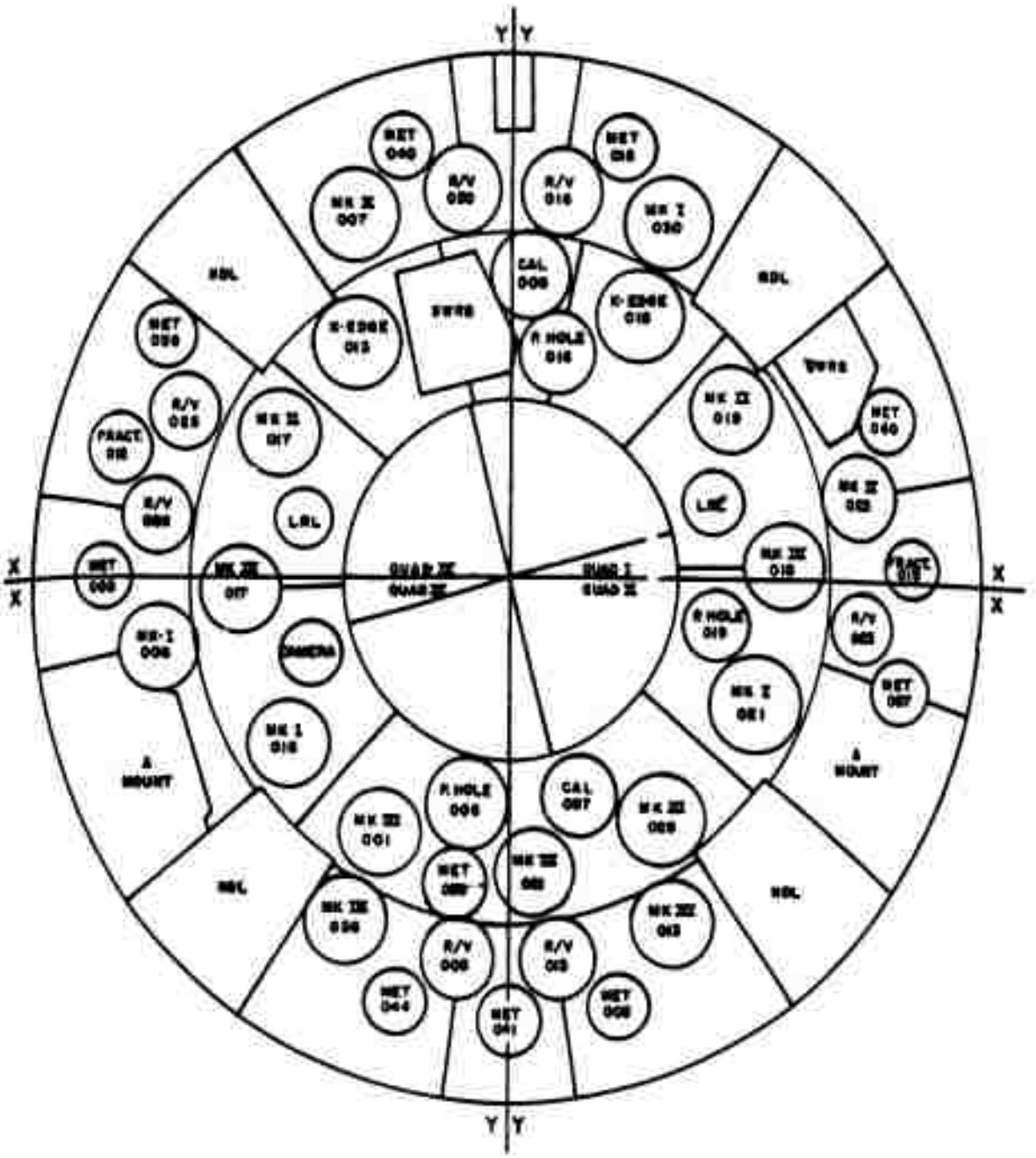

Figure 2.5 Pod S2 instrument layout, Shot Star Fish Prime.

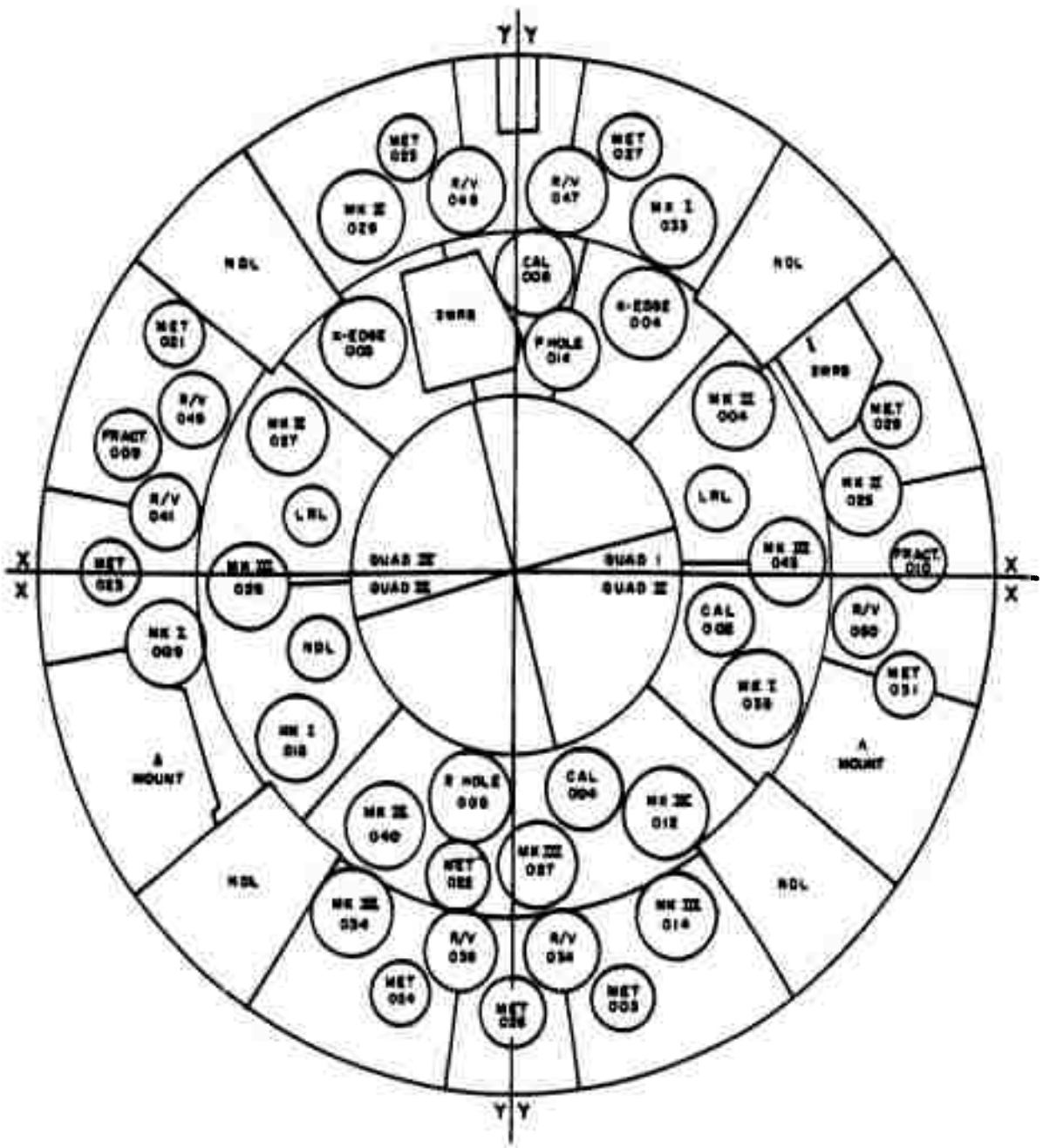

Figure 2.6 Pod S3 instrument layout, Shot Star Fish Prime.

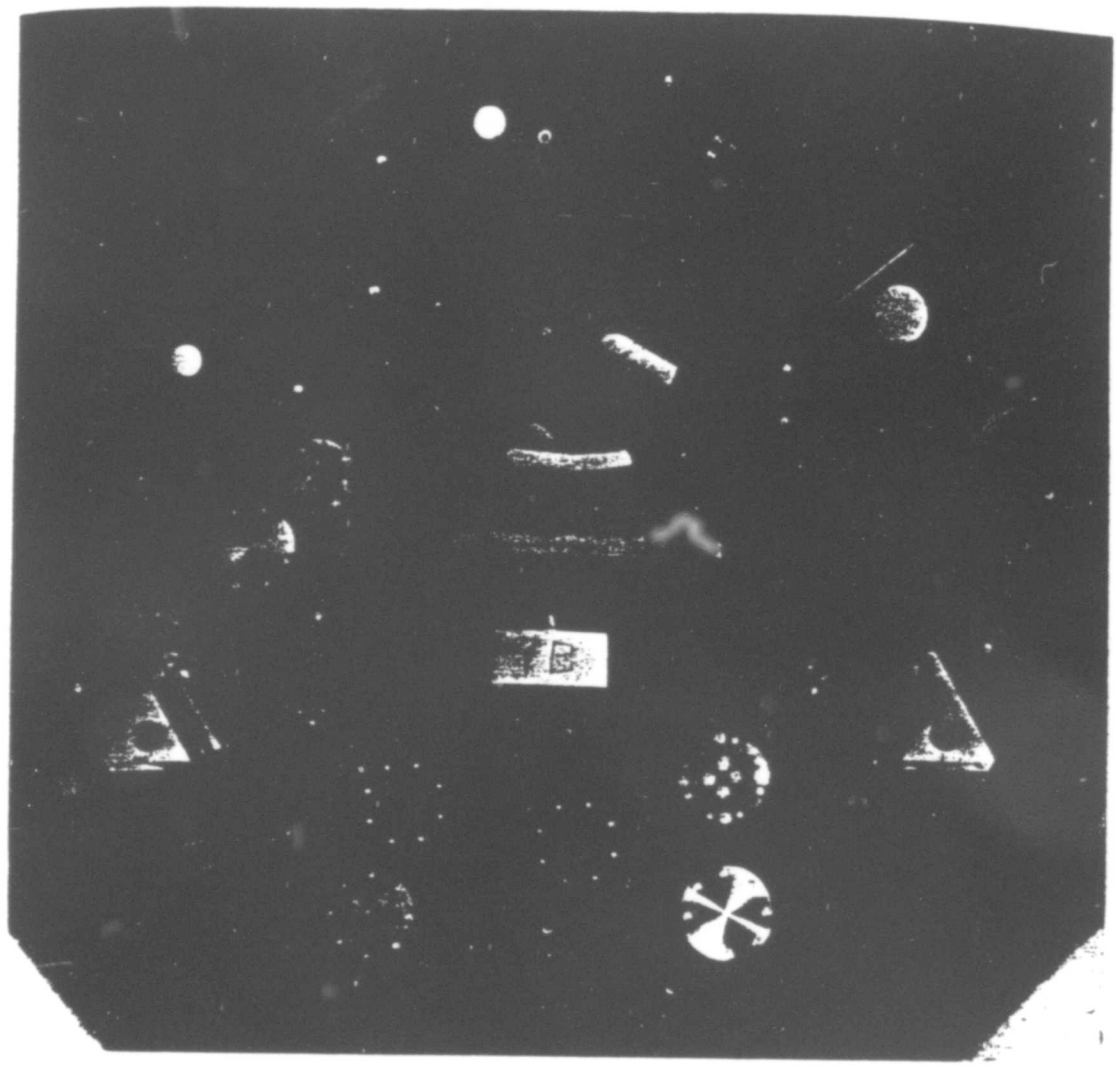

Figure 2.7 Pod S1 instrument plate. (ARA photo)

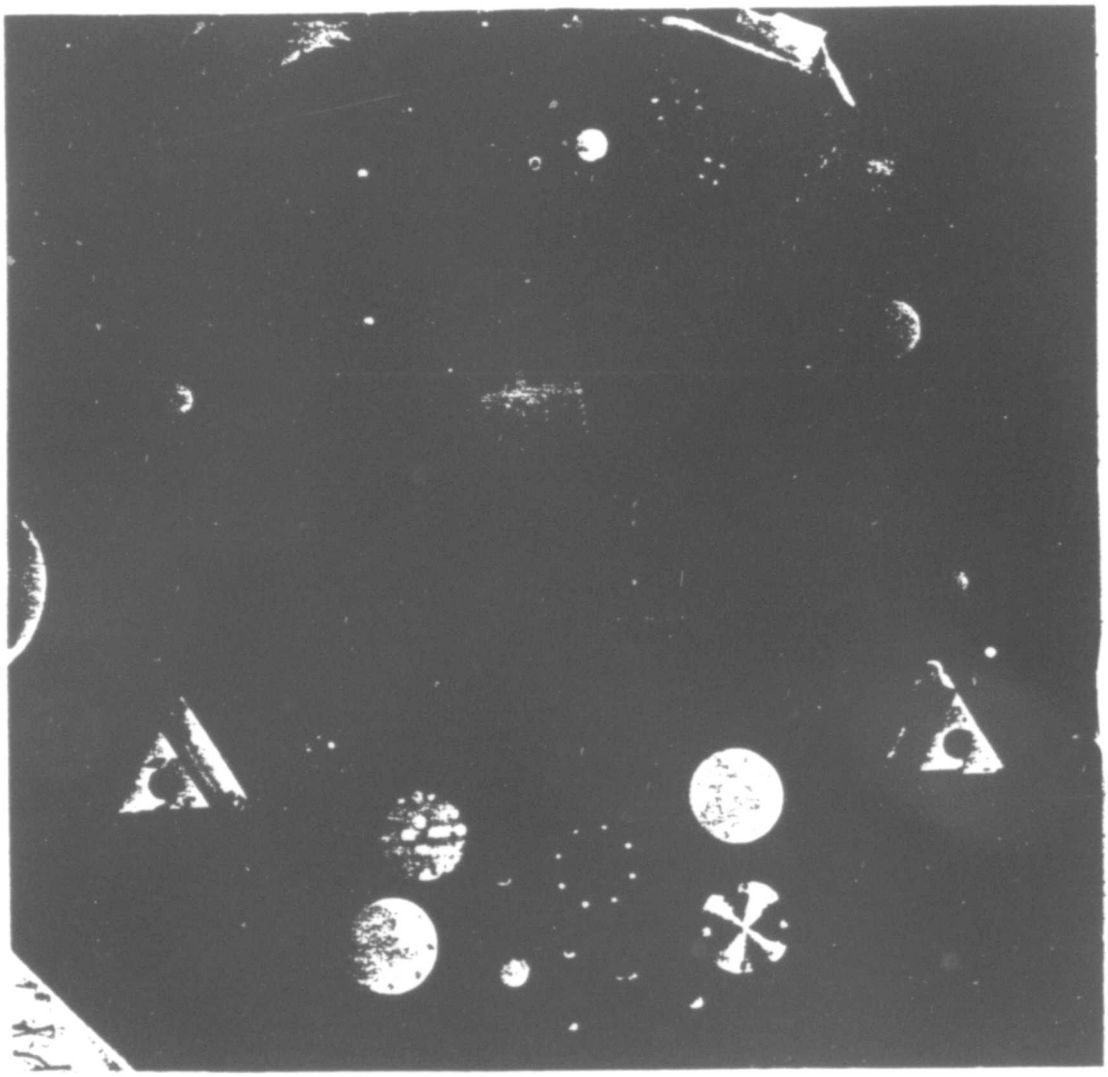

Figure 2.8 Pod S2 instrument plate. (ARA photo)

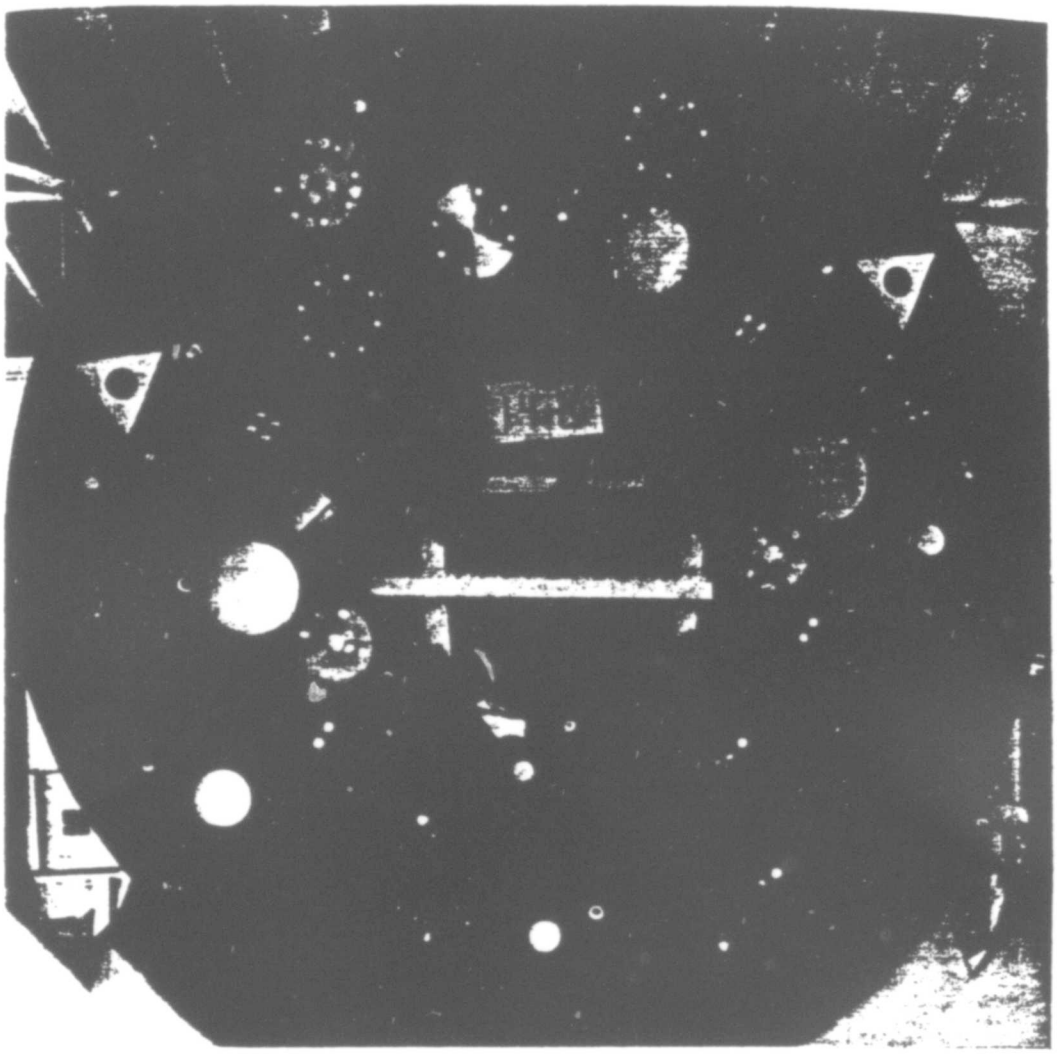

Figure 2.9 Pod S3 instrument plate. (ARA photo)

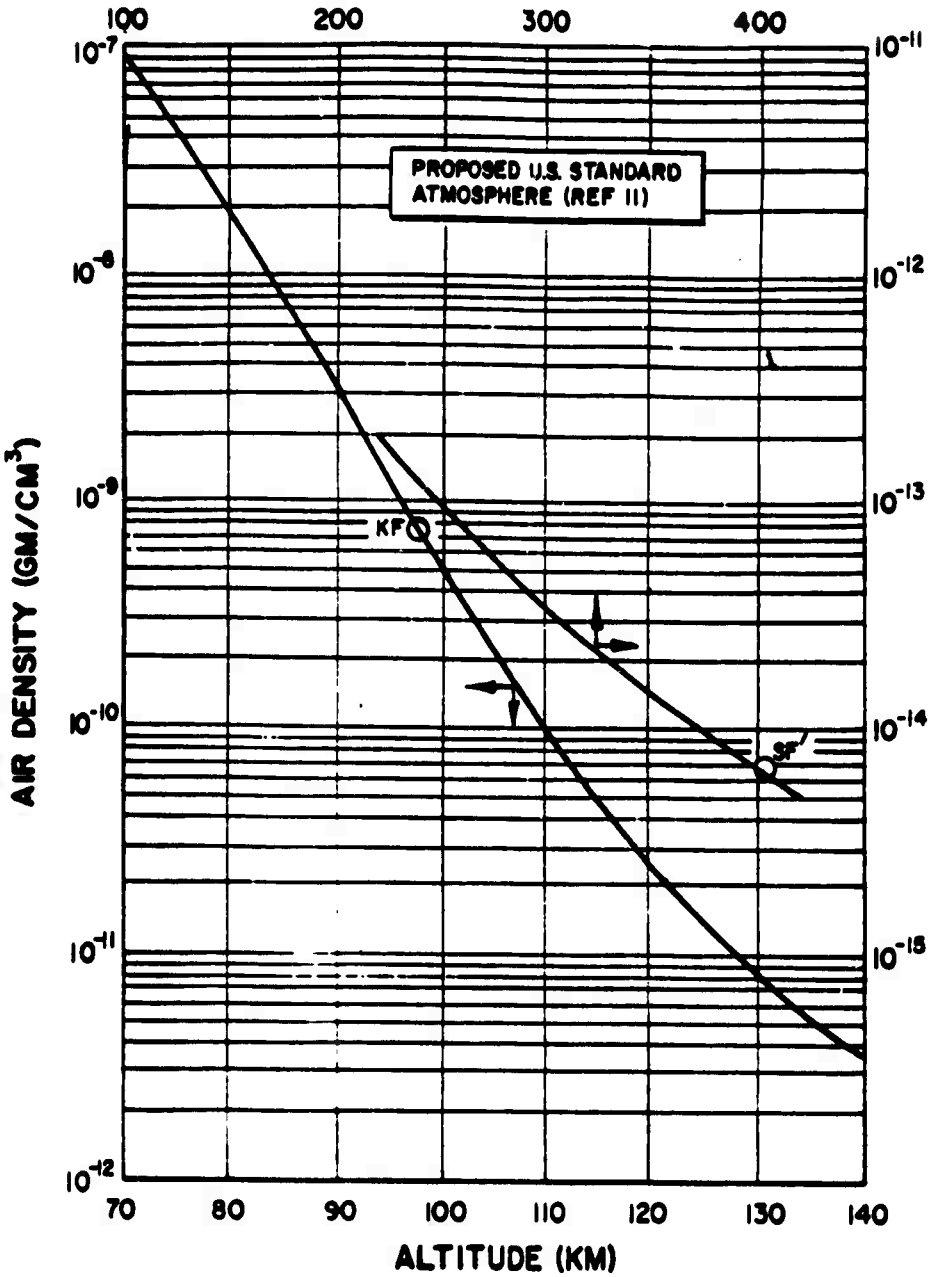

Figure 2.10 Air density versus altitude.

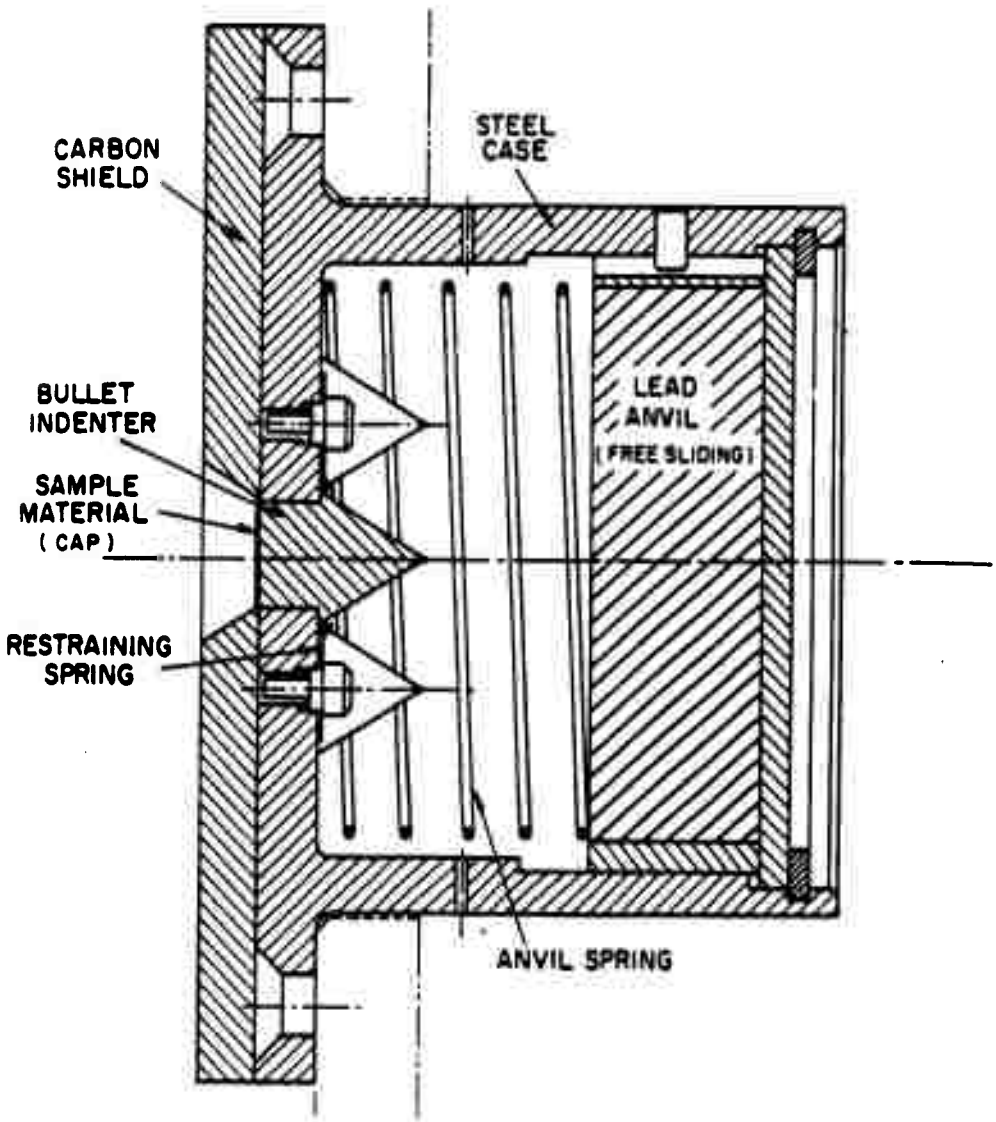

Figure 2.11 Mk 1 indenter gage.

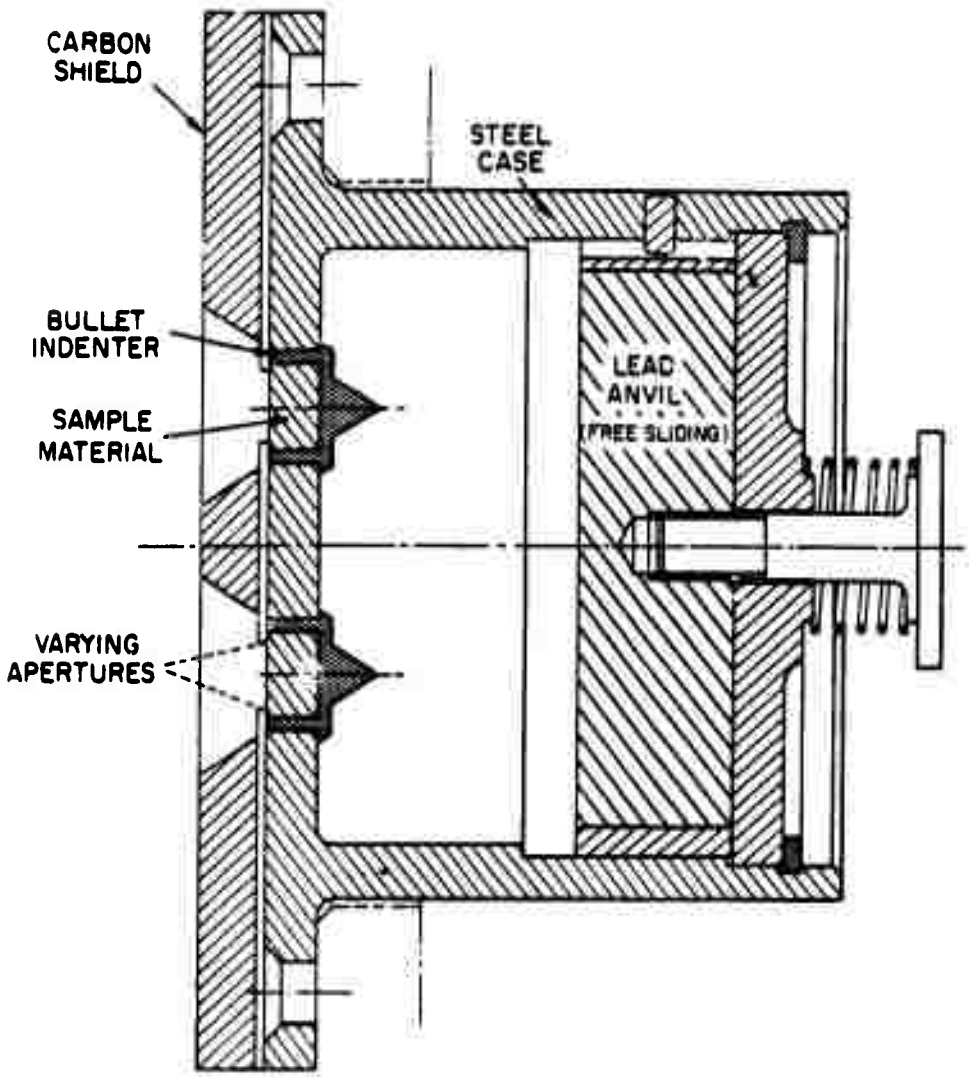

Figure 2.12 Mk 2 indenter gage.

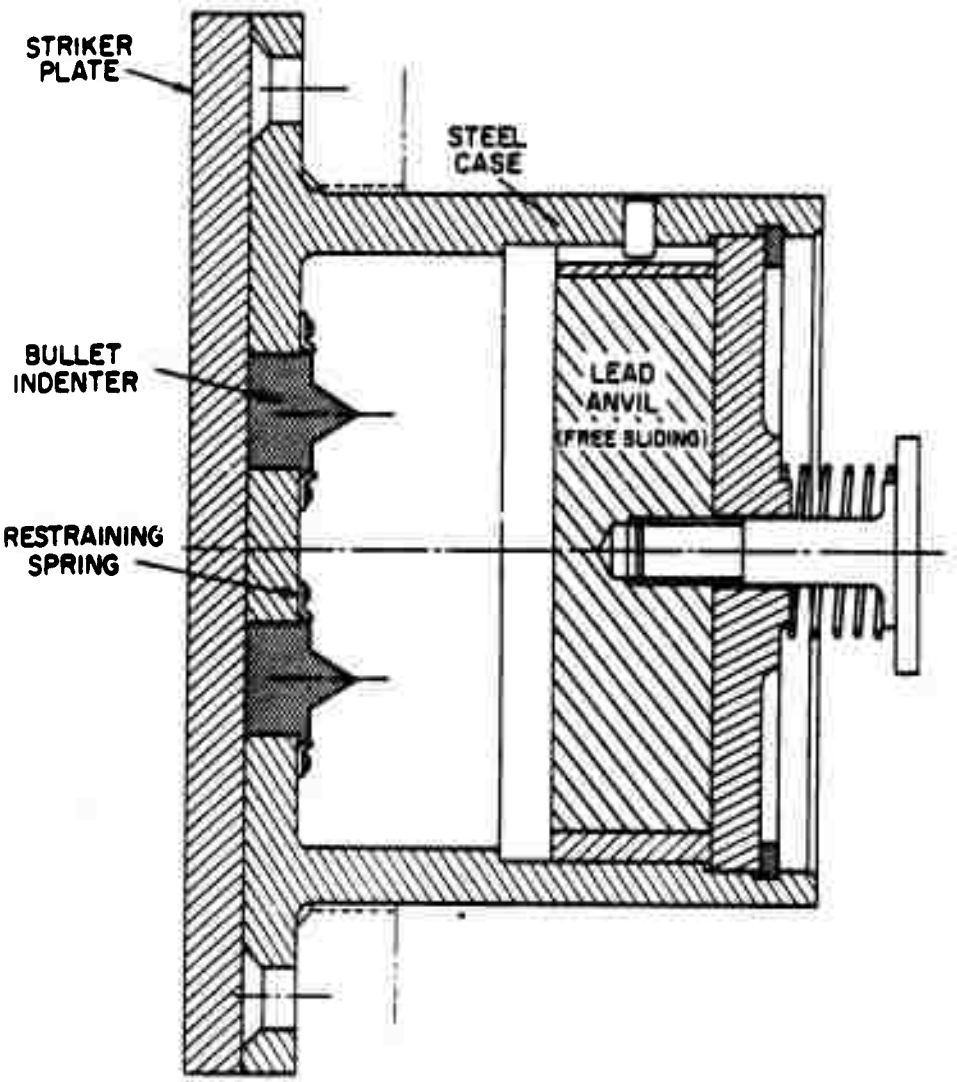

Figure 2.13 Mk 3 indenter gage.

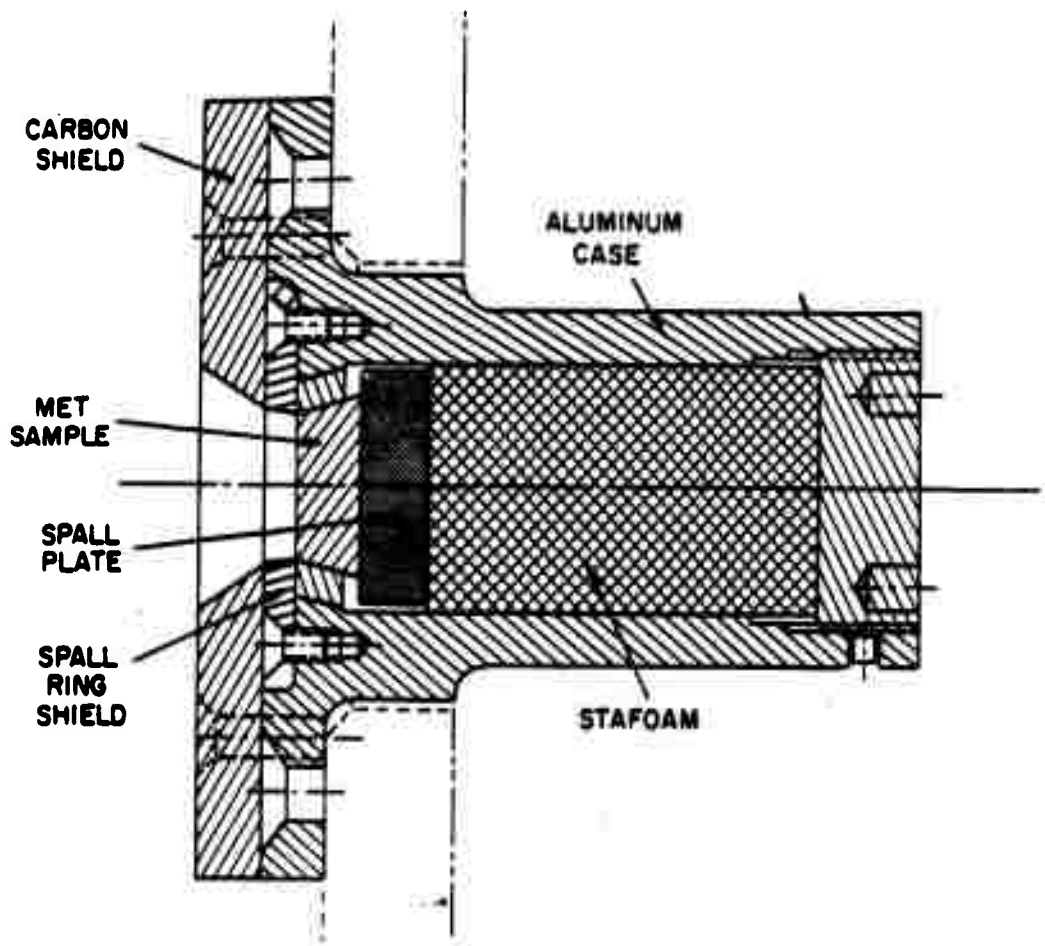

Figure 2.14 Metallurgy gage.

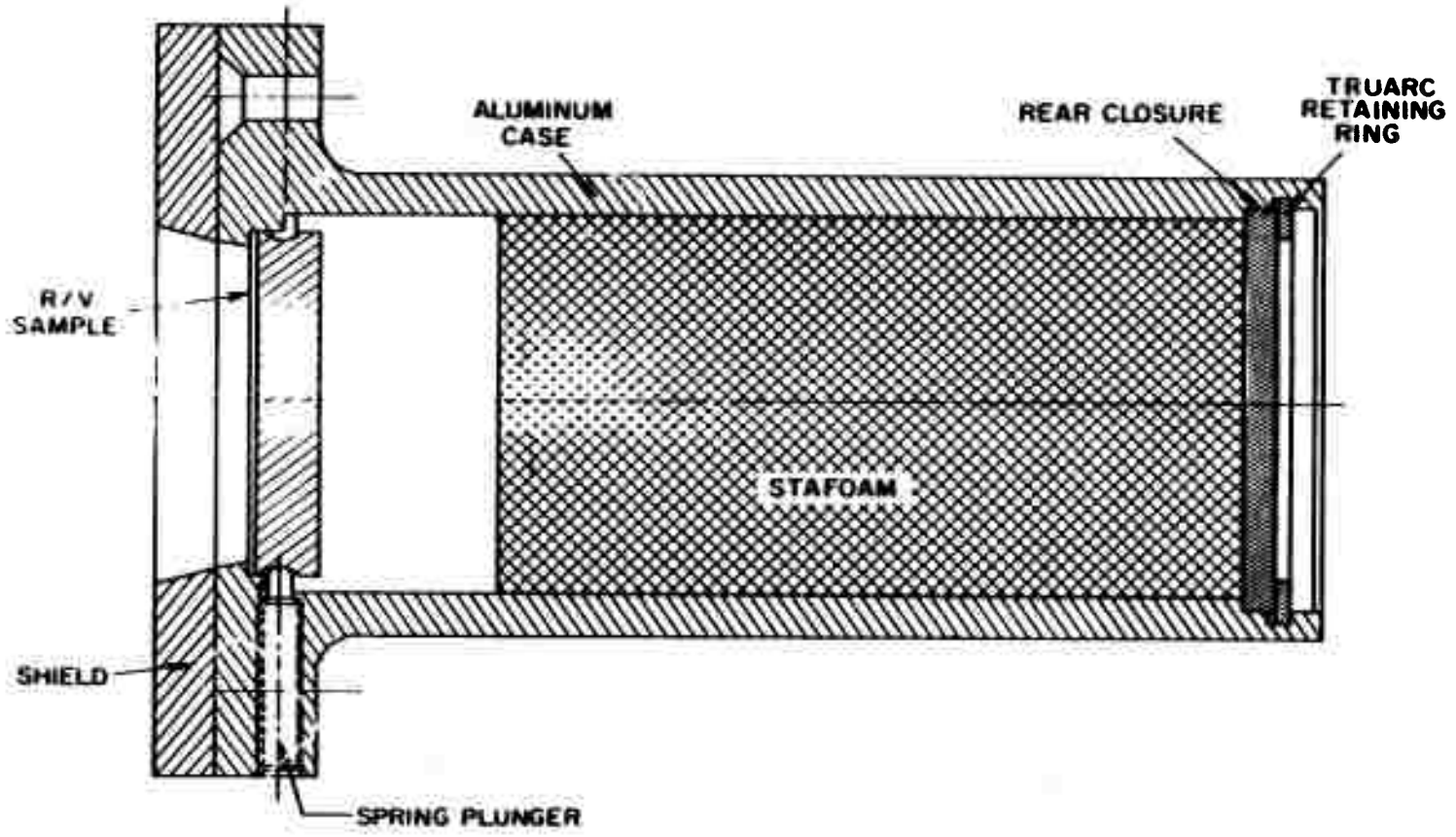

Figure 2.15 R/V gage.

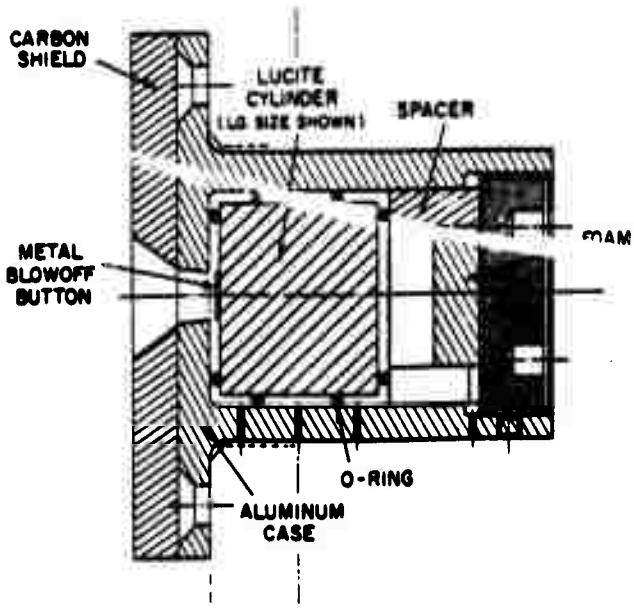

Figure 2.16 Fracture gage.

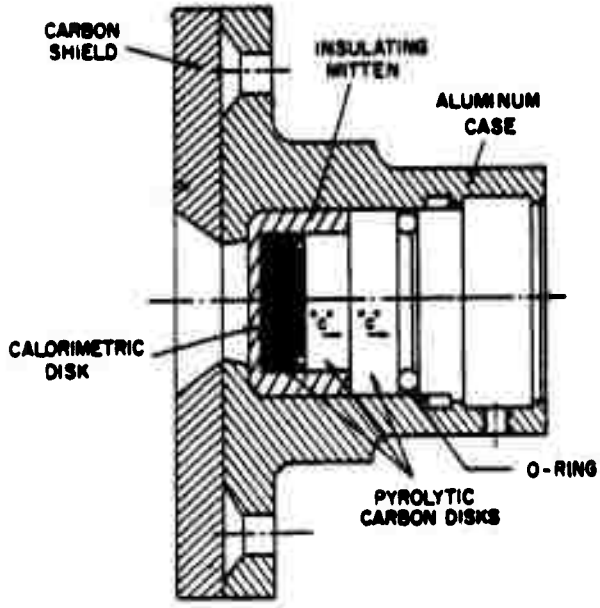

Figure 2.17 Calorimeter gage.

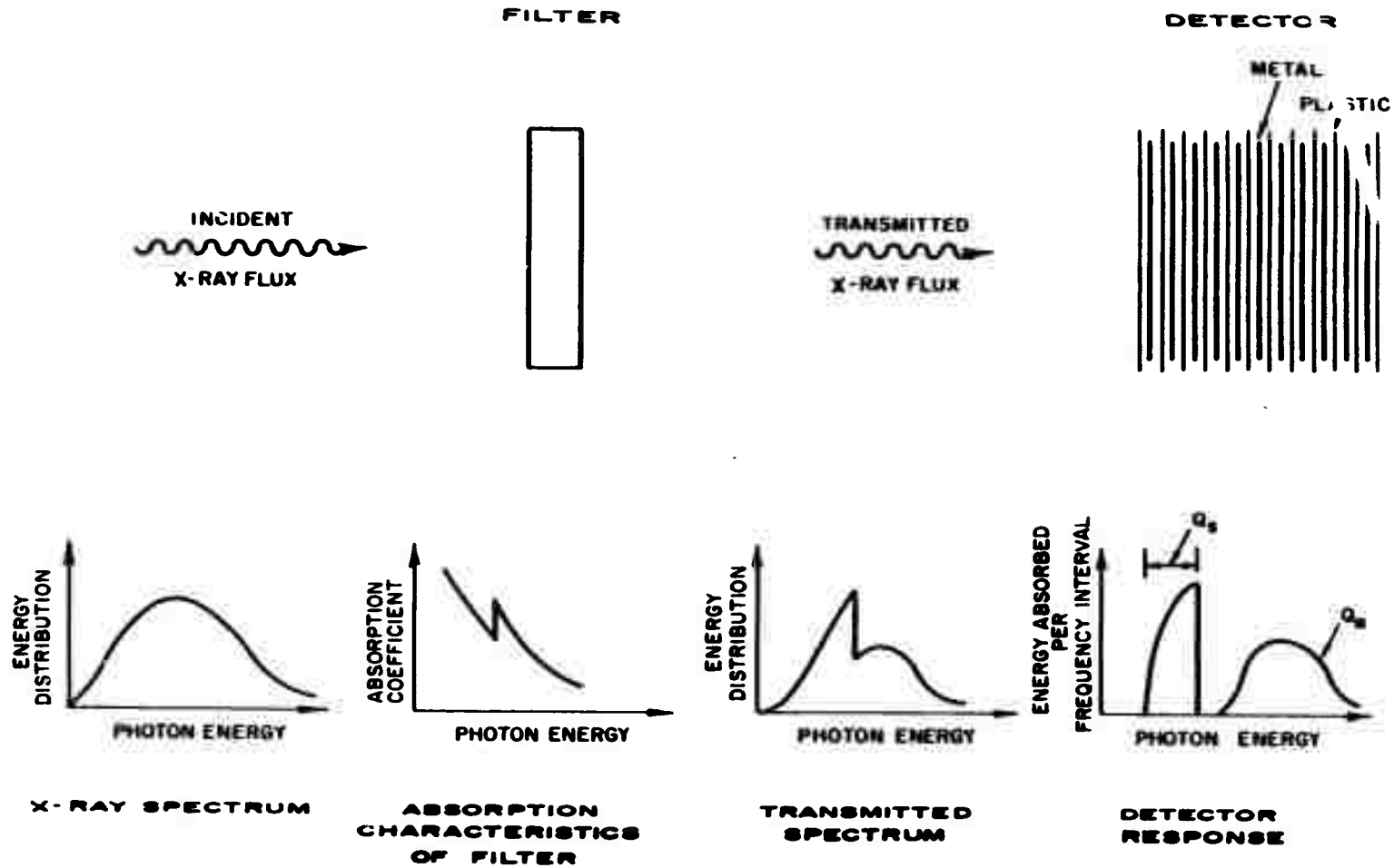

Figure 2.18 Qualitative description of K-edge experiment.

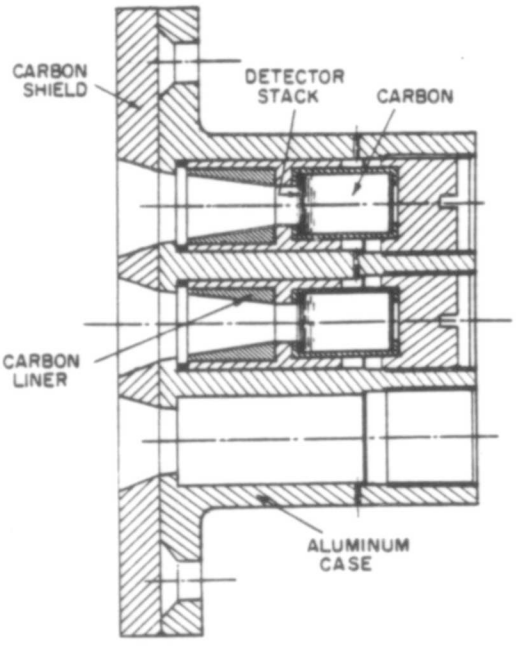

Figure 2.19 K-edge gage.

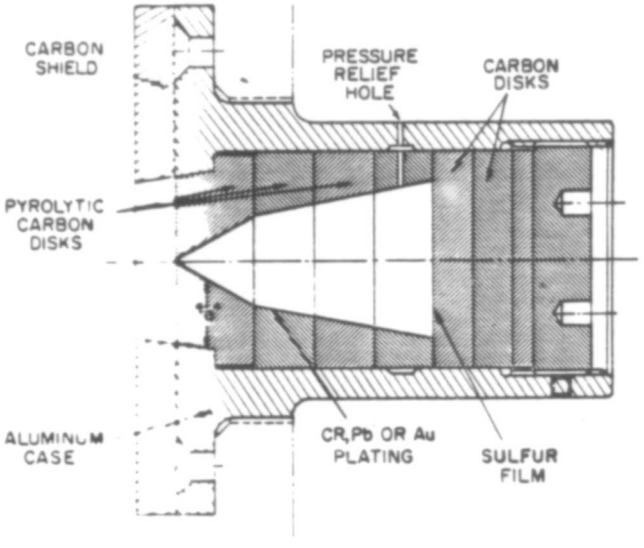

Figure 2.20 Plated hole gage.

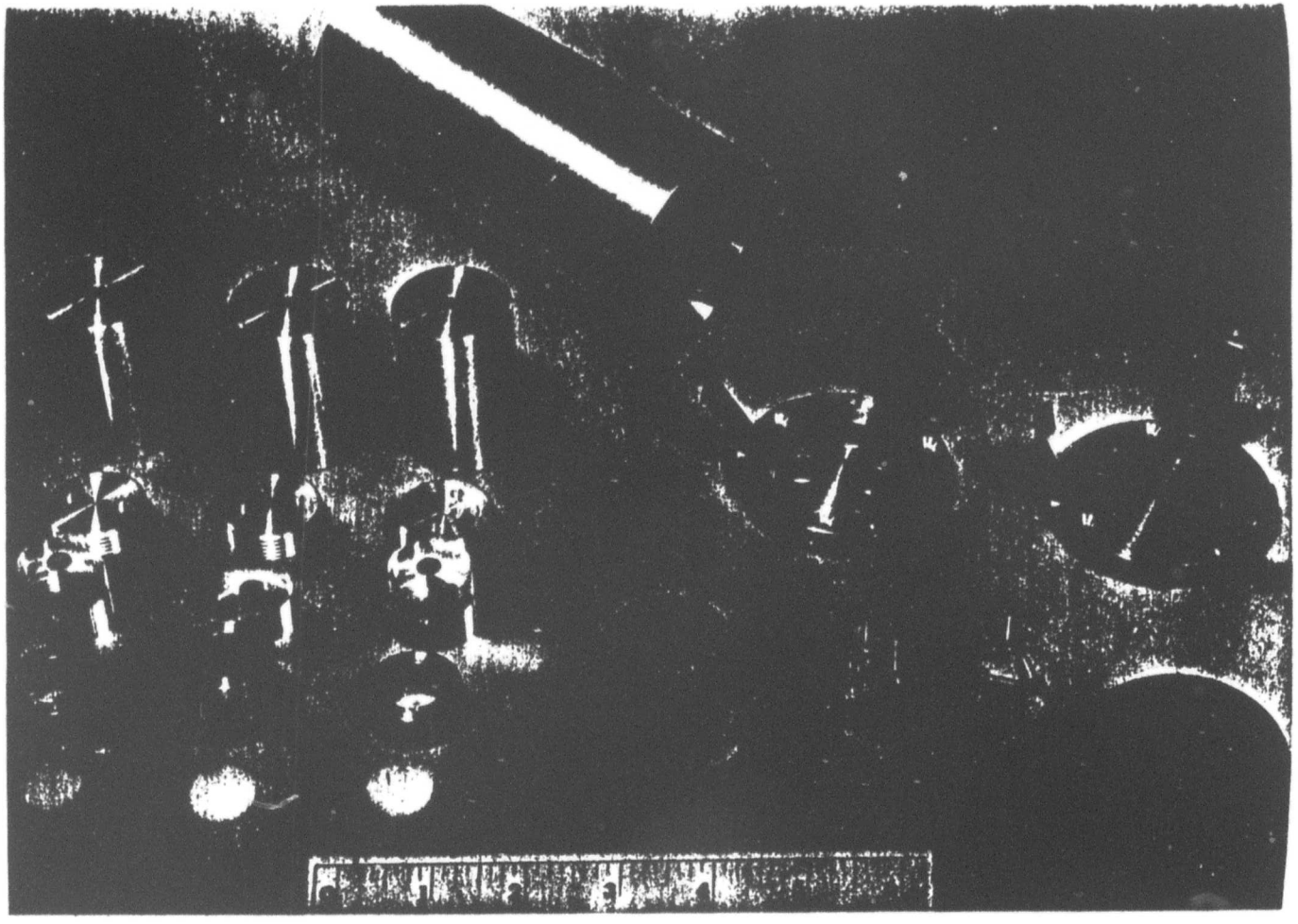

Figure 2.21 (Marshmallow) fracture gage assembly and holder. (ARA photo)

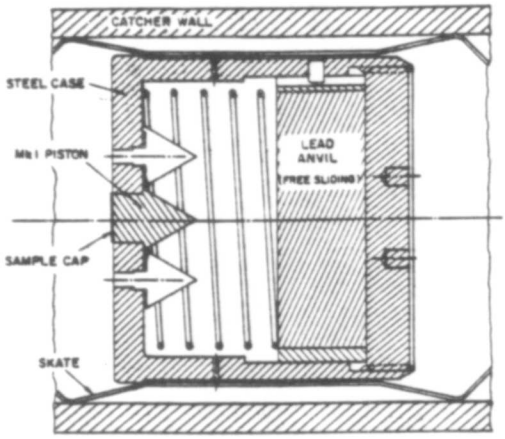

Figure 2.22 Mk 1 indenter.

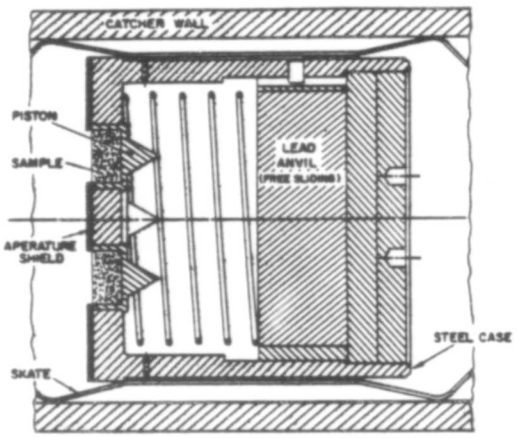

Figure 2.23 Mk 2 indenter.

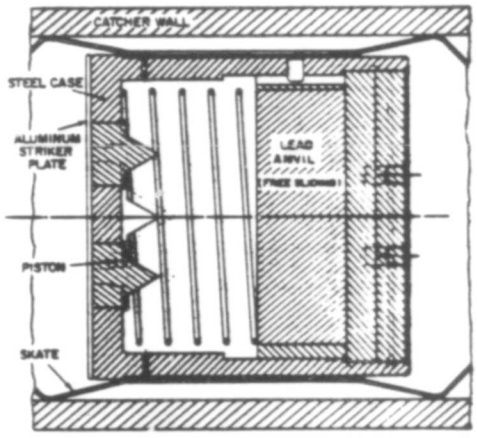

Figure 2.24 Mk 3 indenter

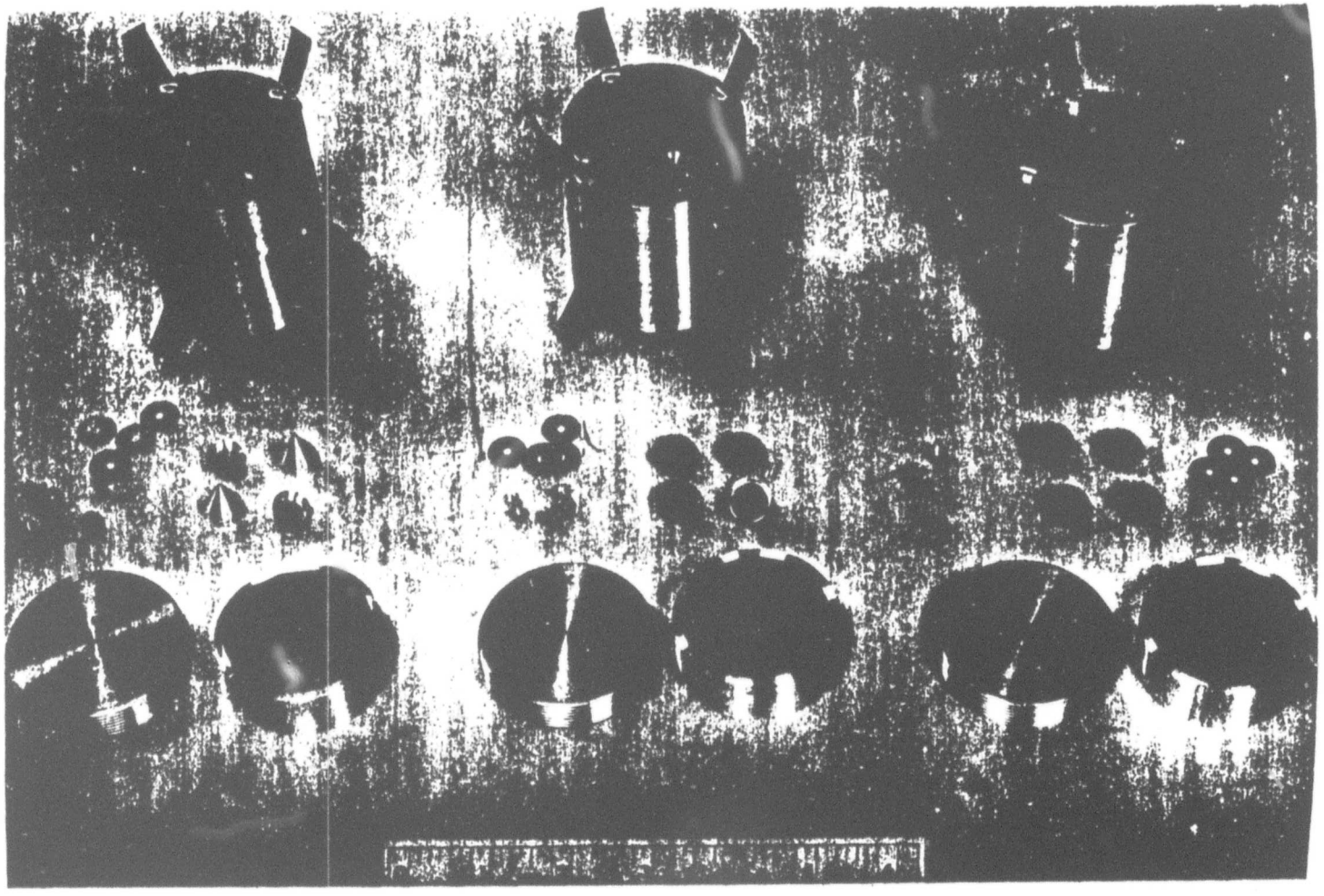

Figure 2.25 Mk 1, Mk 2, and Mk 3 indenter gages. (ARA photo)

CHAPTER 3

RESULTS AND DISCUSSION

The three instrumented pods from Star Fish Prime were recovered and returned to Johnston Island by H+9 hours. D-day was 8 July 1962 and H-hour was 2300; detonation date and time in world (Zulu) time were 9 July, 090009. 0290 hours. All Project 8B instruments were intact. It was found that the radioactivity levels of the pods were low enough to permit removal of the instruments without resorting to remote handling. The highest radiation level at H+9 hours was 2000 mr/hr at the surface of the rear bulkhead of Pod S2.

X-ray effects were immediately obvious on the three Project 8B pods. However, on only two pods were the instruments exposed to the X-ray flux; the Pod S1 orientation was such that the contained instruments had been completely shadowed. Determination of the unexpectedly large misorientations of Pods S2 and S3 was possible to within a degree or better. All instruments were removed within four hours of return. Figure 3.1 shows S3 upon recovery; the other two pods appeared in similar condition.

By H+36 hours, all gages had been disassembled, rinsed carefully in fresh water, and sorted for subsequent inspection. Beginning on D+2, preliminary examination of each element was undertaken and reported in the Project 8B POIR. The considerably more extensive study of the instruments accomplished in the ensuing data reduction program at Allied Research lead to the results presented in this chapter.

3.1 FLIGHT CONDITIONS

3.1.1 Trajectory and Burst Data.

At the time of missile lift-off, it was reported that the gyro motor in Pod S1 had attained a speed of about 3600 rpm instead of the design speed of 5700 rpm. All indications are that this pod tumbled after separation. As far as is known the gyro motors in Pods S2 and S3 reached and maintained their intended speeds. Nevertheless, the gyros failed to limit the pods' precession.

The trajectories of missile and pods were close to those planned as were the ejection and burst sequences. Reentry, parachute deployment, and recovery events were satisfactory.

From tracking data, the burst position, positions of the pods, and their slant ranges to the burst have been determined accurately (Reference 16). These

data are presented in Table 3. 1 using the Bravo coordinate system. The Bravo reference system employs x and y distances along a plane tangent to earth at Point John on Johnston Island. The altitude, z coordinate, is the distance above the tangent plane.

Also in Table 3. 1 is presented a summary of various burst time data; Figure 3. 2 illustrates the pod-burst positions.

3.1.2 Pod Orientations.

Inspection of the Pods S2 and S3 revealed X-ray shadows cast by various projections. The image edges were exceedingly sharp, particularly in the case of shadows cast by metallic projections, thus permitting accurate measurements of the angle of incidence of the X-ray flux. In the case of Pod S1, it was apparent that its orientation was such that only the side and nose were illuminated, the instruments on the aft bulkhead being completely shadowed.

Two types of pod orientation measurements were made. A plane called the burst plane is formed by the longitudinal axis of the pod and the nuclear detonation (see Figure 3. 3). The angle measured in this plane between the longitudinal pod axis and the burst is the off-axis angle, θ. It is zero for a directly tail-on orientation and 180° for a nose-on orientation. This angle was determined by measuring the shadow length and the height of the object casting the shadow. On Pods S2 and S3 such items as the Thor attachment fittings and the Mark 3 indenter striker plates furnished good references for this measurement.

The other orientation angle of interest is the roll attitude of the pod. This is the angle, ϕ, measured in the plane of the instrument bulkhead between the burst plane and the YY pod axis, the latter being defined as passing through the pod umbilical fitting. Positive roll angles are defined as measured clockwise from the YY axis when looking at the instrument bulkhead. As before, the shadows produced by the cylindrical instruments protruding above the rear bulkhead were used to determine the roll angle.

The off-axis angle for S1 could not be accurately determined, because none of the protruding fittings were exposed. It is possible, however, to estimate a lower bound for the off-axis angle. Since no shadows or evidence of any X-ray impingement on rear bulkhead fittings was found, it was necessary to use the shadowing produced by the X-rays on the cylindrical portion of the pod as a basis for the roll measurement. Because these shadows were also sharp and distinct, an accurate measurement was possible. This angle and other measurements are presented in Table 3. 1.

3.2 SPECTRAL GAGES AND DATA

3.2.1 Introduction. There were three types of instruments in the SF' pods designed specifically to obtain information on the X-ray flux characteristics; the carbon calorimeter for measuring total energy, the plated hole for determining the spectral shape, and SRI's K-edge detector which also was to record spectral characteristics. Because of the misorientation of the pods, however, these instruments either failed to view the flux at all, or else failed to operate correctly. Fortunately, other experimental data and theoretical calculations are available which allow a reasonable estimate of the X-ray flux and radiating temperature to be made.

Reference 10 gives results of a two-dimensional, radiation-hydrodynamic code calculation of the weapon output.

Results of X-ray diagnostic experiments are reported in Reference 31. These data support the theoretical calculations within fairly broad limits, although indicating a slightly lower flux. While not required in this report, an estimate has been made of the flux and effective radiating temperature as seen by the pods. Since it is the author's judgment that the code calculations are probably an upper limit on the flux, has been chosen as the effective yield.

Using the effective yield of and the pod ranges from Table 3.1, one finds the free-field flux at the three pods to be:

S1

S2

S3

Placing objective limits on the accuracy of these numbers is not possible, but the problem has been considered, and the authors believe the effective yield is unlikely to be in error by more than ± 20%.

Although the diagnostic instruments failed, the X-ray flux produced effects which are a function of the total flux and its spectrum. These effects are melting of materials to various depths when the melted material is shielded by varying thicknesses of X-ray attenuators. In principle, a sufficient amount of such data would allow the flux and spectrum to be determined. In practice, this is usually not the case for several reasons. The spectrum is complicated, and there is usually insufficient nonredundant data to obtain much resolution in the unfolding. The basic data have errors which will appear as errors in the unfolded spectrum and, along with other problems, make it difficult to show that the spectrum is unique. The melt or heating effects may be insensitive to parts of the spectrum, e.g., the high- and low-

energy tails. There are uncertainties in the thermodynamic properties of the materials and in their response under very short heating pulses; also, the presence of X-ray-induced shock waves can conceivably affect the results.

All of the above problems were present in the analysis of the pod melt data and have made it impossible to make a useful unfolding of the spectrum. The data are consistent with the total flux values given. At the time the analysis was made, the effect of the iron in the weapon case was not realized and this was not taken into account. A reanalysis using this information would perhaps give more useful results. The following sections present all the melt data but do not go into its analysis. It is hoped that this will be done in a later report if more useful results can be obtained.

3.2.2 Raw Physical Data. The X-ray effects studied were the following: (1) melt depths produced in steel, (2) melt depths produced in aluminum, (3) variation of melt depth produced in aluminum as a function of a preceding filter thickness, and (4) variation of melt depth produced in steel as a function of a preceding filter thickness. Data in each of these categories were obtained from both Pods S2 and S3. It can be shown that item (2) and item (3) lead to redundant information; the resulting three types of data from the two pods yield six independent views of the X-ray flux.

The physical effects arose, it is interesting to note, because the pods were tilted, and would not have occurred had proper orientation been achieved. Also, the particular tilt angles involved ($\sim 42^{\circ}$) were fortunate in that from the standpoint of data reduction accuracy the tilts were optimal. Reference to Figures 3.4, 3.5, and 3.11 will illustrate how the effects were produced by the obliquely impinging X-rays. In Figure 3.4 (A) the X-rays are shown penetrating the edge of a striker plate attached to the Mk 3 indenter gage.

The distance traveled through the striker before reaching the steel case varied from zero at the case edge to some maximum distance determined by the strike thickness. At the outer edge of the steel case, unprotected by the striker, the flux was sufficiently intense to produce melting and vaporization. However, at some distance in from the edge the flux fell to an intensity which was just insufficient to produce any melting at all. This distance clearly was determined by the X-ray absorption characteristics of the striker and steel case, and the thermal parameters of the steel. The crescent-shaped region on the top surface of the case wherein surface melting occurred is clearly defined in Figure 3.4 (B). The remaining surface area was heated more or less but not melted. Since there were seven different striker materials, each case showed a crescent area of different dimensions. From Pod S2, five cases had crescents wide enough to permit study, whereas from the Pod S3 only three were deemed useful.

A similar situation, illustrated in Figure 3.5 (A), existed for the carbon-covered aluminum R/V gages. Here, instead of dealing with the crescent area around the outside of the case, the surface melting produced under the carbon shield around the center hole was studied. Just as with the crescents on the Mk 3 cases, the R/V case crescents are simply the region in which the X-ray flux, having traversed the carbon shield, was still of sufficient intensity to cause surface melting of the aluminum. Figure 3.5 (B) presents a photograph of a representative R/V gage face and shows the crescents clearly.

A third and somewhat less important situation in terms of data acquired resulted from X-ray impingment of the Mk 1 aluminum pistons, both solid and capped. These piston data merely supplemented those obtained from the S3 R/V gage crescents just discussed. From the two aluminum pistons it was possible to measure aluminum melt depth. Figure 3.11 shows the Mk 1 piston-case arrangement at the moment of X-ray exposure.

3. 2. 3 Data Extraction.

Mk 3 Case Crescents.

The single most valuable source of data was the Mk 3 steel case crescent. The measurement of interest was the width of the crescent, or more precisely, the width at which melting of the steel case ceased; in general, the two were virtually identical, the problem lying in identifying the exact positions. It is interesting to note that the width of the crescent is the same everywhere if measured parallel to the direction of the X-ray flux (see sketch). Consequently, it was possible to determine the crescent width anywhere on the crescent, although the position of least error clearly is found dead center. From the crescent width measurement, the corresponding striker distance penetrated by the flux can be calculated.

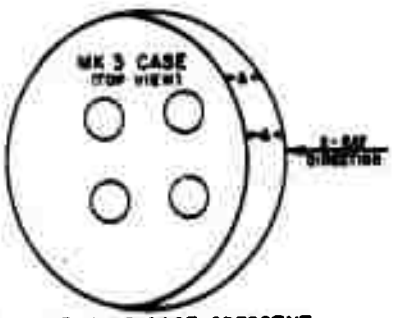

SKETCH OF MK 3 CASE CRESCENT

The technique used for determining the position where surface melting ceased was the following. A wedge-shaped section was cut from the case through the crescent (see sketch) such that one face of the wedge was parallel to the X-ray direction. Wherever possible, this face was cut near the widest part of the crescent, but in a few instances this was not possible because of bolt holes interfering. The side was then polished, etched, and examined under a high-power traveling-stage microscope. Because the wedge sections

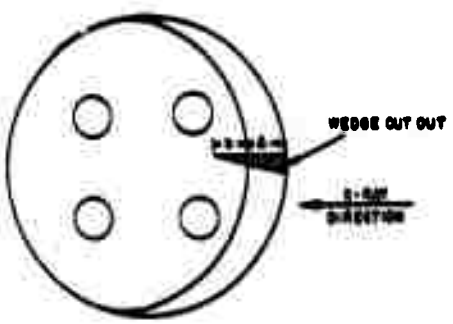

SKETCH OF CRESCENT SECTIONING

included a portion of the original and unablated surface (region "b" in the sketch), it was possible to plot a profile of the surface which showed how it had eroded in the crescent region ("Δ" in the sketch). The profile enabled one to determine the position where surface melting occurred, with good accuracy.

An interesting feature of most cases was the almost complete absence of a melt layer over the eroded area. The existence of tiny inclusions known as sulfide stringers throughout the unmelted region of the steel case, all finger shaped and oriented parallel to the gage axis, acted as tiny melt sensors, due to the fact that upon melting and resolidifying of the steel these stringers distort or disappear. Along the entire distance of the eroded surface line, these stringers usually extended right to the surface and ended abruptly, as though sliced through. Occasionally, a very thin melt layer remained on the surface (see Figure 3. 6 for example), but in general the melt layer was either completely or almost completely gone. Apparently, the sweeping action of the vapor trapped between the striker bottom, which did not melt, and the case was quite strong. As a result, identification of the position where surface melting ceased was possible from a simple plot of the surface profile. When determining the location of zero surface melting, it was necessary to shave and repolish each section several times and average the profiles in order to minimize the effect of random surface irregularities.

The profiles obtained from the five S2 cases examined are shown in Figure 3. 7, the three from Pod S3 in Figure 3. 8. Table 3.2 presents the data of interest.

Although there were several different striker materials from which crescent erosion data were obtained, in principle the data were all redundant. This is because over the photon energies which influenced the crescent width, primarily above 5 kev, the slopes of the X-ray absorption coefficients from the different strikers are virtually identical, and there are no absorption edges. At least, within the uncertainties and errors associated with this whole technique, the slopes deviate so slightly over this range as to be essentially identical. As a result, the difference in crescent widths is not because different regions of the spectrum were affected differently by the absorption characteristics of the strikers, but rather, the crescent widths reflected only the variation in striker densities.

There is an implicit assumption in the foregoing remarks, and that is that the energy below roughly 5 kev transmitted through the striker at the inner crescent edge is small compared to the rest. The assumption is undoubtedly very good, simply because of the very high absorption coefficients at low energies.

Considering the striker-crescent data of Table 3.2 again, these can be used to estimate some of the experimental errors inherent in this technique. A best estimate of the value

$$\left(\frac{\mu}{\rho}\right)_s \; h_s$$

where $\left(\frac{\mu}{\rho}\right)_s$ = X-ray absorption coefficient of a given striker material at a given wavelength, cm^2/gm

h_s = mass distance through which the X-rays penetrated a striker to the maximum crescent width, gm/cm^2

can be obtained by averaging values for the several strikers studied and then noting the deviations from the average value. In theory all the values of $\left(\frac{\mu}{\rho}\right)_s h_s$ should be identical. Choosing 7 kev as a representative wavelength, the following table tabulates the pertinent quantities for the two pods (the graphs of $\left(\frac{\mu}{\rho}\right)$ can be found in Appendix D):

The deviation of the measured value of $(\frac{\mu}{\rho})_s h_s$ from the average S2 value is at most only 12-1/2 percent, easily attributable to experimental errors. The maximum deviation of the S3 values is comparable, 14 percent. There were obviously higher experimental errors associated with the S3 data compared to those of the S2 data, and in addition, there were less data with which to work. It was possible to justify using crescent data from only three S3 cases—those with the C-124, Be, CH_2 strikers—for the reason that the crescents on the carbon and CNP covered cases were too narrow. The errors in width due to a slight misalignment of striker and case edges, or to a slight beveling of the striker edge, or just ordinary measuring errors were deemed potentially too large to permit inclusion of the data from these two cases.

To summarize, there are now two pieces of non-redundant data which could be used to help describe the X-ray spectrum. One piece of the data consists of five observations from the S2 striker-steel case system. The other independent bit of data consists of three observations from the S3 striker-steel case system. For the purpose of calculation, a representative striker can be picked from each group as having the average characteristics.

Steel Melt Depths.

The erosion profiles of Figure 3.7 through the Mk 3 case crescents can be used to extract two additional pieces of independent, non-redundant data. These are the melt depths in unshielded steel in both pods. From the erosion profiles a number of values can be determined by estimating where the extrapolated profile would intersect the edge. An average melt value is then calculated. This procedure is necessary because the profiles become highly uncertain very close to the edge, in addition to which the exact edge position is somewhat uncertain. It should be remarked that the profiles are, as best as can be determined, actually the boundaries between the solid steel and the X-ray-melted regions. When in the course of measuring the profile position a residual layer of melt was encountered, it was quite obvious, and the boundary position was easily ascertained.

Table 3.3 presents the estimates of profile-edge intersections for the five profiles available from Pod S2. These are averaged and the result is converted into a slant penetration distance h_m (because of the oblique incidence angle of the X-ray flux). Also in Table 3.3 are similar estimates for the three profiles from Pod S3. These data are much more uncertain than

those from S2 for several reasons. Errors due to edge position estimation, profile extrapolation, or striker edge alignment have a larger influence on the S3 result. Also, rather than five profiles to average there are but three. The two steel melt depths determined are the following:

R/V Case Crescents and Melting.

The third source of independent data on the X-ray spectrum is determined from the response of aluminum when struck by the flux, both filtered and unfiltered. It is too involved explaining in words the categories in which the various data to be presented fall, as well as the applicable redundancies; hence, the following outline is offered:

Independent Data Piece (1) Al Response in Pod S2
- (a) Al preceded by carbon filter
- (b) Al melt depths from,
  1. solid Al piston
  2. capped Al piston
  3. R/V case profiles

} redundant

Independent Data Piece (2) Al Response in Pod S3
- (a) Al preceded by carbon filter
- (b) Al melt depths from,
  1. R/V case profiles
  2. upper bound data

} redundant

The aluminum data are not redundant with the steel data, because aluminum has no K-edge in the energy region where most of the flux is present as does iron. This means that the phase change positions in aluminum have a different sensitivity to the spectral shape than those in the steel. Also it is interesting to note that the melt depth data for aluminum give a view of the spectrum redundant with that of the carbon filter-Al detector system, unlike the analogous sets of steel data. This characteristic results from the fact that neither aluminum nor carbon have an absorption edge above 5 kev, and the slopes of the absorption curves are essentially identical in the region of flux, whereas none of the strikers have absorption edges above 5 kev but iron does, at 7.1 kev.

With these introductory remarks, consider now the data acquired. Using the techniques described earlier, one S2 and two S3 aluminum R/V cases were sectioned through the center of their melted crescent-shaped regions (see sketch). After polishing and etching, profiles of the surface were obtained

SKETCH OF
R/V GAGE SECTIONING

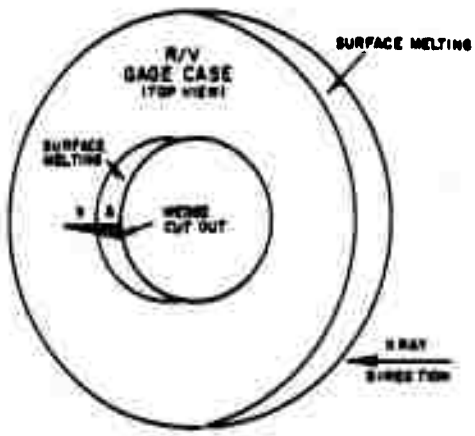

and are displayed in Figure 3.9. A curious feature of the surface in the eroded region, Δ, was the nearly complete absence of melt, which had been swept out from between the carbon shield and the case by the explosive force of the trapped blowoff vapors (see Figure 3.10). Recognition of re-solidified melt was not difficult; sectioned resolidified material over the lip of the inside hole was clear. Consequently, it is certain that the profiles of Figure 3.9 represent the melt-solid boundary.

Table 3.4 presents the crescent width of each sectioned case and the corresponding maximum distance of carbon shield penetrated by the X-rays. Again, the visible crescent width corresponds almost exactly to the surface melting width.

The depth of melt measurements were made in several ways which will be described briefly.

Pod S2. The erosion of two solid aluminum pistons was measured. At a point near the edge of the unshadowed portion of the piston surface, the blowoff pressures swept away the melt layer toward the shadowed regions (where the pressure was zero), and thus the erosion depth measured at this part of the surface approximated the true melt depth, although in reality it was somewhat less. A second measurement came from the Al piston which was capped by an Al disk 0.003 ± 0.0002 inch thick. The piston under the cap had melted (the glue was so thin and transparent to X-rays as to be unimportant), and the total melt depth was taken to be the cap thickness plus the erosion depth of the piston face. Finally, two erosion depth

measurements were obtained from the sectioned R/V case mentioned earlier. The edge of the inside hole viewed the X-rays directly, and the erosion profile under this carbon was reasonably linear so that the profile-case edge intersection could be estimated easily. The depth of this intersection is converted to the slant penetration distance, h_m, which is the true melt depth.

Pod S3. The erosion profile-case intersection could be estimated for the two cases sectioned. With appropriate conversions this data yields the Pod S3 aluminum melt depths. An upper bound estimate of the melt depth was made also. The upper limit comes from the fact that the aluminum Mk 1 piston face under the 0.003-inch Al cap did not melt.

The depth of melt data are presented in Table 3.5, and an average value is calculated for each pod. The two melt depths are:

As emphasized previously, the melt depth data and the R/V crescent width data are redundant. That this is in fact true can be verified quickly by checking the quantity $(\frac{\mu}{\rho})_{Al}\, h_m$ against $(\frac{\mu}{\rho})_{carbon}\, h_c$. The two quantities should be equal at a given range, to within experimental errors; at 7 kev it is found that:

	Pod S2	Pod S3
$(\frac{\mu}{\rho})_{Al}\, h_m$		
$(\frac{\mu}{\rho})_{carbon}\, h_c$		

3.3 IMPULSE GAGE AND DATA

Perhaps the most important class of data extracted from the SF' X-ray experiment was the measurement of the blowoff-induced impulse for a variety

of materials. Despite the loss of about half the SF' impulse data because of the inversion of one pod and the misorientation of the remaining two, a substantial amount of data of good accuracy has been obtained.

The results to be presented in the succeeding sections are introduced according to the gage type from which they are obtained. With regard to the Mk 1 and 2 indenters, it is necessary to discuss first a method which evaluates each indent (data point) such that its validity or spuriousness can be determined. A certain number of otherwise seemingly valid data points are shown to be spurious. The impulse results are then presented. The results from the Mk 3 indenters do not require this preliminary evaluation.

It will be shown that the following number of pistons or samples gave valid data:

	Pod S2	Pod S3
Mk 1	15 out of 16 pistons	1 out of 16 pistons
Mk 2	4 out of 16 pistons	1 out of 16 pistons
Mk 3	7 out of 7 samples	7 our of 7 samples

3.3.1 Mk 1 and 2 Indenter Results.

Data Validity Study.

An analysis of all the Mark 1 and 2 pistons was made by the Biophysics Division at AFSWC to determine the radioactivity level of each piston. By orienting each piston properly it was possible to obtain a count rate from the exposed face, the tip, and two side-on positions. The purpose of this effort was primarily to decide which pistons fired because of X-ray blowoff and which pistons fired at some later time from an entirely unrelated force. The technique developed acts as a kind of filter whereby the genuine data stand out clearly, and bad or uncertain data, often ostensibly

valid, appear as invalid. The reasoning behind this analysis plus the criteria set up to categorize the data are presented below.

It was found from photographic data (Reference 18) that the expansion rate of the weapon debris, that is the vaporized fission and case materials, was approximately 1.6×10^8 cm/sec. At Pods S2 and S3, then, the debris arrived about 8 and 14 milliseconds after the burst, whereas the X-rays arrived considerably earlier, .04 and .07 millisecond. The distance of travel for the piston to impact the anvil was about a centimeter, so that for even the slowest moving of the pistons known definitely to have fired (about 250 cm/sec), the time of travel was only 4 milliseconds. The conclusion to be drawn is obvious: a piston which fired because of X-ray-induced blowoff would no longer have its face exposed to the outside environment by the time of debris arrival; an X-ray-fired piston would be within the indenter gage, at least partially protected and obscured by the gage front.

It is clear then that a piston not fired will be hit by the weapon debris on its exposed front face, whereas a fired piston will suffer a considerably diffused coating of debris which impinges all over rather than primarily on the face. Hence, by determining the radiation level of a particular piston and its distribution, a decision should be possible about its having fired. As will be evident shortly this study was in fact highly successful in evaluating the validity of the indent data from the Mark 1 and 2 indenters.

Mark 1 Data.

The radioactivity rates found by the Biophysics Division at AFSWC for each piston are presented in Tables 3.6 and 3.7 (Reference 19). Looking at the Mark 1 count rate data first, it is noted that the pistons can be separated into two clear-cut groups: (1) pistons with count rates below 10,000 cpm in

all four positions, and (2) pistons with front face count rates above 20,000 cpm, the other three positions yielding lower count rates than the face. On the basis of the earlier discussion it is obvious that pistons falling into the first category fired before the debris arrived, that is, by the X-ray blowoff, and that the second category pistons did not fire prior to debris arrival. There is one exception, however. Mark 1 pistons whose cap came off are indeterminate. In every case where the cap was off, the count rate was low. That the caps probably came off after the debris had arrived is implied by two pistons in Pod S3, Case 033 Piston 3 and Case 018 Piston 4. These two pistons when retrieved were found unfired. Also, their caps were off. Yet the count rates on their faces were quite low, the conclusion being that the caps came off after debris impingement.

The criteria applied to the Mark 1 data can be summarized by the following table.

MARK 1 CRITERIA

Count Rate on Face	Cap	Fired by X-rays?
High (>20,000 cpm)	On	No
	Off	Not applicable
Low (< 10,000 cpm)	On	Yes
	Off	?

The validity of the Mark 1 data has been analyzed in Tables 3.8 and 3.9, which contain the following information: whether a particular piston was found in a fired condition, if an indent was made, if the cap was on or off, if the count rate on the face was high or low and the corresponding deduction as to its having fired, and what the final conclusion about the piston is. Consulting Table 3.9 listing the Pod S3 pistons, it is noted that there was but one piston (arrow) which one can say definitely fired before the debris arrived. Interestingly, there were several pistons, notably Case 035, that ostensibly had fired and indented but which this count rate analysis showed to be spurious since they fired after debris impingement.

Although four fired pistons cannot be evaluated with certainty (question marks in table) only two of them resulted in indents, so that of the sixteen Mark 1 pistons in this Pod S3 only two give data which cannot be appraised. In view of the several spurious indents mentioned in Case 035, however, it would be best to discard these two indents.

A point worth noting is that in these data, as well as in all the Mark 1 and 2 data, there was a situation which might have arisen, produced a serious inconsistency, and thrown some doubt on the entire technique: Namely, a deduced firing (cap on, low count rate) whereas the piston was actually found in an unfired condition. Fortunately, neither this nor any other inconsistency occurred.

Turning to the Pod S2 Mark 1 data, Table 3.8 it is seen that the count rate was low for every piston face. Although some pistons are technically uncertain because of missing caps, it is believed justifiable from the consistency of the remaining data to conclude that all the pistons were fired by the blowoff impulse. There is no evidence to suggest that any may have fired later, such as was true in Pod S3, and furthermore, there is a count rate characteristic which tends to support the above assumption. This is that the uncapped pistons had side orientation count rates similar to those which remained capped, not significantly higher as generally is true when the debris engulfs an unfired piston (refer to Table 3. 11 for example).

There is no ready explanation for the lack of indent from Piston 2, Case 006. The count rate gives no unequivocal answer. Perhaps the piston cocked and jammed; this could happen if one of the two restraining springs had accidently been installed double thickness.

To summarize the evaluation of the Mark 1 indenter data by means of the count rate criteria, of the six indents observed in Pod S3 only one can be considered valid with any certainty. The remaining indents are either clearly spurious (three) or indeterminable (two) and rejected. It appears likely that all the indents made in Pod S2 were the result of the blowoff impulse, half being definitely attributable to blowoff, the other half being uncertain but with good argument in favor of this conclusion.

Mark 2 Data.

The Mark 2 count rates determined for four areas on each piston are presented in Tables 3.10 and 3.11. Unlike the Mark 1 data, the count rates on the faces do not fall into just two clearly defined and separated categories but rather into three, where the new category is intermediate to the two extremes. The definitions are almost as clear cut as before, but the conclusions are not quite as certain as to the meaning of the count rate now; nevertheless, screening of the data still results in vastly improved evaluation of a given indent's validity.

While the new grouping of the count rates introduces some uncertainty into the technique, the fact that the Mark 2 pistons remained intact, no caps to be lost, removes an even more important source of ambiguity in the results.

Careful consideration of the count-rate data on the piston face led to the following three groups: (1) below 3,000 cpm, (2) 10,000 through 18,000 cpm, and (3) 24,000 cpm and greater. The explanation for the low and high count-rate collections is straightforward. The pistons fired by the X-ray blowoff received no direct debris impingement on the face and, hence, display a low count rate. Correspondingly, the unfired pistons were struck face-on by the debris, and their faces are comparatively highly radioactive (as well as their sides, the debris apparently penetrating the small gap between the piston and the hole wall). On the other hand, the reason for the intermediate radioactivity is somewhat obscure. An attractive but otherwise speculative explanation is that these pistons cocked, jammed in their hole, and were, in effect, moving so slowly that they were not free of their holes by the time of the debris arrival. Although not being entirely out of the way, nevertheless, they were partially shielded from the debris and thus were coated to some intermediate degree. Since a number of Mark 2 pistons did indeed hit the anvil side-on rather than point-on, and this behavior can be attributed to cocking, the foregoing explanation gains some support. However, the meaning of the data in this intermediate category remains somewhat uncertain, and, in fact, if the supposition of cocking is correct, the data is clearly of little value because an unknown fraction of the impulse energy or momentum was lost in the jamming action.

The criteria applied to the Mark 2 data are presented in the following table:

MARK 2 CRITERIA

Count Rate	Fired by X-ray?
High (>24,000 cpm)	No
Intermediate (10,000 < cpm < 24,000)	?
Low (< 3,000 cpm)	Yes

The evaluation of the Mark 2 indent data is presented in Tables 3.12 and 3.13. The setup of the tables is similar to the Mark 1 tables and shows whether a given piston made an indent, if it was found in a fired condition, into what category the count rate fell, and if it indicated the piston had fired, and what the final conclusion about the piston is.

Reviewing first the Pod S3 data, it is seen that although only two pistons were recovered in an unfired condition, and of the others seven had indented, only two pistons were concluded definitely to have fired. Interestingly, these particular two pistons were both Devcon samples. Looking ahead for a moment, of the two Devcons in the middle pod (see Table 3.12), one fired and the other probably fired, but is uncertain. The rather astonishing conclusion is that Devcon, which covered the Teak instrument pod in Operation Hardtack in 1958 for the express purpose of protecting the pod against the X-ray blowoff impulse, was an exceedingly poor choice. Of all the Mark 2 or Mark 1 materials it has been shown that only Devcon and tin definitely generated a sufficient blowoff pulse to fire the piston under the low flux conditions of the far pod.

To continue with the Pod S3 comments, another interesting point is evident. Of the three pistons for which the firing is uncertain, only one made a measurable indent. Similarly, of the two Devcon pistons which definitely fired, one made no indent, and the other made such a small indent that the firing threshold energy was just barely exceeded, the threshold impulse for this piston being Consequently, there was but one definitely valid indent and only one possible indent rejected because of firing uncertainty.

Considering the Pod S2 Mark 2 data, every piston was recovered in a fired condition. However, of the sixteen pistons, the count rate criteria show definitely that three did not fire and eight did fire as a result of the X-rays, the remaining five pistons being uncertain because the count rate fell into the intermediate group. Three of the five uncertain pistons had not indented and the fourth had struck side-on, making it valueless. The potential loss of data by discarding the one remaining indent value is not large.

There are four pistons (arrowed in Table 3.12) which fired prior to debris arrival and apparently produced indents. Four others fired legitimately but either hit side-on indicating that cocking and jamming occurred, or in one case did not indent at all. It is unfortunate also that there was no duplication between any two of the valid indented samples.

Summarising the Mark 2 count-rate analysis of the fourteen apparently fired pistons initially considered in Pod S3, it was found that only one indent was clearly valid. There were six other indents, but they were either spurious (five) or uncertain (one). The evaluation of the Pod S2 pistons brought out that half fired because of the blowoff impulse, but only half of these, four, produced measurable indents.

Mark 1 Impulses.

The elimination of spurious indent data by the foregoing count-rate analysis provides high confidence in the validity of the remaining data presented here and in the following section.

The raw indent data, pertinent parameters, and corrected impulses are presented for the nonspurious Mk 1 indents from Pods S2 and S3 in Tables 3.14 and 3.15. Indents which were shown definitely to be invalid have not been treated. Although a number of S2 indents cannot be verified without question by the count-rate evaluation, the argument given in the preceding section for their validity has been accepted and the data consequently have been reduced. As a result, all the pistons except three in the S2 gages yielded impulse data, whereas all of the pistons except one in Pod S3 failed to yield impulse data.

It can be shown that the interpretation and reduction of the data is not complicated by whether the piston was found with its sample cap on or off; it is necessary only to use the proper piston mass. The explanation is the following. If the cap remained on, as it did in a few instances, the blowoff energy and momentum are completely contained within the piston and cap

system. That situation is, in a sense, ideal, and the momentum is theoretically all accounted for in the movement of the piston. When the cap came off, on the other hand, the sequence of events must be examined a little more closely. The cap and piston dimensions were such that the compressive pulse generated by the X-ray blowoff was entirely within the piston by the time that the leading edge of the pulse, having been reflected from the tip, returned to the cap-piston interface. This returning pulse was, of course, a tension wave and as such was responsible for the separation of the cap from the piston when the tension exceeded the tensile strength of the glue bond. No other boundary tension existed prior to the first return of this pulse. Thus, in instances where the caps came off, it is probable that they separated after only one traversal of the piston by the blowoff pulse, the caps simply falling out of the gage (the piston, gage, and pod fell away, to be precise). Support of this analysis comes from the fact that none of the caps were found inside the gages. The glue bond should have broken almost immediately upon incidence of the leading edge of the tension wave, thus resulting in containment of virtually all the momentum and energy of the pulse within the piston proper. However, even in the event that the pulse should have succeeded in re-entering the cap appreciably, the cap thicknesses and acoustic properties were such that at any given time only a small fraction of the momentum could have been within it. Consequently, whether the cap remained attached or not, it is certain that the initial blowoff energy or momentum was essentially all contained within the piston. The losses due to breaking glue bonds or to trapping of momentum within the cap are believed small. In reducing the data it is necessary only to adjust the piston mass by the loss of the cap mass.

It will be noted in Table 3.14 that the indent data from the two aluminum-capped pistons has not been reduced even though the count-rate analysis showed the indents to be due to the X-ray impulse. The defect involved was fortunately unique to these two pistons. Discarding this data was necessitated by the fact that the Al caps were not separated from the pistons in the manner just described, but rather because they were literally blown off. Unintentionally, the caps had been made too thin, 0.003 inch, so that the X-ray flux transmitted through the caps was still of sufficient intensity to produce melting of the piston faces. Certainly, there was then generated enough vapor pressure, either from the aluminum face or, more important, from the glue, to pop off the cap. Two uncertainties are thereby injected into the analysis. First, an unknown and possibly appreciable impulse was given to the piston

from the cap mass and its velocity because of this internal blowoff, and, second, the moment of cap separation is now unknown; the blowoff pulse generated in the front of the cap may or may not have been transferred to the piston.

Therefore, the S2 data from the Al-capped pistons have been discarded. It is interesting to observe that the indents (and thus the impulses) of these pistons are considerably larger than their solid Al, uncapped counterparts. This discrepancy apparently confirms the questionable validity of the data.

Why the S2 copper-capped piston failed to indent is not known. It has been suggested that two restraining springs were accidentally assembled, thus causing the piston to cock, jam in its hole, and expend its kinetic energy working down the hole.

In determining the face area exposed to the X-ray flux (see Figure 3.11) an unavoidable uncertainty in the value exists for two reasons. First, it was not possible to determine the exposed area for each piston individually, because the exposure boundary was too uncertain, generally; melt slopped or splashed over into the unexposed portion. It turned out that it was possible to measure the exposed area for only two pistons on each pod with any degree of accuracy. The exposed areas were virtually identical for both pods, 52%. Thus, it was necessary to apply the exposed area measured and averaged from only two pistons to the data from all the other pistons. But since there were variations in the surface height of the pistons because of the various cap thicknesses, as well as variations in shank lengths and seating of the pistons in their holes (the piston could sit over to one side since there was .006-inch clearance), the shadowing of the piston faces by the carbon shield varied from piston to piston. Consequently, the true exposed area varied from piston to piston and was not necessarily the 52% value used in the calculations. A second source of uncertainty lies in determining the exposed area itself on the pistons actually examined. Even for these selected pistons, there was some uncertainty in the boundary position for various reasons. Consequently, the figure of 52% exposure must have an associated error attached to it. A reasonable estimate is believed to be $\pm$ 8%.

Although the upper edge of the carbon shield shadowed the Mk 1 piston caps (see Figure 3.11) there was a certain thickness of carbon through which the X-rays could traverse and still be of sufficient intensity to melt the cap. Hence, one would expect a crescent-shaped region on the cap surface, adjacent to the fully exposed area, in which melting occurred, but to a progressively diminished degree as one travels away from the exposed

region. Also, the relative widths of this shadowed crescent should depend on the X-ray and thermal characteristics of the cap material, in general being in proportion to the effect observed in the exposed region. Another interesting point is that the shadowed crescent should be quite small on the caps from the far pod. Observation showed that all this was clearly the case. The partially melted crescent region is clearly visible in the photographs of Figure 3.12, where an S2 zinc cap and Al solid piston are shown. The three regions discussed are illustrated for two metals having contrasting responses to the X-ray flux; the zinc is rather easily melted, the aluminum is not. The flow of melted material is, as would be expected, toward the shadowed region; a high pressure gradient existed between the two regions.

As a result of the partial exposure, one component direction of the resultant impulse on the piston was such as to produce a torque about the center of mass. (Had the entire cap surface been exposed as planned, regardless of the X-ray flux angle, the impulsive force would have been parallel to the piston axis, and no torques would have arisen.) Consequently, the pistons attempted to rotate or cock in their holes as they moved forward. It is difficult to estimate the energy or momentum losses involved with this process, but it is felt that several factors combined in the Mk 1 design to minimize its importance. The most influential factor was the optimal piston length to diameter ratio which precluded severe cocking angles during the initial movement and afforded time for the constraint of the hole to straighten out the piston direction. This factor was missing in the Mk 2 piston design, to be discussed shortly, as evidenced by the almost complete loss of data there, even from Pod S2. In evaluating the Mk 1 data, then, it is necessary to keep in mind the uncertainty introduced by the cocking and scuffing losses. However, the remarkable indent agreement between identical Mk 1 samples, for Pod S2, as well as the excellent agreement of the Mk 1 Al impulses with the Mk 3 Al impulses tend to confirm that the data are meaningful.

The impact tilts shown in the tables were determined from the character of the anvil indents and indicate a slight cocking of the piston in flight. The tilt values are not excessive and are not a problem in applying the anvil calibration. Appendixes B and C discuss the anvil indent calibrations and the analysis of tilted indents. The correction for the energy absorbed by the restraining springs is developed and graphically displayed in Appendix C.

With these calibrations and corrections, the quantities in Tables 3.14 and 3.15 are self-explanatory.

The single seemingly valid impulse value extracted from the S3 gages, for tin, is highly uncertain. The impulse delivered was so close to the minimum permitting firing that almost all the initial kinetic energy of the piston went into deflecting the restraining springs (note the difference between KE_r and KE_o, the final and initial energies, respectively). The twin of this Sn-capped piston failed to fire; apparently, it did not experience even the minimum impulse. Therefore, it is believed that this S3 tin impulse value should be considered as very approximate.

Mark 2 Impulses.

The exposed samples in the Mk 2 gages were non-metallic R/V or plastic materials which, in general, were appreciably more transparent to the X-rays than the metals capping the Mk 1 pistons. For this reason, as discussed in Section 2.3.1, the Mk 2 piston design was unlike that of the Mk 1 piston, the exposed sample being a cylindrical plug glued into the recessed metal piston shell. Although embodying highly desirable features, the specific design parameters used, in conjunction with various ramifications of the ped mis-orientation, resulted in such an erratic firing pattern that even the indents validated by the count-rate analysis become suspect. The reasons for and the uncertainties associated with this Mk3 data will be developed in the following text. First, however, the available data will be presented.

It was concluded from the count-rate analysis that of the S3 gage indents only one was attributable to X-ray blowoff, and that of the five indents found in the S2 gages four were clearly X-ray induced while one was uncertain. The data are presented in Tables 3.16 and 3.17 including the one questionable indent from the S2 Avcoite sample. The tables are virtually self-explanatory; the same corrections and calibrations applied to the Mk 1 data are applied here and have been treated in detail in Appendixes B and C.

The interpretation of the Mk 2 data is not complicated by samples or cap loss, as was true for some Mk 1 data. The blowoff energy and momentum delivered to the Mk 2 pistons was completely trapped. If sample loss or front surface spalling had occurred, then an analysis of the possible momentum change would again have been required. No spalling or sample loss was observed from any of the pistons.

Determining the exposed sample areas was considerably simplified by the fact that all the samples ablated cleanly, that is, there was not a melt

layer splashed over into the unexposed area and obscuring the boundary (Figure 3.13). On all samples the area exposed was clear cut, the materials apparently went directly from solid to gaseous blowoff products. The areas exposed to the X-rays were different for the two pods because of the aperture shields used. The value varied little from piston to piston in Pod S2, and a representative value of .50 cm^2 was used in the calculations.

A crescent-shaped region bridging the exposed to the unexposed areas was again evident on all samples wherein the X-rays traversed a portion of the carbon shield prior to hitting the sample (refer to Figure 3.11, which illustrates this point for the Mk 2 samples even though picturing a Mk 1 sample). The uncertainty in the effective blowoff area is thus present again, but generally, this transition region is estimated to affect the representative area measurement by less than $\pm$ 10%.

Ostensibly at least, the data reduced for the Mk 2 pistons seem thus far to be trustworthy; the count-rate tests were passed, spall or sample separation did not occur, and the various measurements, parameters, and corrections could be applied straightforwardly to determine the impulse values. Yet, there are several disquieting aspects to the data which result in some question about their accuracy.

In particular, it is apparent that cocking and jamming of the pistons in their holes was an acute problem with the Mk 2 design. All pistons that had fired were examined, and in every case polished scuff marks on the shank were found and are considered evidence of jamming. The marks were invariably found most clearly on one side of the shank up near the front surface and on the other side of the shank down near the start of the tip. It is concluded that what had happened was the following. The unequal blowoff pattern produced a torque on the piston about its center of mass so that it cocked until restrained by two points of contact with the hole, the front edge and the bottom of the shank. At the same time the piston was moving forward, hence the polishing and scuffing of the piston at the two points of contact. As the piston progressed, it also ricocheted back and forth. It is speculated that the Mk 2 shank length to diameter ratio was so low that the bore could not effectively dampen the side to side movement. In addition, a protective coating had been applied to the magnesium pistons which was comparatively rough and may well have contributed to any seizing.

Confirming the foregoing evidence is the fact that of the eight S2 pistons known to have fired from the X-ray impulse (see Table 3.12) one did not indent at all, three hit the anvil side-on, and of the four which indented,

three had large impact tilts, 18° to 30°. Of the two valid S3 firings, one piston impacted at 30° and the other not at all. This evidence suggests strongly that severe cocking and jamming was common to all the Mk 2 pistons and that the energy lost thereby was appreciable for certain pistons.

It is not possible to evaluate these data in terms of impulse self-consistency between identical samples, since no duplicate indents were obtained. Nor are there any cross checks with other data sources, as was possible between the aluminum Mk 1 and Mk 3 samples.

The conclusion is the following. It is a certainty that cocking of the Mk 2 pistons occurred and momentum and energy were thereby lost. The error introduced into the impulse data is unknown, but may be substantial. The impulse values, therefore, should be considered as lower bounds.

Mark 1 and 2 Uncertainties and Errors.

A summary of the relevant errors and uncertainties affecting the impulse values of the Mk 1 and 2 indenter gages is given in this section. Wherever possible a quantitative estimate of the uncertainty is made.

Indent Size. Any error in measuring the size of the anvil indent becomes a magnified error in the impulse value, inasmuch as the impulse varies as the three halves power of the indent diameter. The probable impulse error diminishes with increasing impulse values from as much as about ± 30% at the very lowest (S3) impulse to perhaps ± 5 percent at the highest. The error inherent in the calibration curve itself is probably very small, less than a few percent at all energy values.

Restraining Springs. The uncertainties associated with correcting for the effect of the piston restraining springs have been treated in Appendix C. For all S2 Mk 1 and 2 impulse data, the uncertainty arising from variations in the spring constants and other parameters is less than a few percent. The uncertainty associated with the S3 pod data (only one data point for each type of gage) is on the order of 50%.

Piston Weights. These are known extremely accurately and contribute essentially no uncertainty to the impulse values. Only for those Mk 1 pistons whose caps came off is there some mass uncertainty involved. It has been estimated as no more than ± 3%.

Blowoff Areas. For the Mk 1 and 2 pistons alike, errors in the exposed area value used in the data reduction are reflected directly into impulse errors. The several components contributing to this one uncertainty are the following: (a) deviations from the representative area value which

was used for all pistons from a given gage type, (b) measuring errors in the representative area considered, and (c) the unknown degree of contribution to the total impulse from the partially screened region. The overall uncertainty of this error source is estimated at less than ± 15%.

Mk 1 Energy Loss. For those pistons losing their caps, the energy loss through trapping of some energy and momentum in the cap can be assessed. In the ideal case, the piston separates from the cap, which remains stationary, and moves off with virtually all the momentum. The worst possible case would occur if the piston separated slightly but the cap moved along with it at the same average velocity. There, through total momentum conservation, it is clear that the momentum of the piston is reduced by the amount carried by the pursuing cap. The momentum ratio of cap to piston is just the mass ratio; since these caps to piston mass ratios are at most 6%, then this figure represents the maximum impulse uncertainty for this effect.

Cocking Losses. Attaching an error value on the data from cocking and jamming effects is not possible. As indicated in the foregoing discussions, it appears that the Mk 2 impulse data were subject to severe cocking effects and should be considered lower bound, whereas the Mk 1 data may have been affected nominally.

An estimate of the total error associated with the impulse data can be made with the above individual error sources, but excepting cocking losses:

S2 Total Error.	± 20%	(Mk 1 and 2 Data)
S3 Total Error.	± 60%	(Mk 1 and 2 Data)

A cocking correction would shift the impulse data to higher values.

3.3.2 Mark 3 Indenter Results.

Data Validity.

The Mark 3 indenter system has been discussed in detail in Section 2.3.1. The principal departure of this gage from the Mk 1 and 2 devices is that the blowoff impulse is measured indirectly and depends on the transmission of momentum from the exposed material (the striker) to the piston which then traps this momentum. Advantages and disadvantages alike result from this design. An advantage which becomes obvious immediately upon presentation of the data is that the Mk 3 design was such that its

function was not impaired by the pod misorientation, as were the Mk 1 and 2 gages. The impulse data from not only the S2 gages but the S3 gages as well are consistent and, as will be shown, valid. This fortunate situation arose from two sources; first, the Mk 3 design exposed one large striker disk to the X-rays, not small individual piston faces, so that the entire striker was unshadowed by surrounding objects, despite the pod tilt. Thus, the blowoff pulse traveling through the striker was generated equally across the entire front surface and was a plane parallel wave when it entered the pistons, so that no torques were introduced. Second, the momentum enhancement phenomenon meant that the momentum delivered to the piston was, except for the Be and Al strikers, larger than that generated in the striker. These factors resulted in proper operation of the devices in both pods simply because the pistons experienced fairly large impulses normal to their front faces (for those strikers generating impulses above the firing minimum).

It is not possible to make an evaluation of the indent data validity for the Mk 3 gages similar to that presented for the Mk 1 and 2 gages. That analysis depended upon measuring the radioactivity of the exposed pistons; here, however, the pistons were completely shielded by the strikers which intercepted the weapon debris. Nevertheless, it is possible to argue convincingly that the Mk 3 impulse data is valid for the reasons outlined below:

No Prefiring. It is obvious when a piston fired prior to the X-ray burst. The X-rays penetrate the striker and image the projected piston hole on the lead anvil by either lightly melting the anvil surface or by vaporizing the surface oil film. One S3 pod piston did, in fact, prefire, and the projected hole was clearly imaged on the anvil. It is certain that none of the other pistons prefired since no other images were found. The transmitted X-ray flux would have been sufficient through any other striker to produce a similar image.

Certification Test Implications. The results of Tiger Fish, wherein no burst occurred, showed that firing of the pistons during reentry accelerations would be marginal. It should be mentioned that the restraining springs of the Mk 3 gages were reduced in tension subsequently such that Mk 1 Tigerfish results are more appropriate here. Had any pistons not been fired by the X-ray impulse, the conclusion is that they might have barely fired during reentry. This indicator is indeterminate.

Control Piston Results. The control piston, one in each Mk 3 gage, was shortened so that the blowoff pulse could not be transmitted to it

through the striker. However, the pulse could be felt by the control piston much attenuated after it had traversed the steel gage wall and entered the piston via the small flange pressed against the inside gage face (see Figure 2.13). Hence, the control piston could be fired by the X-ray impulse, but with a much reduced velocity compared to the test pistons. Now the criterion by which one can evaluate the indent validity is the following. If spurious post-burst impulses or decelerations fired the pistons in a given gage, then all the indents, including the control, should be the same. If the control indent is smaller than the test indents, then the test data is probably valid. In all gages the control piston either did not fire or produced an indent smaller than the test indents.

The general conclusion is then that the Mk 3 indenters fired from X-ray-induced impulses except for one that clearly prefired. The data are valid with a high degree of certainty.

Data Presentation.

The X-ray-induced blowoff impulses for the various Mk 3 striker materials are displayed in Tables 3.18 and 3.19 for Pods S2 and S3, respectively. These impulses, it should be remembered, are from an X-ray flux incident on the strikers at an angle about 42° off normal. No attempt has been made to adjust the data to normal incidence values.

The calibration curve by which the piston kinetic energy is obtained from the indent diameters is discussed and presented in Appendix B. Also, the restraining spring correction used to determine initial kinetic energy, KE_o, is treated in Appendix C. Enhancement factors and related parameters are presented in Table 3.20 with the sources indicated for the various values.

Certain features of the impulse data are of interest. The theory that the control pistons were not fired during reentry or water impact but by the weakly transmitted X-ray impulse gains additional support by the way in which the S2 control indents increase in size with increasing impulse. The low-impulse striker, carbon, failed even to fire the control while the highest impulse (unadjusted) material, polyethylene, produced the largest control indent. The S3 controls failed either to fire or to indent, the transmitted impulses evidently being too small in all cases. Had reentry or water impact decelerations been responsible for the firing of any pistons, the pattern of firing and indent values in Tables 3.18 and 3.19 simply would not have been explainable.

Of note also is the fact that wherever the impulse was sufficient to fire more than one test piston, above a few hundred taps, the values are very close. Deviation from a mean or average impulse value is generally less than five or six percent. In the case of the S3 C-124 gage there was some inconsistency. It appears, however, that in this instance the two weakly indenting pistons probably cocked and jammed in their holes. The high-impact tilts imply that conclusion, and as a result those two data points are discarded. The one large diameter, low-tilt indent, is believed correct. The one low-indent value found on the S3 polyethylene anvil is undoubtedly attributable also to cocking, and it too has been discarded.

The S2 carbon striker apparently produced one indent. However, because of the large-impact tilt and the misalignment of the indent with the hole axis, it is clear that the true impulse value is highly uncertain. The carbon evidently did succeed in barely generating the minimum firing energy as evidenced

by the fact that the other two test pistons fired. This minimum value is very uncertain, but on the order of the corresponding minimum firing impulse is (a tap is 1 dyne-sec/cm^2). Hence, the impulse for carbon is very crudely determined to be about this value. Similarly the S2 beryllium impulse is very uncertain but somewhere between the minimum firing value of and the indent value of

We do not know that the S3 carbon and beryllium impulses were zero, only that they were below the minimum firing impulses. Also, the values for the S3 CNP and the carbon paint lie between the values shown and the minimum firing value, since in each instance one of the pistons remained unfired.

The results of Table 3.19 show that the

Steel Case Perturbation.

A problem arose which was of some concern during the data reduction program. For various reasons, the Mk 3 case material was steel, whereas aluminum should have been used so that the striker-case interface would have been the same as the striker-piston interface. The steel case, during the traversal of the blowoff pulse across the interface, moved a smaller distance than the aluminum piston, thus generating a shear wave in the striker at the circumference of the piston. The effect of the shear wave on the momentum delivered to the piston was unknown and feared appreciable. It will be shown now, however, that except for the beryllium and aluminum strikers the upper bound error introduced into the impulse values by the shear wave was very small.

A shear wave disturbance travels from the periphery toward the center of the piston face, principally in the striker. The area A'(t) traversed at any given moment is:

$$A'(t) = \pi v_r t \left[2r_o - v_r t\right]$$

where: v_r = shear wave velocity

SKETCH SHOWING SHEAR PROPAGATION

At the same time, a compressive wave is passing through the whole piston-striker interface, normal to the piston face. Or at any instant, the area in which the compressive pulse is not interfered with by the shear wave is:

$$A(t) = \pi(r_o - v_r t)^2$$

It appears that the worst case, or the maximum effect the shear wave could have on the net momentum transmission going on across the boundary, would be to reduce it to zero in the region already reached by the shear wave. Putting a net negative momentum or particle movement into the piston is impossible under the circumstances of a non-bonded interface, because the tensile stress necessary to produce a negative momentum cannot be sustained under these conditions.

Hence, the worst case is that when the shear wave reaches a given radial position, the net transfer of momentum across that position drops to zero. After a time, τ, the compressive wave traveling into the piston is over, and the shear wave does not effect the particle movement in the piston. That is, after time, τ, the stress across the boundary ahead of the shear front is zero.

It appears, then, that the effect of the shear wave on the piston momentum exists only during the traversal time of the compressive wave, and at most, cuts off momentum transferral in the area it has passed over. We can calculate the momentum that can be passed across the striker-piston interface; assume the compressive pulse to be square wave in character, that is, the peak pressure is constant for a time, τ :

$$dM = A(t) \cdot P_o \, dt$$

where:

A_o = total piston face area

$A(t)$ = piston area not traversed by the shear wave at any time

dM = the total momentum transmitted by the compressive wave into the piston in a time interval dt across the area $A(t)$

P_o = peak pressure of compressive pulse—assumed constant for a time $o \rightarrow \tau$

then:

$$M = P_o \int_o^{\tau} A(t)\, dt$$

$$M = \pi P_o \int_o^{\tau} (r_o^2 - 2r_o v_r t + v_r^2 t^2)\, dt$$

$$M = A_o P_o \tau \left\{ 1 - \frac{v_r \tau}{r_o} + \frac{1}{3}\left(\frac{v_r \tau}{r_o}\right)^2 \right\}$$

The bracketed term is the fraction of the theoretical maximum momentum which can cross the interface under the worst-case conditions assumed.

Consider the magnitude of this term for the various strikers, assuming a compressive pulse length of 30 shakes, which is a reasonable value:

$$\tau = 3 \times 10^{-7} \text{ sec}$$

$$r_o = .71 \text{ cm}$$

Mat'l	Shear Vel.	$M/P_o \tau A_o$ Lower Limit	Maximum Impulse Error
	cm/sec		percent
C	1.3×10^5 [b]	.95	5
Be	9.0×10^5 [a]	.67	33
Al	3.0×10^5 [a]	.87	13
CNP	1.3×10^5 [b]	.95	5
C-124	1.5×10^5 [b]	.94	6
AV-2	1.6×10^5 [b]	.93	7
CH_2	0.5×10^5 [a]	.98	2

[a] Reference 20

[b] 60% of sound velocity

Thus, the reduction in true impulse due to this shear wave interaction is small except for beryllium and aluminum. It should be stressed, however, that these error values are upper limits; transfer of momentum across the area reached by the shear wave may well have occurred to some extent, and the assumption of a square pulse rather than a more realistic shape such as a triangular pulse increases the amount of momentum which can be effected by the shear wave.

Mark 3 Errors and Uncertainties.

A summary of the uncertainties and errors associated with the Mk 3 data is given below. The steel case error discussed separately in the previous section is systematic, that is, it results always in a net impulse loss.

Indent Size. Indent-measuring errors translate into impulse errors through the three-halves power of the indent size. Thus, the impulse value is somewhat sensitive to this error. It is estimated that for indent diameters above about 1 mm the impulse uncertainty is less than $\pm$ 6%; the remaining impulse data in Tables 3.18 and 3.19 from indents around .35 mm have errors estimated at 25%.

Restraining Springs. The uncertainties arising from variations in the spring parameters are discussed in Appendix C. This error is insignificant, less than a few percent, for all impulses, except for several that were close to the minimum firing impulse, that is, indent diameters close to .3 mm. For those very low values, the uncertainty is on the order of 50%.

External Impulses. The effect of disturbances or impulses originating outside the indenter gage on the momentum transfer process occurring at the striker-piston interface have been studied. It can be shown that except for the polyethylene striker gage, any external impulse such as that generated by the carbon shield will not be felt by the piston while it is still in contact with the striker. This error source in any event is considered to be negligible.

Calculated Enhancement Factors. For those gages where the momentum enhancement was calculated from acoustic data, error is introduced by uncertainties in the values taken for (a) acoustic impedance of aluminum, (b) sound velocity of striker material, and (c) density of striker material. Assuming an uncertainty in the value of aluminum's acoustic impedance of $\pm$ 10%, the largest corresponding uncertainty in any of the enhancement factors would be $\pm$ 5%. Also, although the effective sound velocity of some of the materials may be highly uncertain, it has little effect in general on the enhancement factor calculated. This error results in less than a $\pm$ 5% error in the enhancement factor. The density error can be neglected,as it is inconsequential.

AFSWC Enhancement Factors. The enhancement factors supplied by AFSWC are the result of PUFF Code calculations with experimentally determined equation-of-state data and are inherently more applicable to the high-stress conditions of the Mk 3 gages. It is estimated that the values determined for these materials, CNP, C-124, Avcoat-2, are accurate to within $\pm$ 5%.

Cocking Losses. Again,the energy losses resulting from pistons cocking or scuffing along their holes is unknown. However, except for certain gages where only one piston fired, it is possible to sort out the jammed pistons. For the remaining indents, cocking is believed to have involved negligible losses. The momentum delivery to the pistons did not encourage cocking, unlike the Mk 1 and 2 gage situation. Wherever comparison between two or more pistons in the same gage was possible, it was obvious which piston had acted anomalously; also, impact tilts give an indication of cocking.

An estimate of the total error associated with the impulse data can be made from the foregoing component errors and the systematic shear wave error.

Striker	Total Errors	
	Pod S2 percent	Pod S3 percent
Graphite	± 57	NA
Beryllium	+ 65 - 57	NA
Aluminum	+ 16 - 10	--
Carbon Paint	--	± 57
CNP	+ 10 - 8	± 57
C-124	+ 10 - 8	+ 10 - 8
CH_2	± 9	± 9

To these total errors, however, must be added the unknown cocking losses. This effect is undoubtedly most important for the low-impulse pistons which are already characterized by high uncertainties. Correction of the data for cocking would tend to increase the impulse values.

3.4 MATERIAL ABLATION DATA

It has been possible to determine for seventeen materials the total ablation which resulted from X-ray exposure and relatively free blowoff conditions. Ablation, as used in connection with the study discussed in this section, refers to the material irretrievably lost from the surface of a sample due only to blowoff, not to spall. It appears certain, however, that none of the samples treated here spalled from the front surface. Just what the precise mechanism was that produced the ablation for a given material, whether it was sublimation, melt and vaporization, or whatever, has not been investigated. Clearly it was not the same for all materials. In certain materials, for example Teflon, no visual evidence of melt exists, suggesting that sublimation was the ablating mechanism. On the other hand, aluminum displayed a lumpy surface characteristic of a melted layer which resolidified; presumably, only the vaporized front surface and perhaps a fraction of the melt layer escaped. Although varying from material to material, the mechanism by which each responded to the X-ray pulse was, it can be assumed,

characteristic of the material itself and would recur under similar conditions. Therein lies the value of the ablation data to be presented.

The ablation data were obtained from three sources; (1) the striker plates of the Mk 3 indenter gages, (2) the R/V gage samples, and (3) the samples used in the Mk 2 indenter pistons. A number of materials were represented in two of the three categories, thus giving not only additional data on some samples but also permitting a crude cross check on the uncertainties associated with the categories themselves. Despite the differences in size and exposed area, the responses of the three sample types to X-ray exposure were essentially the same. Most important was the fact that the outward expansion of blowoff vapors was relatively free, the samples being unenclosed. It is true, however, that the striker plate arrangement was in a sense more ideal. The sample area was considerably larger than either the R/V or Mk 2 areas. Yet it is believed that the area differences have resulted in only a small effect, if any, on the ablation, since a study of the data has not revealed any systematic differences attributable to area differences. The variations in ablation found in the samples which were in both the R/V gage and the Mk 2 piston, for example, seem to be attributable only to experimental errors; no consistent bias is discernible.

The techniques for determining the ablation losses were essentially the same for all three data sources. The samples had been weighed prior to the shot to one ten-thousandth of a gram using a Mettler balance (except for the Be strikers which were too heavy). At least a month after the shot, the samples were weighed again on a similar balance. The weight difference clearly represented the mass ablated, subject to one correction to be described below. A second, and mass-independent measurement of the ablation, was accomplished by directly measuring the linear difference between the original surface and the remaining surface, since some of the original surface remained on the R/V and Mk 2 samples, or by measuring the initial and final striker sample thicknesses with a micrometer and thus determining the thickness ablated.

As mentioned above, one correction to the weight data was found necessary. It was discovered upon return to the mainland that the S1 samples had apparently gained weight. The S1 samples, it will be remembered, had not viewed the burst and so had not lost mass. The fact that they all gained weight seemed primarily due to water absorption. Known low-absorbing materials such as aluminum and teflon, for instance, gained least. Consequently, the correction to the ablation data consisted of adding to the raw weight loss

data the weight gained by the corresponding sample in the S1 pod. This procedure assumes that the water absorbed and the weight gained by an S2 and S3 sample was about the same as its S1 counterpart, and that the change in surface character by X-ray exposure had a small effect on the absorptivity. Admittedly, this correction is rather approximate; nevertheless, in principle it is correct and, as a study of the data quickly revealed, it invariably made the weight ablation data more self-consistent as well as more consistent with the linear ablation data. The fact that the absolute moisture content of a given sample may have varied from pre-shot to post-shot weighings does not introduce any error into the procedure, since the S1, S2, and S3 samples were all weighed at the same time after having had long times, at least a month, in identical environments to stabilize. The difference in moisture content from pre- to post-shot weighings is implicitly accounted for by the S1 sample weight change.

The weight gain of the S1 samples is given in Table 3.21. These values change with time and the environment of the samples and thus are not particularly important in themselves, only as corrections. The post-shot striker and R/V sample weighings were made in August 1962, and the Mk 2 weighings were done in March 1963.

The ablation data will now be presented and discussed by sample type.

R/V Samples.

Pages 107 & 108 deleted.

Striker Plates.

The striker plates covering the Mk 3 indenter gages offered large exposed areas to the X-rays. Unlike the samples already discussed, the strikers were all completely unshadowed so that no original surface remained with which to compare the ablated surface. However, in anticipation of this ablation analysis, the strikers, whose surfaces were highly parallel, were carefully measured for thickness beforehand. Then, the thicknesses were measured subsequent to recovery and the linear erosion determined straightforwardly. Also, the strikers were carefully weighed before and after the burst, where possible, in order to obtain weight loss data.

The ablation data calculated from both weight loss and linear loss measurements are presented in Table 3.25. It is unfortunate that the beryllium strikers were too heavy for the precision balances available in the field. As a consequence, no weight loss data are available. However, as noted in the table, no linear loss could be detected micrometrically to the accuracy of the measuring device, $\pm$ .0013 cm.

The corrections applied to the raw weight loss figures were, as before, simply the weight gain of the Pod S1 counterpart strikers. Only polyethylene was not represented on Pod S1, and so a correction could not be applied. Therefore, the values in the "Weight Loss" and "Linear Loss" columns are low for CH_2. One would suspect, however, that the correction would have a small effect on these values for two reasons; polyethylene is non-moisture-absorbing, and the mass ablated, at least in Pod S2, was high, thus minimizing the influence of the correction. With regard to the remaining strikers, the correction produced less than a 20% change in the raw data except for the graphite, where the net loss was so close to zero that other experimental errors overwhelm the significance of the very small loss value. In general, then, the importance of the correction on the striker ablation data is not great.

Comparison of data derived from weight losses with that linearly measured is possible for a limited number of samples. Good agreement is evident in general; although an apparent discrepancy exists for carbon paint, it is possible that it can be accounted for by the uncertainty in the density value of 1.5 gm/cm^2 assumed in order to calculate the "Linear Loss" value.

A cross comparison of striker plate data with either R/V sample or Mk 2 sample data exists for only one material, C-124, which in addition to having been a striker plate was also included in the R/V gage. For both Pods S2 and

S3 it can be seen from Tables 3.22 and 3.25 that the ablation data are remarkably consistent for this sample. This provides some assurance that the difference in blowoff areas had only a small effect, if any, on the amount of unit area ablation.

Graphical Summary.

Errors and Uncertainties.

It would be specious to attempt a quantitative estimate of the errors associated with the ablation data already presented. Instead, the major sources of errors will be pointed out and the probable best data suggested.

Clearly, the fact that the weight losses are very small differences between two large numbers means that any small errors or spurious changes in the total weight values will reflect as large errors in the ablation data. This one characteristic of the mass loss determination technique introduces the largest error. The mass loss (corrected) varies from as low as about 1/3% of the total sample weight in Pod S3 to at most a few percent of the sample weight for the S2 striker samples. Hence, the ablation data sensitivity to errors in total weight measurements is obvious.

On the other hand, the linear measurements obtained by means of depth- or thickness-measuring gages are relatively free of the analogous problem of defining small distances on large thicknesses, at least for the Mk2 and R/V samples, because the total sample thickness was not involved in the measurement. The small difference problem does enter into the picture on the striker samples, but where measuring difficulty was encountered, it was due primarily to a different phenomenon, that of surface bubbling or melting wherein the irregularity and unevenness of the surface prevented estimating the effective surface level. Striker samples from which final thicknesses could be obtained generally ablated evenly, and the resulting surface was reasonably smooth.

Some of the error sources considered important in their potential influence on the ablation data are the following:

Weight Corrections. The corrections added to the raw mass loss data are, for the Mk 2 and R/V samples in particular, large sources of uncertainty. In a few extreme instances, for example, the correction is larger than the data value. Yet the validity of the correction itself is uncertain, since it is the result of factors which may not have affected all pods the same. Its application is rationalized by the fact that since all the S1 samples gained weight, some adjustment of the S2 and S3 data seems necessary, and the corrections, as uncertain as they may be, definitely make the S2 and S3 data more consistent in all respects.

Extraneous Weight Changes. Erratic, unsystematic weight additions or losses to the samples which then result, as above, in magnified errors in the mass loss data may have occurred. These could have resulted from the

handling after the pre-shot weighing as well as from the handling and washing prior to the post-shot weighing. Abrasion, chipping, salt accretion all could contribute randomly to the spurious weight change of the samples.

Dimensional Changes. Permanent changes in the thickness of the striker samples due to water absorption or the initial heat gradient after X-ray exposure could introduce a linear thickness measuring error. This phenomenon apparently is evident in the CNP striker, which is thicker after exposure than initially. This source of error is probably not important with respect to the R/V and Mk 2 samples because of the method of measurement employed.

Area Measurement Errors. The exposed area, or the area from which ablation occurred is not always known accurately. This error applies, of course, only to the mass loss data, but it does apply to all three sources of ablation data. The Mk2 sample area used in the computations was an average value from which the individual exposed areas may have deviated up to $\pm$ 8%, as an estimate. Also, for both the R/V and Mk 2 samples, there was a partially shadowed region in which the ablation varied from maximum to zero. This region for certain materials may have represented as much as 10% of the exposed area, and in this region the amount of blowoff is difficult to estimate. Even on the strikers, which were fully exposed, there was a small and unaccounted for area around the vertical edge of the striker facing the X-rays, which ablated to an unknown degree. In general, however, this mass loss is estimated to be small compared to the total mass lost from the top surface.

In view of the potentially large errors that could have affected the ablation data, the agreement of data from one source to another and the generally small deviation of data on a given material from an average value are remarkable. With regard to which measuring technique yielded the best results, i.e., results having the fewest errors and uncertainties associated with them, the answer is that for the strikers and Mk 2 samples it is a tossup. However, the direct linear measurements made on the R/V samples are probably more accurate than the weight loss data.

3.5 OTHER GAGES AND DATA

The remaining instruments or data will be treated only briefly in this section, because, except for the correlation gages, there either was no data obtainable, or else it is being reduced under a different contract.

3.5.1 Gages with No Useful Data.

K-Edge Gages. The off-axis misalignment of the pods, 42 degrees, greatly exceeded the acceptance angle of the K-edge instrument. Consequently, none of the incident radiation impinged on the detector stack, and no spectrum data could be obtained. The recovered filters and instrument parts were subjected to a visual examination for possible unpremeditated data relevant to the spectral study described in Section 3.2, but nothing of importance was found.

Fracture Gages. No data could be extracted from the gages in either pod. The X-ray angle prevented the flux from reaching the metal button.

Carbon Calorimeter. Because of the incidence angle, only a small fraction of the calorimetric disk was irradiated. Close inspection showed that, while some of the temperature crayons became sufficiently hot to flow in the S2 pod gages, apparently not even the minimum temperature of 150° F was reached by either calorimeter. None of the Pod S3 crayons either flowed or changed color. No meaningful data could be obtained from this instrument. Because of the highly complex thermal diffusion problem imposed by the flux-gage orientation and shadowing, not even a lower bound to the incident X-ray energy could be determined.

S2 Plated Hole Gages. With regard to the lead-plated and chrome-plated gages, there were no data. In the case of the lead, no pattern of removal of the lead from the carbon disk existed which might be attributable to the X-rays. In the first disk of the chrome-plated gage, most of the plating appeared to be gone. There was one small area remaining, but no significant relationship to the incident X-ray beam was apparent.

The gold-plated gage, however, showed an elliptical pattern of gold removal which was clearly the result of the X-ray deposition. Unfortunately, however, there was no way to interpret the meaning of the gold-no-gold boundary; contrary to expectations it did not necessarily correspond to the solid-vapor or solid-melt phase change interface, because the gold film was sufficiently thin to evaporate off at temperatures below vaporization. Hence no spectral data was extracted from this gage.

This spectral gage design was discarded after the SF' event for the above reason. Its successor, whose design was the result of the SF' experience, is described in Section 5.3.

S3 Plated Hole Gages. With regard to the chrome-plated gage, most of the chrome was gone on the first disk, generally from the area which was shadowed from the X-ray beam. Although the pattern of the remaining chrome plate was symmetric to the X-ray pattern on the front of the instrument, it was not consistent with what would be expected. A slight heating effect was visible on a small part of the second disk. which extended to about the depth one would expect from the angle of incidence. No useful data was obtained from this gage.

In the gold-plated gage an elongated elliptical area of plated gold was gone from the first disk Its orientation and length corresponded to what would be the expected illumination of the plated surface. The pattern extended to essentially the end of the front disk However, for the same reasons outlined before, no meaningful interpretation of the effect could be made.

3.5.2 R/V Gages. Of the two exposed sets of R/V samples tested, those in Pod S2 received the greatest amount of X-ray damage. In general, each sample of this set received severe surface burning with accompanying loss of surface material over approximately 70% of the sample surface, and mechanical damage in the form of layer delamination and failure of R/V composite material. Each of the seven different samples are discussed only briefly below because a thorough study was accomplished elsewhere (see Reference 23). Also, in Section 3.4 the mass loss data from these samples is presented.

Pod S2 Visual Descriptions.

page 115 deleted.

3.5.3 Metallurgy Gages. Surface melting effects indicated that approximately 40% of the samples' surface areas was exposed to the X-radiation. These gages will not be discussed further here inasmuch as they are currently being analyzed at Allied Research under DASA contract No. DA-49-146-XZ-168 and will be reported separately.

3.5.4 Correlation Gages. The three fracture gages and three indenters discussed in Section 2.3.3 were returned to Allied Research for analysis in September 1962. The purpose of these instruments was partly to provide additional effects data but, more important, to check for experimental consistency between the two different environments of SF' and Marshmallow. The data from the Marshmallow gages are reduced and reported in this section; comparison to SF' results is beyond the scope of this report.

Fracture Gage Data.

Careful visual and microscopic examination of the fracture gages showed no fractures or spalls whatsoever. Although there had been a slight misalignment of the gages as evidenced by the flowoff pattern found, still the major fraction of the button areas had been exposed and blew off. Two of the three zinc buttons were loose but intact inside the

gage housing; fragments of the third were found. From the small amount of material loss over the exposed area of the button it is possible that the flux level at this station was below that anticipated.

At some time during their residence in the tunnel, probably subsequent to the burst, the lucite cylinders reached their softening temperature, estimated near 100° C. The four O-rings isolating the cylinder from the housing left deep imprints in the lucite indicating a general long-term heating rather than a flash transient type of heat input.

Mark 1 Indenter.

No data could be extracted from this instrument. The entire assembly had been crushed and torn apart, the anvil being so distorted that it is unknown whether or not any indents were made.

Mark 2 Indenter.

This instrument functioned properly, and the impulse data obtained is presented in Table 3.26. There is no evidence of the pistons cocking in their holes; the impact tilts were small, and the impulse was delivered uniformly across the piston face. On the other hand, an unknown velocity increment may have been given the pistons from debris impact. The flight times to impact, during which the pistons were vulnerable to this mechanism, were between 1 and 2 milliseconds. This source of error in the impulse values is difficult to estimate but believed small. The amount of debris accretion on the piston faces is virtually unnoticeable.

Mark 3 Indenter Gage.

This instrument was returned intact and mechanically had functioned perfectly. However, a design error precludes a meaningful interpretation of the indent data. The aluminum striker plate was too thin; the result was that the striker-piston interface was heated appreciably, and inelastic deformation of the striker occurred. The machine marks on the piston face were imprinted on the striker, and corresponding to the gap between piston and hole wall, a ridge on the striker exists where it penetrated the gap inelastically. Under these conditions, the theory treating the wave propagation and momentum transfer becomes inapplicable; consequently, no data are reported for this gage.

Material Ablation.

The four Mk 2 samples were studied with the purpose of obtaining erosion data on those materials. A detailed explanation of various considerations and the procedures used for the analogous study of the SF' Mk 2 materials has been given in Section 3.4 and need not be repeated here. It is sufficient to remark that mass loss was determined for each piston by means of a highly sensitive Mettler balance (see "Weight Loss" column in Table 3.27). In addition, a direct measurement of the linear surface recession was possible since there was a ring of material left unexposed to the X-rays (the aperture effect) which gave the position of the original surface. A height-measuring dial indicator gage simply measured the difference between the original and eroded surfaces (see "Measured Loss" column in Table 3.27). The linear recession has been calculated from the "Weight Loss" data (see the next to the last column in Table 3.27) so that a comparison of the data from the two measuring techniques can be made; comparison of the two final columns shows excellent agreement.

With regard to spallation, it seems certain that except for the pyrographite none of the samples spalled. The surfaces were examined rather carefully, and they had only the characteristic stippled appearance that X-ray exposure seems to produce in many such materials. The as in Star Fish, was eroded more deeply in the resinous area. The plug, however, did come out of the shank slightly, and now the original surface protrudes about 1/32 inch. It is doubtful that it was originally glued in this position, although there is that possibility. A more likely explanation is that because of the low impedance of the compared to the Al piston, the piston shell and plug attempted to go in opposite directions, and did in fact succeed in separating slightly before the relevant force fell below the retarding frictional forces.

The carbon had delaminated such that the dislodged piece was not of even thickness, but rather wedge shaped as sketched. However, not much

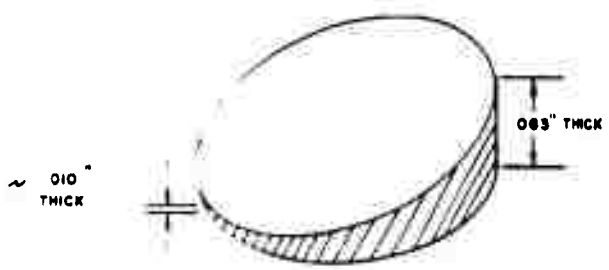

SKETCH OF PYROGRAPHITE PIECE

importance should be attached to this spalled piece. The pyrographite stock from which this sample came could be pried apart easily by fingernail if the right spot was found. With this type of behavior, estimating spall tensions is rather difficult.

TABLE 3.1 SUMMARY OF BURST AND TRAJECTORY DATA, SF[1]

Burst Date.....	9 July world (Zulu) time (8 July Local time)	Ref. 17
Burst Time.....	090009.0290 world (Zulu) time	Ref. 17
Burst Height.....	400.2 km	Ref. 16
Total Yield.....	1.3 Mt	Ref. 10
Radiated Yield....		Ref. 10
X-Ray Conversion....		Ref. 10
Initial Debris Velocity.....	1.6×10^8 cm/sec	Ref. 18 Ref. 10
Debris Arrival at Pods.....	5.4 millisec (S1) 7.6 millisec (S2) 14.4 millisec (S3)	
Pod Ranges.....	8.74 km (S1) 12.25 km (S2) 23.40 km (S3)	Ref. 16 Ref. 16 Ref. 16

Position of Point John.....	16° 44' 03.30" north (Latitude) 169° 231' 41.48" west (Longitude)	
Burst Position (Bravo System).....	x = - 11.57 km (East is positive) y = - 31.30 km (North is positive) z = + 400.2 km (Vertical is positive)	Ref. 16

Pod Positional Differences from Burst (Bravo System) — Ref. 16

	S1	S2	S3
Δx	- .0595 km	+ .0582 km	+ .818 km
Δy	+ .471	+ .711	+ 1.078
Δz	-8.72	-12.25	- 23.4
Slant Range	8.74	12.25	23.4

Pod Orientation Angles

θ... Off axis tilt
ϕ... Roll angle

	S1	S2	S3
θ	$>135^\circ$	$43 \pm 1/2^\circ$	$41 \pm 1/2^\circ$
ϕ	$61 \pm 1^\circ$	$0 \pm 1/2^\circ$	$35.5 \pm 1^\circ$

[1] This is X-ray energy radiated into 4π steradians, the output was asymmetric and greater than this in the direction of the pods. See Section 3.2 for a discussion of this point.

TABLE 3. 2 CRESCENT WIDTHS AND CORRESPONDING STRIKER TRAVERSAL

Striker Material	Crescent Width, Δ	Striker Penetration, h_s

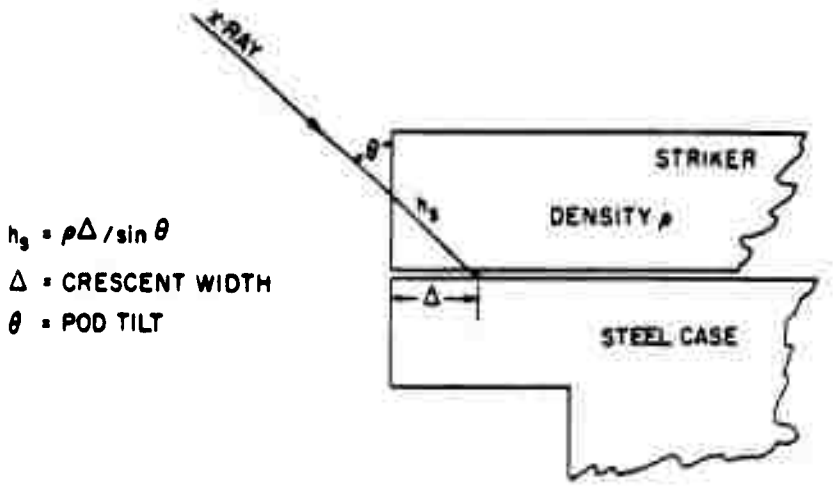

TABLE 3. 3 MELT DEPTHS IN STEEL

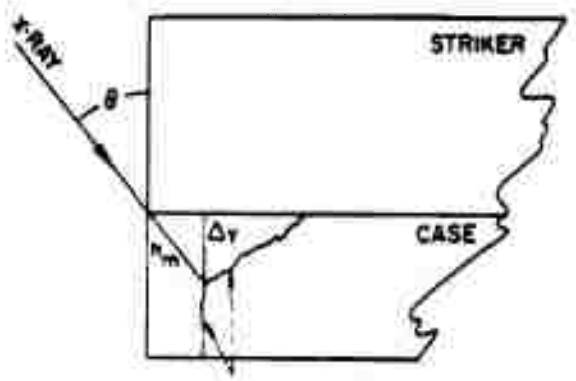

TABLE 3.4 CRESCENT WIDTHS AND CORRESPONDING CARBON SHIELD TRAVERSAL

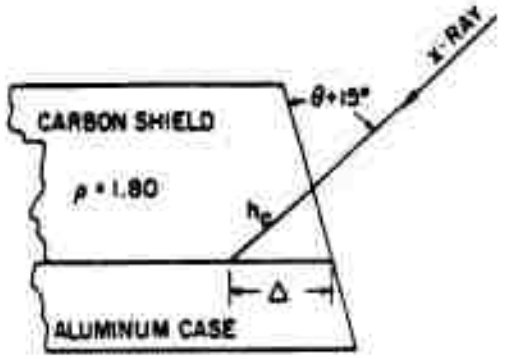

$$h_c = \frac{\rho \Delta \cos 15°}{\sin(\theta + 15°)}$$

Δ = CRESCENT WIDTH

θ = POD TILT

TABLE 3.5 MELT DEPTHS IN ALUMINUM

Data Source	Vertical Erosion, Δy	Slant Melt Depth, h_m
	cm	gm/cm^2
Pod S2, $\theta = 43^\circ$		
Solid MK1 Piston		
Case 030		
Case 021		
MK1 Piston + Cap		
Case 30		
Case 006		
R/V Case Profiles		
Case 016		
Case 016 Repolished		
Pod S3, $\theta = 41^\circ$		
R/V Case Profiles		
Case 049		
Case 050		
Capped MK1 Pistons		
Upper Bound		

Illustration of Terms

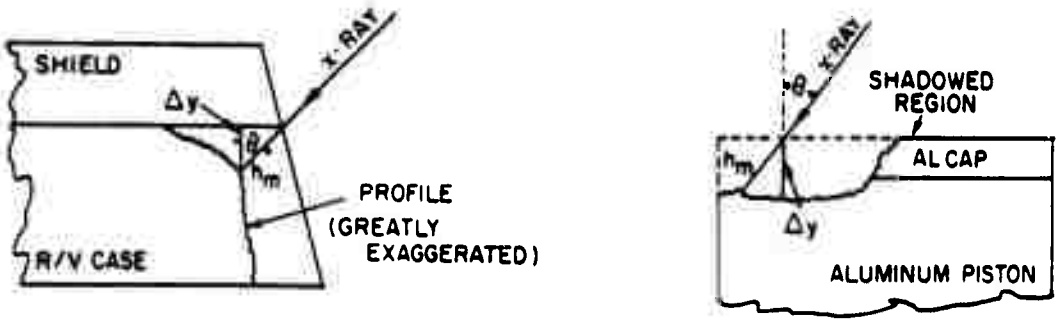

TABLE 3.6 COUNT RATES, POD S2, MK 1 INDENTERS

Gage	Sample	Position	CPMx10^3[a]	Gage	Sample	Position	CPMx10^3
016	1. Mg	F	0.7	021	1. Cu	F	0.6
		1	0.9			1	0.4
		2	0.9			2	0.5
		3	0.7			3	0.6
	2. Fe	F	7.9		2. Al (solid)	F	0.4
		1	1.1			1	1.1
		2	2.4			2	1.1
		3	1.1			3	1.0
	3. Sn	F	2.6		3. Zn	F	0.9
		1	3.1			1	0.4
		2	7.6			2	0.4
		3	2.0			3	0.5
	4. Au	F	0.8		4. Au	F	0.5
		1	0.4			1	0.3
		2	0.5			2	0.4
		3	0.6			3	0.4
030	1. Mg	F	1.9	006	1. Fe	F	5.3
		1	1.7			1	0.9
		2	2.3			2	1.4
		3	1.1			3	1.4
	2. Al (solid)	F	2.5		2. Cu	F	0.6
		1	1.1			1	2.3
		2	1.1			2	0.8
		3	0.8			3	0.7
	3. Al	F	1.4		3. Sn	F	3.8
		1	0.6			1	2.9
		2	0.4			2	1.5
		3	0.5			3	1.1
	4. Zn	F	1.4		4. Al	F	1.0
		1	0.8			1	1.0
		2	0.8			2	1.2
		3	0.7			3	1.4

[a]CPM means counts per minute.

TABLE 3.7 COUNT RATES, POD S3, MK 1 INDENTERS

Gage	Sample	Position	CPMx10^3[a]	Gage	Sample	Position	CPMx10^3
033	1. Mg	F	23.0	009	1. Fe	F	32.3
		1	4.9			1	4.8
		2	3.4			2	4.9
		3	3.7			3	4.8
	2. Fe	F	49.0		2. Zn	F	< 0.1
		1	6.1			1	0.1
		2	7.6			2	0.1
		3	7.4			3	0.1
	3. Cu	F	< 0.1		3. Al	F	41.3
		1	0.1			1	11.1
		2	0.1			2	6.9
		3	0.1			3	7.1
	4. Zn	F	6.8		4. Sn	F	52.1
		1	1.1			1	10.2
		2	1.9			2	7.6
		3	1.0			3	8.9
018	1. Al (solid)	F	30.6	035	1. Al	F	52.6
		1	6.4			1	13.3
		2	4.9			2	9.6
		3	5.3			3	9.2
	2. Sn	F	6.2		2. Mg	F	40.1
		1	2.8			1	8.3
		2	0.8			2	5.8
		3	2.7			3	6.1
	3. Au	F	3.9		3. Al (solid)	F	35.5
		1	1.1			1	7.9
		2	0.9			2	5.3
		3	2.5			3	5.8
	4. Cu	F	< 0.1		4. Au	F	0.2
		1	0.1			1	0.2
		2	0.1			2	0.1
		3	0.1			3	0.2

[a]CPM means counts per minute.

TABLE 3.8 INDENT EVALUATION, POD S2, MK 1 INDENTERS

Gage	Channel	Indent?	Cap?	CPM	Apparent Fire?	Deduced Fire?	Conclusions
016	1 Mg	Yes	On	Lo	Yes	Yes	Yes
	2 Fe	Yes	On	Lo	Yes	Yes	Yes
	3 Sn	Yes	Off	Lo	Yes	?	?
	4 Au	Yes	Off	Lo	Yes	?	?
030	1 Mg	Yes	On	Lo	Yes	Yes	Yes
	2 Al	Yes	On	Lo	Yes	Yes	Yes
	3 Al	Yes	Off	Lo	Yes	?	?
	4 Zn	Yes	On	Lo	Yes	Yes	Yes
021	1 Cu	Yes	Off	Lo	Yes	?	?
	2 Al	Yes	On	Lo	Yes	Yes	Yes
	3 Zn	Yes	On	Lo	Yes	Yes	Yes
	4 Au	Yes	Off	Lo	Yes	?	?
006	1 Fe	Yes	On	Lo	Yes	Yes	Yes
	2 Cu	No	Off	Lo	Yes	?	?
	3 Sn	Yes	Off	Lo	Yes	?	?
	4 Al	Yes	Off	Lo	Yes	?	?

TABLE 3.9 INDENT EVALUATION, POD S3, MK 1 INDENTERS

Gage	Channel	Indent?	Cap?	CPM	Apparent Fired?	Deduced Fire	Conclusion
033	1 Mg	No	On	Hi	No	No	No Fire
	2 Fe	No	On	Hi	No	No	No Fire
	3 Cu	No	Off	Lo	No	?	No Fire
	4 Zn	Yes	Off	Lo	Yes	?	?
018	1 Al	No	On	Hi	No	No	No
	2 Sn	Yes	1/2 On	Lo	Yes	Yes	→ Yes
	3 Au	Yes	Off	Lo	Yes	?	?
	4 Cu	No	Off	Lo	No	?	No
009	1 Fe	No	On	Hi	Yes	No	No
	2 Zn	No	Off	Lo	Yes	?	?
	3 Al	No	1/2 On	Hi	No	No	No
	4 Sn	No	1/2 On	Hi	No	No	No
035	1 Al	Yes	1/2 On	Hi	Yes	No	No
	2 Mg	Yes	On	Hi	Yes	No	No
	3 Al	Yes	On	Hi	Yes	No	No
	4 Au	No	Off	Lo	Yes	?	?

pages 128 & 129 deleted.

TABLE 3.12 INDENT EVALUATION, POD S2, MK 2 INDENTERS

Gage	Channel	Indent?	CPM	Apparent Fire?	Deduced Fire	Conclusion
007		Yes	Lo	Yes	Yes	→Yes, Fired
		Yes	Med	Yes	?	?
		Side On	Lo	Yes	Yes	Yes, but no data
		Yes	Lo	Yes	Yes	→Yes
017		Side On	Lo	Yes	Yes	Yes, but no data
		Side On	Med	Yes	?	?
		Side On	Lo	Yes	Yes	Yes, but no data
		No	Hi	Yes	No	No
023		No	Hi	Yes	No	No
		No	Med	Yes	?	?
		Yes	Lo	Yes	Yes	→Yes
		No	Med	Yes	?	?
019		Yes	Lo	Yes	Yes	→Yes
		No	Lo	Yes	Yes	Yes, but no indent
		No	Hi	Yes	No	No
		No	Med	Yes	?	?

TABLE 3.13 INDENT EVALUATION, POD S3, MK 2 INDENTERS

Gage	Channel	Indent?	CPM	Apparent Fire?	Deduced Fire	Conclusion
029		No	Hi	No	No	No Fire
		No	Hi	No	No	No
		Yes	Hi	Yes	No	No
		Yes	Hi	Yes	No	No
025		No	Hi	Yes	No	No
		Yes	Hi	Yes	No	No
		Yes	Hi	Yes	No	No
		No	Lo	Yes	Yes	Yes, but no indent
027		Yes	Hi	Yes	No	No
		No	Hi	Yes$_2$	No	No
		Yes	Med	Yes	?$_2$	?
		No	Hi	Yes	No	No
004		No	Hi	Yes	No	No
		No	Med	Yes	?	?
		Yes	Lo	Yes	Yes	→ Yes
		?	Med	Yes	?	?

page 132 thru 137 deleted.

TABLE 3.20 STRIKER MATERIALS PARAMETERS

Material	Density (gm/cm^3)	Sound Vel. (m/sec)	Acoustic Impedance ρC	Enhancement Factor
Be	1.84 (a)	12,800 (c)	23.5×10^5	0.747
Carbon Graphite	1.70 (b)	2,250 (f)	3.9×10^5	1.56
Al	2.7 (a)	5,200 (d)	14.0×10^5	1.00
CH_2	0.924 (b)	920 (c)	0.85×10^5	1.88
CNP	1.18 (b)	2,180 (e)	2.57×10^5 (e)	1.69
C-124	1.14 (b)	2,450 (e)	2.8×10^5 (e)	1.67
AV-2	1.10 (b)	2,730 (g)	3.0×10^5	1.65

[a]Rare Metals Handbook (Reference 21)

[b]Measured at ARA

[c]AIP Handbook (Reference 20)

[d]Olson (Reference 22)

[e]Calculated from Enhancement Factor Data Supplied by AFSWC

[f]Calculated from Data supplied by National Carbon Co.

[g]Uncertain, but based on extrapolated data from AFSWC

pages 139 thru 144 deleted.

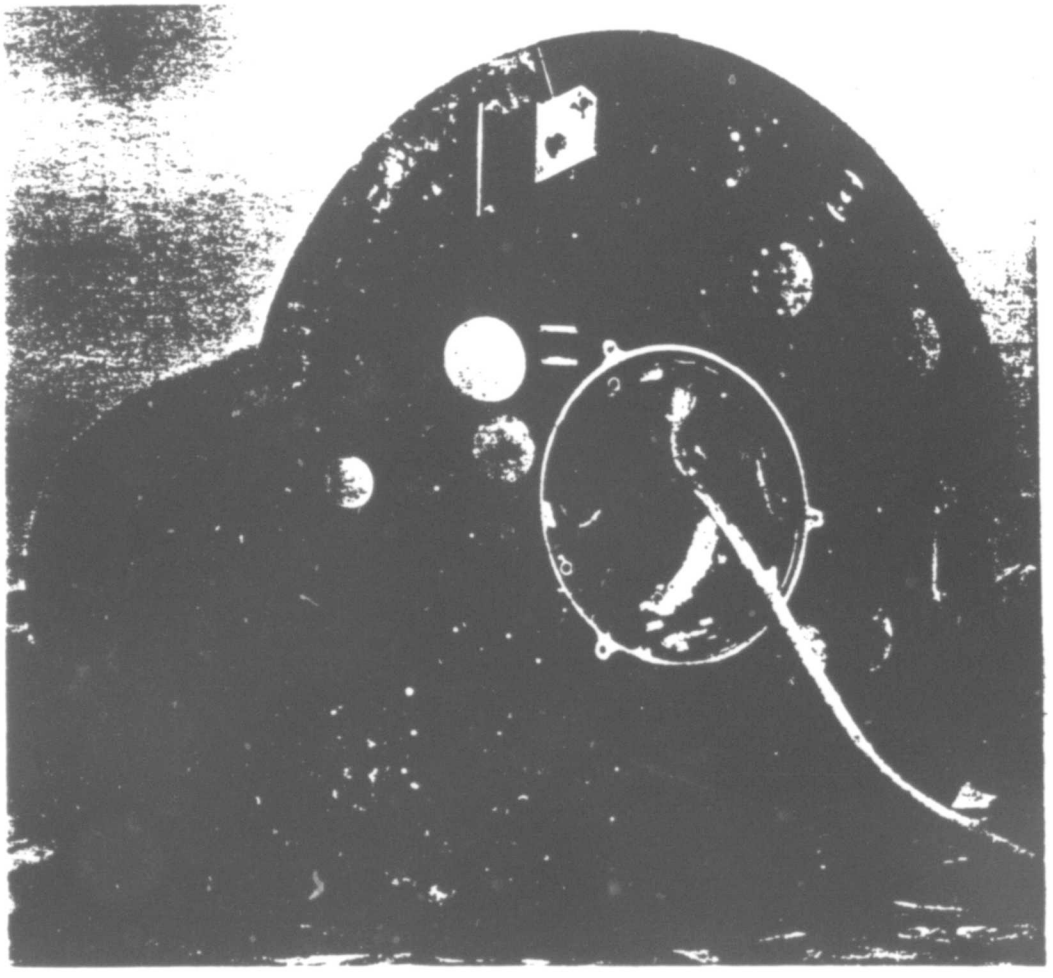

Figure 3.1 View of Pod S3 after recovery. (ARA photo)

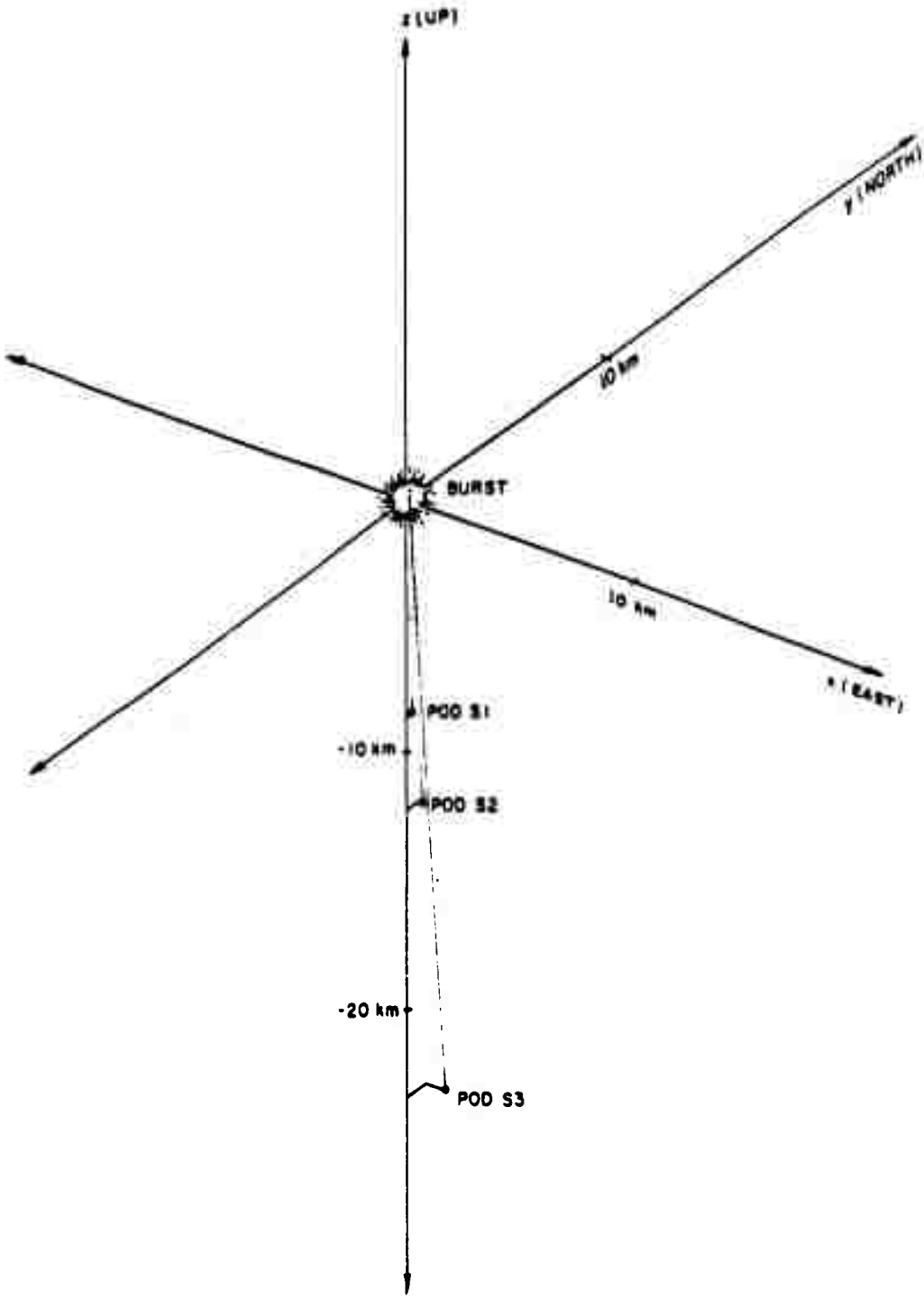

Figure 3.2 Pod-burst positions, Shot Star Fish Prime.

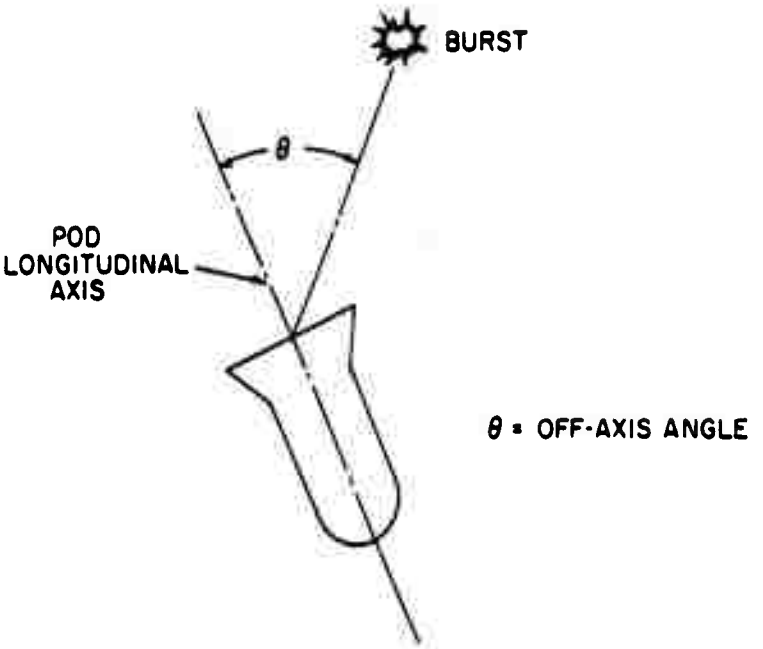

DEFINITION OF OFF-AXIS ANGLE

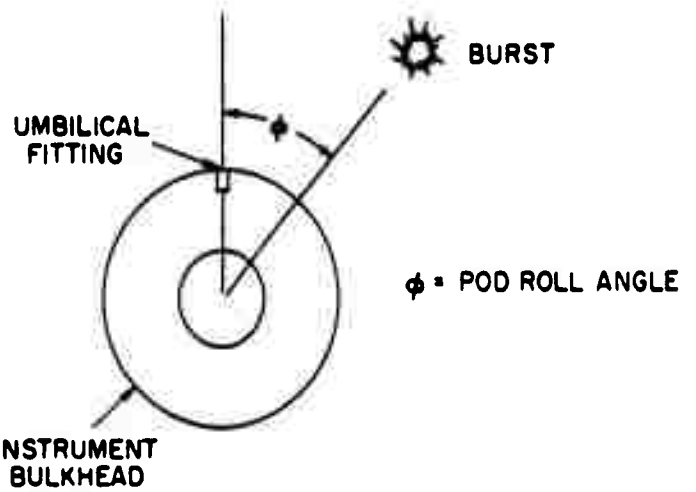

DEFINITION OF ROLL ANGLE

Figure 3.3 Definition of pod attitude.

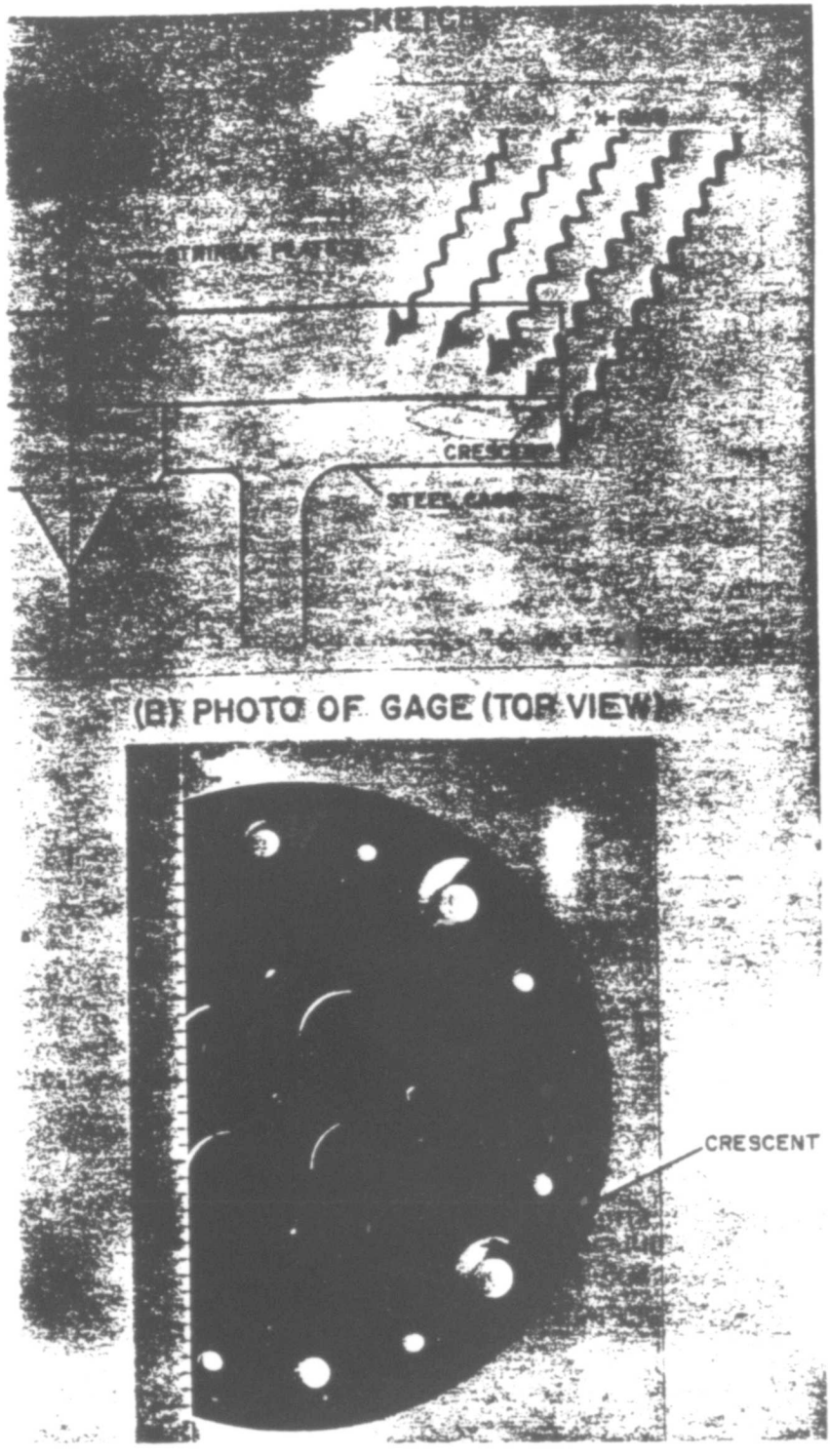

Figure 3.4 X-ray absorption by Mk 3 indenter gage after traversal of striker plate.

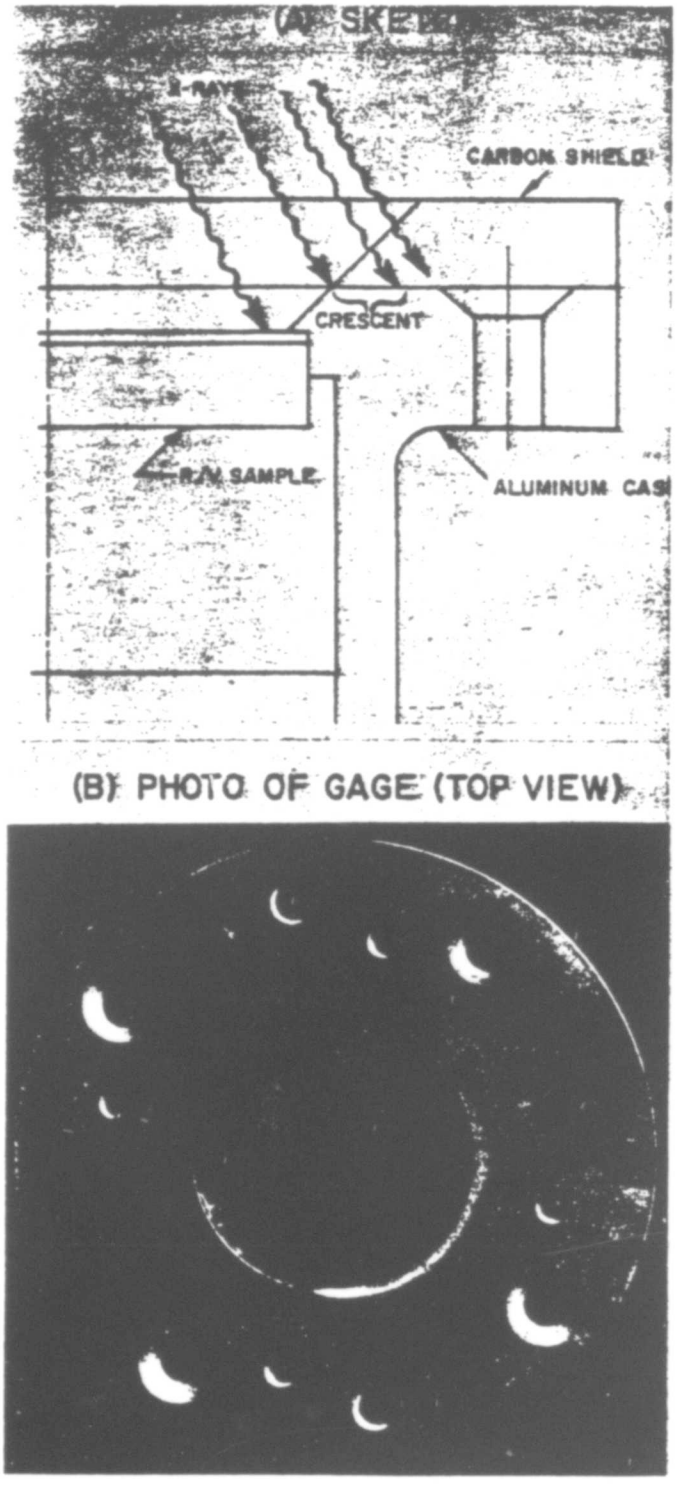

Figure 3.5 X-ray absorption by R/V case after traversal of carbon shield.

pages 150 thru 154 deleted.

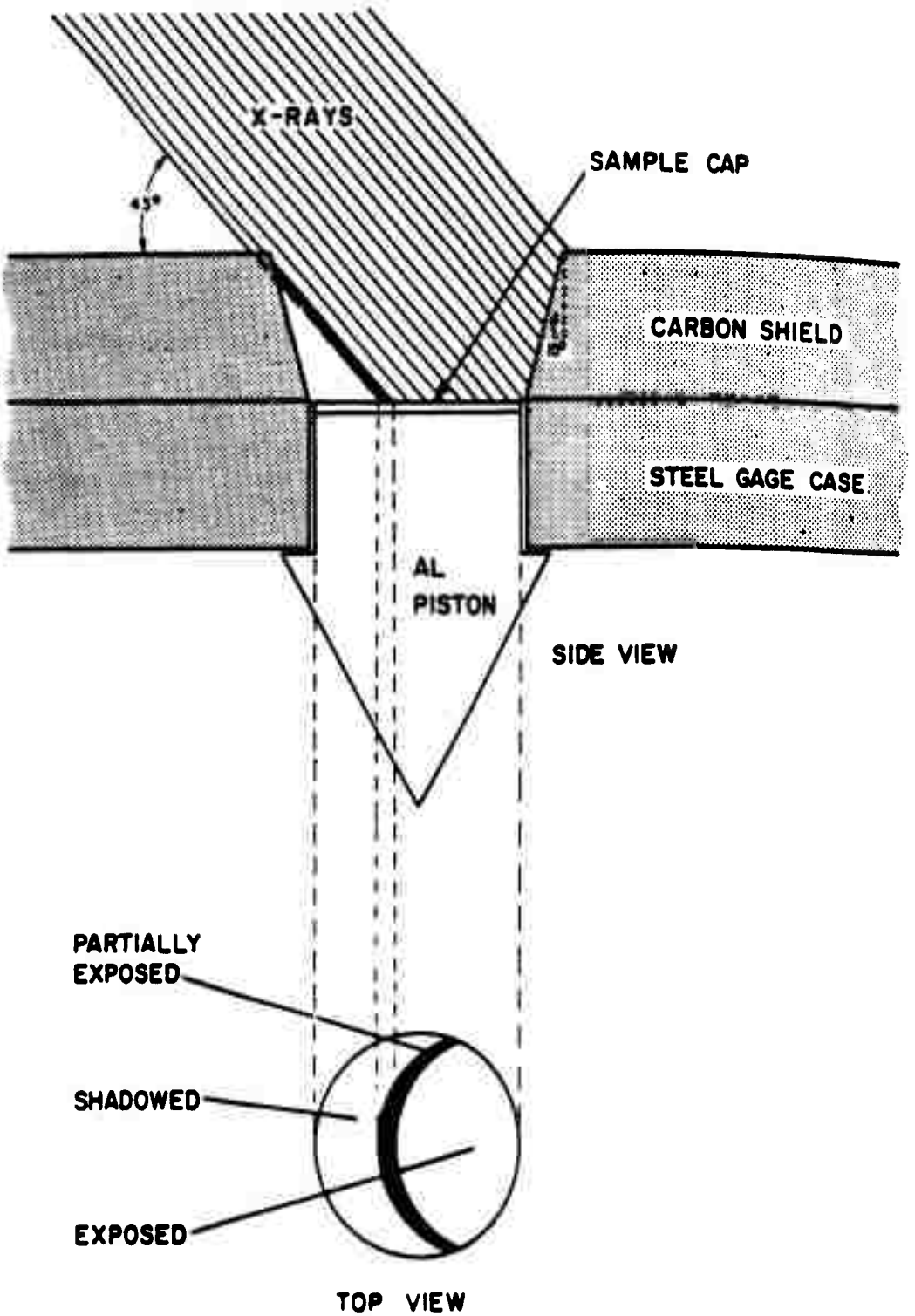

Figure 3.11 Sketch of X-ray exposure of Mk 1 piston.

pages 156 thru 162 deleted.

CHAPTER 4

CONCLUSIONS AND RECOMMENDATIONS

From two SF' pods certain physical effects have been observed which yield good quantitative experimental data about the phenomena associated with high-intensity X-ray deposition. A summary of the major conclusions reached and several recommendations follow.

4.1 CONCLUSIONS

The instrumented pod technique of data acquisition from nuclear detonations is fundamentally sound and was reasonably successful in shot SF'. Although some of the X-ray instruments could not operate properly because of the pod misorientation, it was clear that under a less extreme handicap most of the devices would have performed as designed.

The incident X-ray spectrum was not measured. Other evidence allows the flux to be estimated with reasonable accuracy to be

n Pod S3. For purposes of comparing X-ray impulses, an effective source temperature of indicated.

The range of X-ray-induced impulses observed at Pod S2 (flux at 43° to the normal) was about

4.2 RECOMMENDATIONS

Additional X-ray effects experiments are clearly of value in order to extend the present data to new materials and to more extreme energy regimes.

In the event that pod-type instrument carriers are again utilized, an improvement in pod stability is suggested as a result of the orientation problems encountered in SF'.

PART 2 KING FISH

CHAPTER 5
PROCEDURE

5.1 INSTRUMENT PODS

The two X-ray pods, designed and fabricated by General Dynamics/ Astronautics (GD/A), were essentially identical to those used in Star Fish Prime. A description of the pods as well as of the anticipated reentry and impact conditions imposed upon them can be found in Section 2.1. The third pod carried by the Thor missile was instrumented with Project 8C devices devoted primarily to studying fireball thermal effects.

5.2 FLIGHT SEQUENCES

As in Star Fish Prime, the pods were released from the missile after main engine cutoff but during vernier burn. Because of the somewhat lower burst altitude, however, release occurred later than before. Also the missile trajectory in King Fish (KF) was planned to be flatter so that the pods would land 70 km down range. After vernier cutoff and booster separation, the pods and warhead coasted to an apogee of about 700 km. Burst occurred at an altitude of with a total yield estimated at Thereafter, the sequence of recovery events was to be the same as in Star Fish Prime.

Reliance on a flywheel to supply stabilization to the pods was again attempted. Indications from the certification test, Tiger Fish, had been that the pods could be stabilized to within $\pm 8^{\circ}$ such that the instruments would view the burst directly to within that uncertainty. However, in Star Fish Prime, the two stabilized pods whose gyro motors attained full speed were off axis over 40°. Certainty as to the cause of this deviation was lacking. Consequently, the acceptance angles of the KF X-ray instruments were increased to permit operation even in the event of a 45° misalignment between pod axis and burst line of sight.

5.3 INSTRUMENT MODIFICATIONS

The changes in instrument design for King Fish as compared to Star Fish are specified in this chapter. The theory behind the operation of each instrument has been given in some detail in Section 2.3 and Reference 3 and will not be repeated here. A major design revision occurred with regard to only

one instrument, the plated hole gage which evolved into the spectral gage. Other revisions were generally of a minor nature.

The following list presents the Project 8B instruments carried on the rear bulkhead of each pod. In addition to these gages, certain devices from other agencies, in particular Aeronautical Systems Division (ASD), Lawrence Radiation Laboratory (LRL), Nuclear Defense Laboratory (NDL), and Air Force Special Weapons Center (AFSWC) were included. Figure 5.1 maps the gage array on both KF pods, and Figures 5.2 and 5.3 are photographs of the two instrument bulkheads.

Instrument	Number per Pod
Mk 1 Indenter	4
Mk 2 Indenter	3
Mk 3 Indenter	8
K-edge Detector	2
R/V Composite	7
Spectral gage	2
X-ray Calorimeter	2
Thermal Calorimeter	1
Metallurgy	10
Fracture	2
Orientation sensor	2

A summary of some of the conditions and fluxes assumed for design purposes during Phase I of the KF program were:

KF Conditions Presumed for Instrument Design Purposes	
X-ray Flux* K2	
K3	
Effective Source Temp.	
Debris Arrival Time	1.5 to 2.2 msec
Air Density (95 kev)	$\sim 10^{-9}$ gm/cm^3

* These values took into account the X-ray attenuation due to air absorption.

5.3.1 X-ray Effects Instruments.

Impulse Recorders.

The three types of indenter gages designed for Star Fish were again used in King Fish. The total of fifteen gages was maintained; however, there were three Mk 2 types and eight Mk 3 types instead of the four and seven, respectively, for Star Fish.

Mark I Indenter (4 gages).

The following comments describe the changes to the KF Mk 1 indenters: (1) The piston holes in the carbon shield covering the instrument face were cut back to permit a 45° acceptance angle. (2) The cap thicknesses for both pods were as follows:

Cap	Thickness inch
Al-solid	no cap
Al-cap	.006
Mg-solid	no cap
Fe	.006
Cu	.005
Zn	.010
Sn	.004
Au	.004

Mark 2 Indenter (3 gages).

Changes in the Mk 2 indenters were as follows: (1) the piston holes in the carbon shield were cut back to permit the piston faces a 45° field of view; (2) the Devcon sample was eliminated; (3) each sample was repeated once only; (4) the shadow plates, used to aperture the piston faces, were changed from steel to aluminum; and (5) the samples for both pods were as follows:

Pod K2

Sample	No/Pod	Sample Length inch	Piston Shell	Aperture inch
OTWR(U)	2	.200	Aluminum	.40
OTWR(P)	2	.200	Aluminum	.40
Rad 58 B	2	.200	Aluminum	.40
Avcoite I	2	.200	Aluminum	.40
GEFG	2	.200	Aluminum	.40
Teflon	2	.200	Aluminum	.40

Pod K3

Sample	No/Pod	Sample Length inch	Piston Shell	Aperture inch
OTWR(U)	2	.200	Magnesium	.44
OTWR(P)	2	.200	Magnesium	.44
RAD 58 B	2	.200	Magnesium	.44
Avcoite I	2	.040	Magnesium	.44
GEFG	2	.200	Magnesium	.44
Teflon	2	.200	Magnesium	.44

Mark 3 Indenter (8 Gages).

The following modifications were made to the Mk 3 indenters:

(1) The case material was changed to aluminum. It was realized during the data reduction program for Star Fish Prime that an unnecessary complication had been introduced into the analysis of the momentum transfer from striker to piston by having the case and piston materials dissimilar (iron case and aluminum pistons).

(2) The length of the control piston shank was reduced to preclude the possibility of an easily deformed striker contacting it. The shank length was 0.190 inch.

(3) The striker thickness for a given material was the same for both pods. Conflicting requirements resulted in the criteria used for determining the final striker thicknesses. First, it was desirable for the strikers to be as thin as possible to minimize attenuation and dispersion of the blow-off pulse and to provide little time for disturbances from outside the case to propagate to the pistons through the case flange. On the other hand, the striker had to be sufficiently thick to prevent excessive heating of the piston, which might result in expansion and sticking as well as in acoustic impedance changes. Also, the striker had to be thick enough for the entire pulse to pass the striker-piston interface before the return of the leading edge of the twice-reflected wave.

Hence, two criteria were established. The aluminum piston should become no hotter than 500°C (660°C being the melt temperature of Al). This gave a minimum striker thickness at each range. The second criterion applied was that the striker be thick enough for the leading edge of the pulse to make one traversal of the striker in 2 microseconds. It was assumed that in all samples the pulse length was less than 4 microseconds and that the acoustic velocity for an elastic wave was a satisfactory approximation to the real velocity. This second criterion dominated.

It turned out that for most materials the same minimum thickness was indicated at both ranges. In the several instances where two different thicknesses resulted, the differences were considered small enough to compromise on a single thickness. There was one exception, however; two thicknesses of aluminum were carried in order to discern what effect, if any, a thin striker would have on the momentum transfer.

The striker thicknesses flown in King Fish are listed below:

Material	K2 inch	K3 inch
CNP	.25	.25
Avcoat II	.21	.21
Be	.625	.625
Graphite	.28	.28
Polyethylene, CH_2	.50	.50
Al	.41	.41
Al	.20	----
Teflon	.20	.20
CPG	----	.28

(4) Temperature sensitive paints were tamped into eight shallow holes on the underside of each striker. Knowing the temperature near the rear surface of the striker would have been necessary if a correction for the temperature effect on the enhancement factor was later deemed important.

Metallurgy Experiment (10 gages).

No changes in the metallurgy instruments occurred except for the widening of the hole in the carbon shields to permit a 45° look angle.

R/V Materials (7 gages).

The hole in both the carbon shield and the case was cut back to permit a 45° look angle.

Fracture Experiment (2 gages).

The fracture gages were modified in the following respects: (1) The case and carbon shield hole were cut back to permit a 45° look angle, (2) the blowoff button diameter was increased to 0.5 cm, (3) the two lucite cylinder lengths were changed to .445 and .23 inch. The spacer lengths were adjusted accordingly. Failure of similar gages to fracture in the Marshmallow event made it appear desirable to increase the probability of fracture. Decreasing the lucite cylinder length accomplished this, and

(4) the button materials were: K2, aluminum; K3, magnesium.

5.3.2 Diagnostic Instruments.

Carbon Calorimeter (3 gages).

The carbon calorimeter design was changed as follows: (1) the carbon shield and aluminum case holes were cut back to permit a 45° view, (2) a third calorimeter was included on each pod but shielded such that X-rays could not reach the calorimetric disk, yet thermal energy, such as emitted by a fireball, could effect it (Figure 5.4).

K-Edge Instrument (2 gages).

The following changes were made in the K-edge: (1) The carbon shield hole was cut back to a 45° bevel; however, the case hole was given only a 30° bevel, (2) the detector stacks were brought closer to the filter in order to accommodate greater orientation misalignment (Figure 5.5), and (3) filter thicknesses were revised because of the higher flux levels and lower source temperature involved. The new filter and detector parameters are presented in Tables 5.1 and 5.2.

Spectral Gage (2 gages).

The spectral gage (Figure 5.6) was a modification of the plated hole instrument used in Star Fish. This most recent form has associated with it the same principles of operation as its predecessor. That is, the impinging X-rays penetrate varying thicknesses of carbon, with the spectrum being attenuated selectively, and are absorbed by the detector metal immediately behind the carbon. The position of the melt-solid boundary line on the surface of the metal detector gives a point on an energy density as a function of carbon thickness curve. This datum can, in turn, be related to the character of the incident spectrum. By utilizing more than one detector metal and by utilizing melt depth data, the spectrum becomes accordingly better known. In Section 3.2 the technique for reconstructing the incident X-ray spectrum has been presented in order to determine the SF' spectrum; although the physical data used came from somewhat different circumstances than those described here, the principles remain the same.

As can be seen from Figure 5.6, a conically shaped piece of high-density carbon was used to attenuate the X-rays. Two different detector metals, lead and chrome, were formed in the shape of a conical cup and spaced from the carbon cone approximately 1/16 inch. The chrome, in actuality, was a heavy plating on a steel form; the lead was solid. The space between the carbon cone and the detector cup was vented to allow pressure relief for the vaporizing metal.

This arrangement was believed preferable to the previous design wherein the detector metal was a thin film on the carbon. Experience in Star Fish Prime indicated that identification of the phase change boundaries in such a film was not possible, whereas identification of such boundaries in the Mk 3 indenter metal cases that had been shielded by the striker materials was relatively straightforward. Thus, the present design attempted to capitalize on the Star Fish experience. The one complication introduced by the solid-block type of detector was the effect on the boundary position by conduction of the heat into the block. This point has not been treated in detail, but it appears to result in a negligible error.

Orientation Sensors (2 spikes).

In order to determine the off-axis angle and the roll angle of each pod with respect to the burst, the most simple and direct method has been to utilize the X-ray shadows cast by various protuberances on the rear of the pod. Clearly, the longer the shadow cast, the more accuracy possible in determining these angles. No projection specifically designed for these measurements was included in Star Fish, and as a result, it was necessary to use shadows cast by strikers and fittings. The uncertainties in the measurement were unnecessarily high. Consequently, for King Fish two 3-1/4 -inch spikes were attached to two rear bulkhead instruments such that regardless of the burst direction one of the spikes would project a shadow on the rear, if the off-axis were within 45°. Because the height of the spike tip above the surface could be determined precisely beforehand, the subsequent calculations would result in very small errors.

pages 172 & 173 deleted.

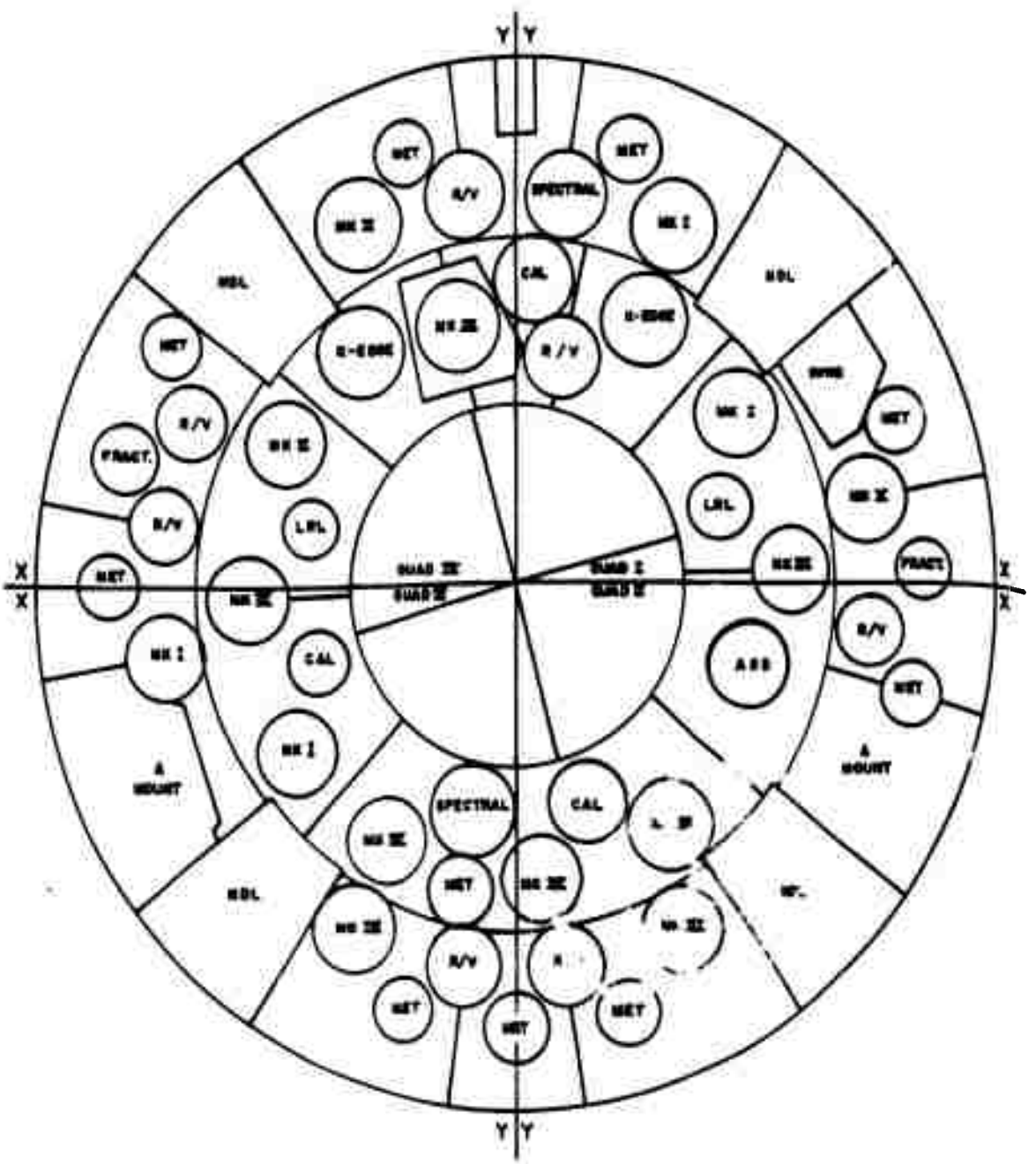

Figure 5.1 Instrument layout, Shot King Fish.

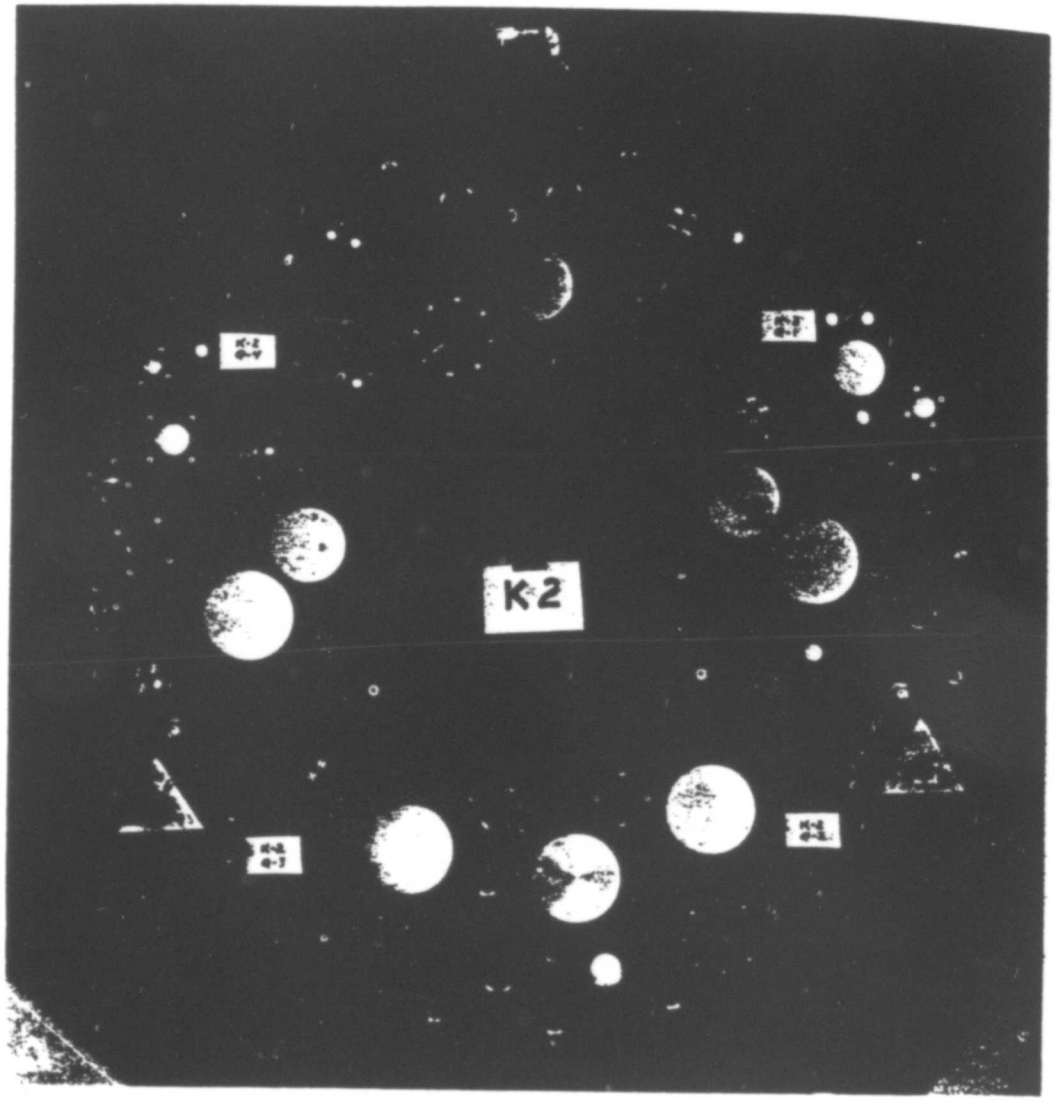

Figure 5.2 Instrument plate, Pod K2. (ARA photo)

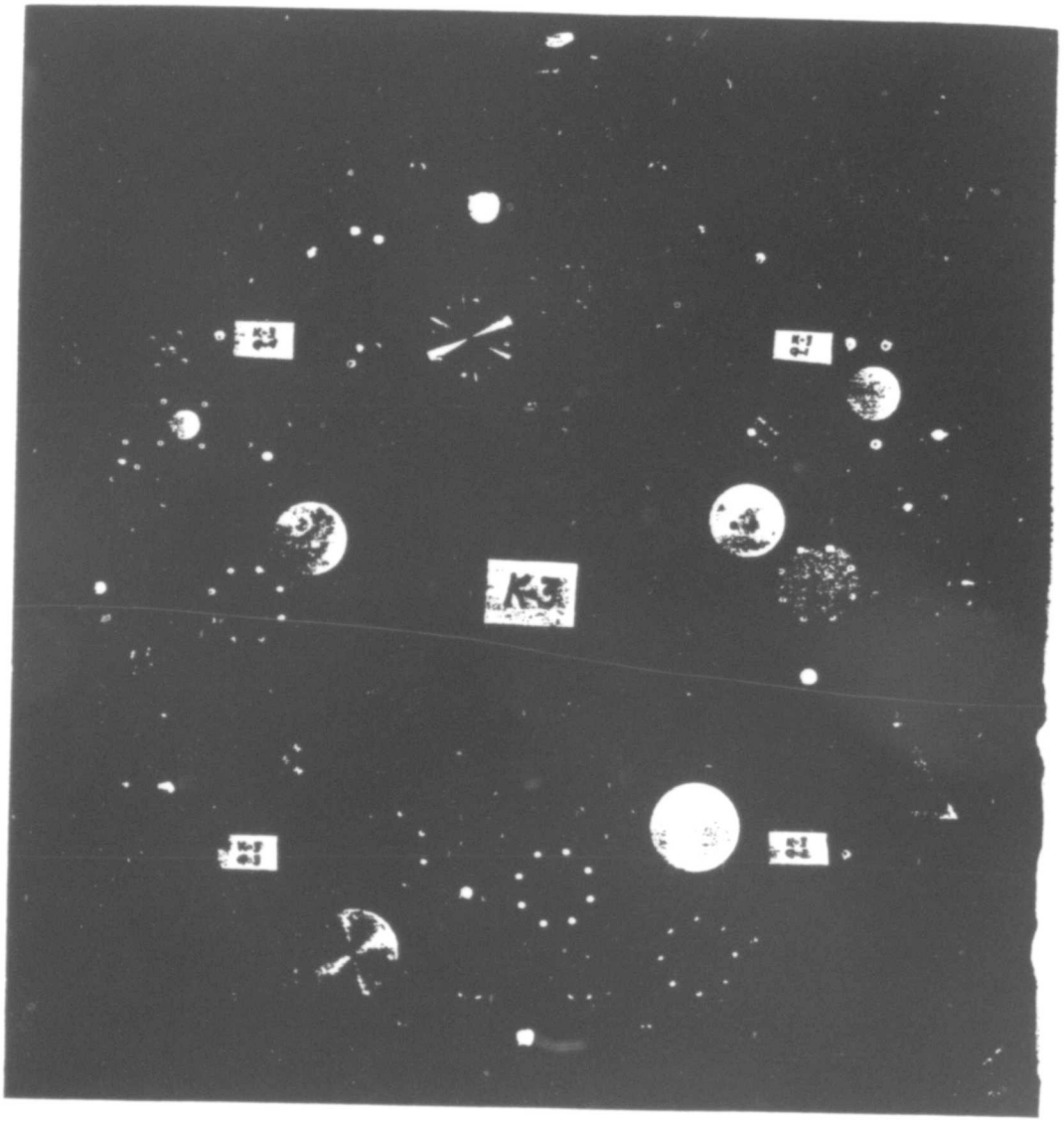

Figure 5.3 Instrument plate, Pod K3. (ARA photo)

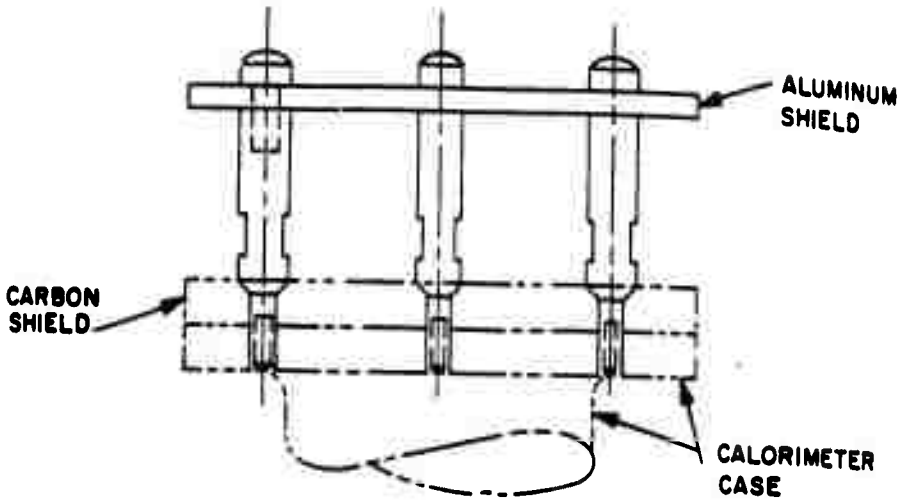

Figure 5.4 Thermal calorimeter assembly, Shot King Fish.

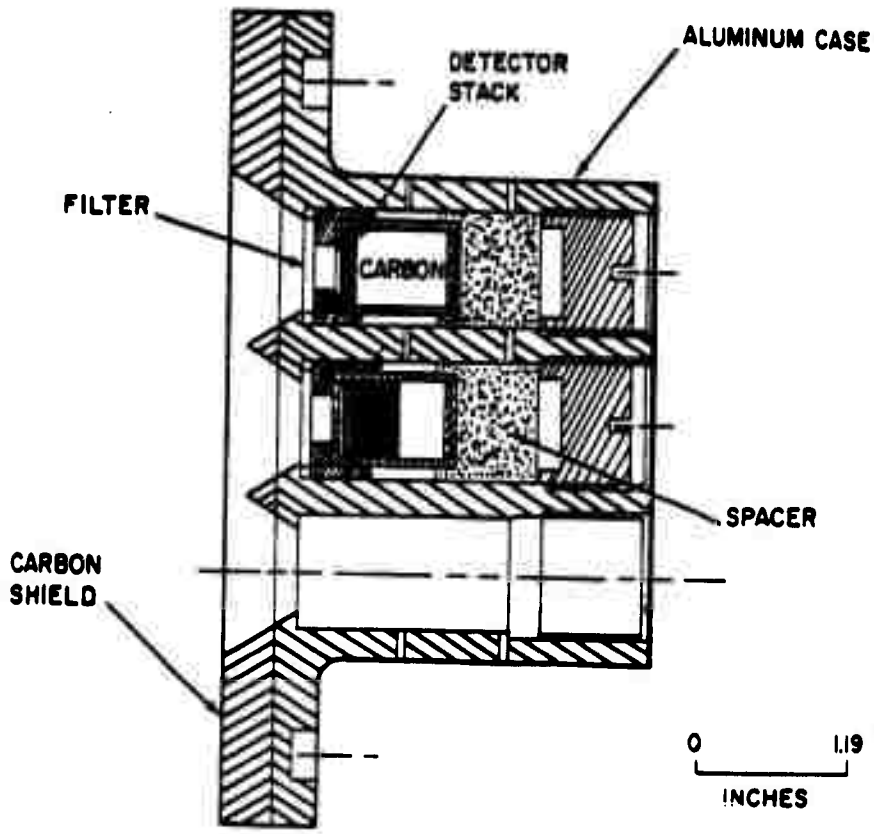

Figure 5 K-edge instrument, Shot King Fish.

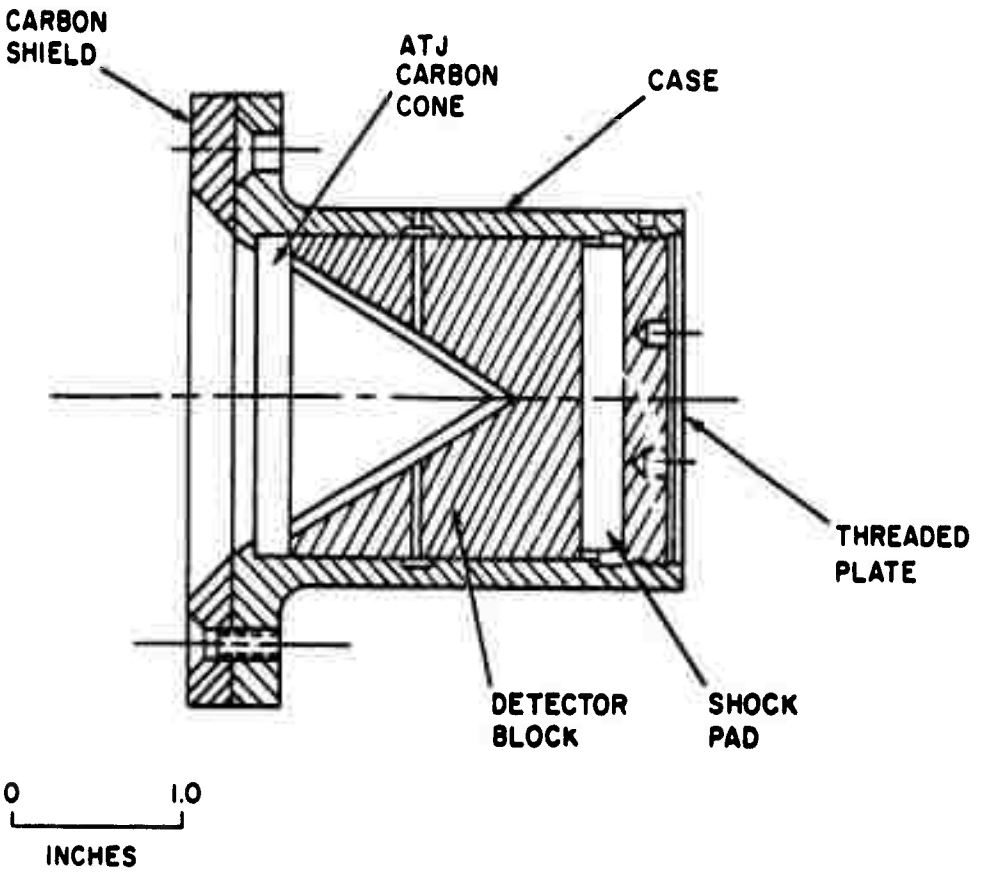

Figure 5.6 Spectral gage, Shot King Fish.

CHAPTER 6
RESULTS

The Thor missile was launched at approximately 1155 Zulu, 1 November 1962. Prior to launch, all pod systems appeared to be functioning satisfactorily. The Thor trajectory was good, and pod release signals were received as planned. Tracking information indicated that the pods were not tumbling.

Shortly after dawn, Pod K2 was located by one of the recovery vessels and returned to the island by helicopter. Examination of the pod showed it to be severely damaged by water impact, which apparently occurred at a nearly horizontal attitude.

As shown in Figure 6.1, the rear bulkhead on which was mounted all the X-ray instrumentation had separated from the pod structure and was lost at sea. Some of the secondary instrumentation, particularly those gages mounted on the internal pod structure were recovered. Pod K3 was not recovered, and all the instrumentation on board was lost. The nose cone and portions of the recovery package of this pod were later located, indicating that severe damage occurred at water impact.

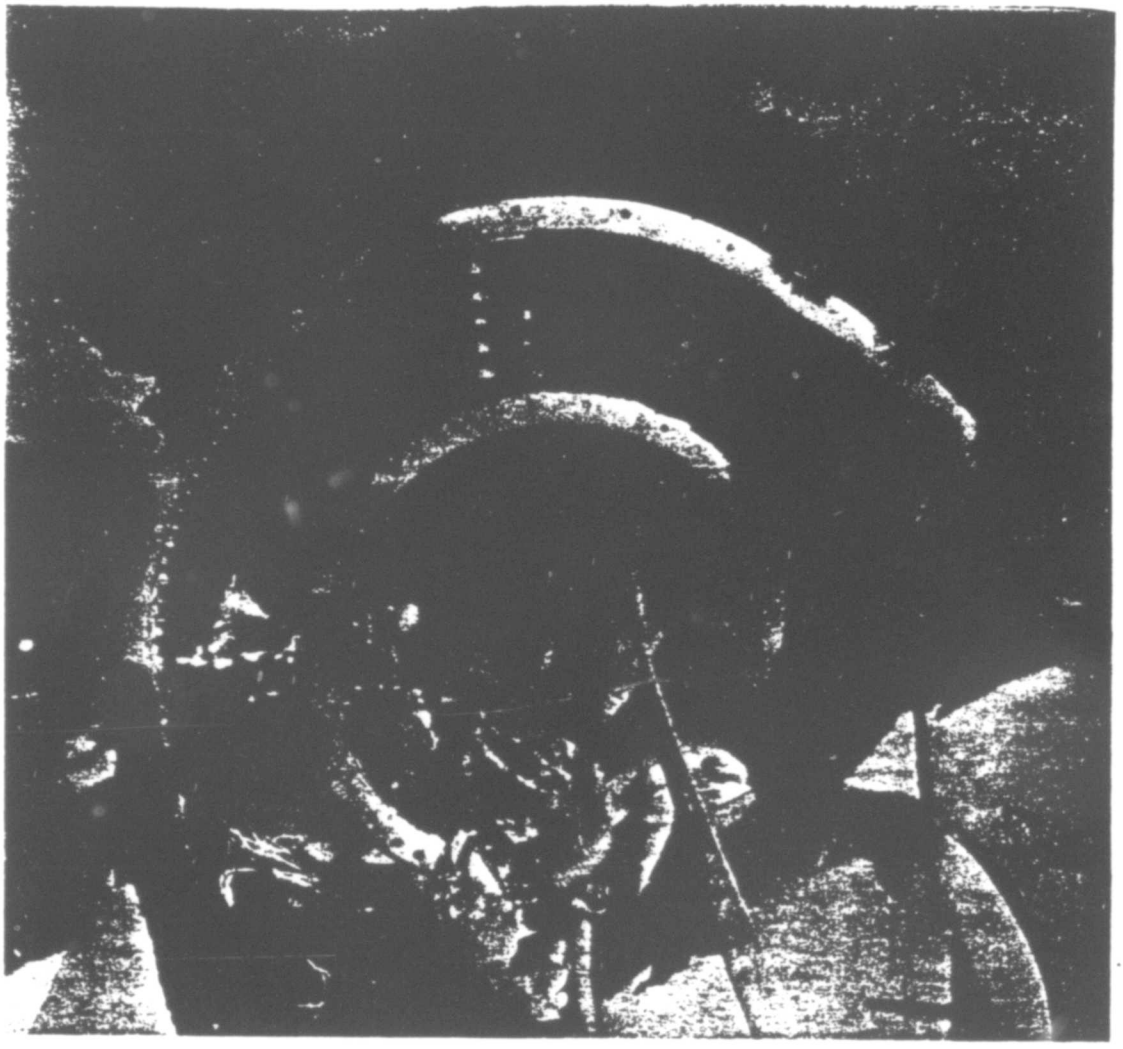

Figure 6.1 Crushed aft end, Pod K2. (ARA photo)

CHAPTER 7
CONCLUSIONS AND RECOMMENDATIONS

Failure to recover any of the Project 8B X-ray instruments due to breakup of the pods following severe water impact permits no conclusions to be reached concerning the King Fish X-ray phenomena.

Two recommendations for future operations involving instrument pods of this type are advanced: (1) Reused recovery equipment must be avoided. (2) A long coiled cable or chain attaching the instrument plate to the pod body and tucked inside the pod might prevent loss of the plate even if it is sheared off.

APPENDIX A

CERTIFICATION TEST, TIGER FISH

A.1 TEST CONDITIONS

On the Tiger Fish shot of 2 May 1962, three pods of the type designed to carry the X-ray instruments in Star Fish were launched into a trajectory planned to simulate the Blue Gill and Star Fish sequence of events, with the exception that there was no nuclear detonation. This event afforded an overall systems check on the Thor and on telemetry. sequencing, pod performance, and the recovery equipment operation.

In addition, this test gave Project 8B an opportunity to observe the performance of the X-ray instruments when subjected to launch, re-entry, and recovery conditions, without nuclear inputs. In this way, it was believed, any obvious design defects might be brought to light and non-X-ray impulsive or thermal inputs estimated. Thus, in two of the three pods, C1 and C3, a prototype of each instrument was carried, except for the Mark 3 indenter which was not available at the time.

At launch, the gyro motor in Pod C1 was inoperative, so there was no stabilization of C1 during its free flight. Its motion was one of random tumbling. From telemetered accelerometer data, it is apparent that upon initiation of re-entry, Pod C1 was oriented tail-first, and although it reversed itself quickly, there was sufficient heating to produce high temperatures on the rear bulkhead and thermal damage to various instruments. The drogue and main chutes, scheduled to open just after re-entry and provide a low velocity water impact, failed; it has been surmised (Reference 24) that the reversed orientation at re-entry precluded the subsequent events necessary to arm and trigger the chutes. As a result, Pod C1 impacted at high velocity, and almost horizontally. Hence, an abnormally high and wrongly directed impulse was experienced by the X-ray instruments at water impact. Add to this the abnormal re-entry heating of the instruments, and it is clear that, except for a certain academic interest, the data contained by the C1 gages is of minimal value to Star Fish interpretation. A brief description of the C1 gages and their conditions will be presented shortly. On the other hand, Pod C3 followed through its programmed sequence adequately for the stated purposes. Although the gyro motor was not operating at full rpm and an appreciable wobble developed, the stability of the pod was sufficient to result in a normal

re-entry and chute deployment. Consequently, the impulsive and thermal data gathered from both the telemetry and X-ray instruments of C3 are applicable to the data reduction and analysis of Star Fish.

A.2 POD C3 INSTRUMENTS

A careful examination of the various C3 X-ray instruments was made and disclosed that, except for the two indenters and the calorimeter, the gages returned in essentially their original conditions.

Fracture Gages. No discernible effects; returned in essentially original condition.

Metallurgy Gage. No discernible effects; returned in essentially original condition.

R/V Gage. Carbon shield cracked; otherwise in essentially original condition.

Plated Hole Gage. No discernible effects; returned in essentially original condition.

K-Edge Gage. Only four filters and five detectors were installed. Of these, only a mylar filter was broken. Examination failed to resolve during which phase the tear occured. Otherwise the instrument was essentially unaffected. The detector laminations had remained distinct.

Carbon Calorimeter. No color change was found in any of the temperature elements, thus indicating the peak temperature of the calorimeter was less than 65°C (150°F). Telemetered temperature data indicated a slightly higher back plate (outside surface) temperature near 200°F. Evidently, the brevity of the peak temperature experienced by the calorimeter prevented its being registered. That the calorimeter became appreciably heated, however, is evidenced by the fact that the crayons became tacky and in some instances flowed; these crayons melt at temperatures that are lower than their indicating temperatures. The heating of the calorimeter is ascribed to the re-entry environment.

Mark 1 Indenters. Two modest indents were found on the anvil of this gage, although all four pistons had fired. The two indents, 1.1 and 1.05 mm in diameter, indicated that terminal piston velocities of 470 and 506 cm/sec, respectively, had been reached. This gage had piston-restraining springs which, statically tested, would let the piston pass under a 50-g load. It is interesting to note that the peak deceleration during re-entry (acting in the direction to fire the pistons) was measured through telemetry at about 40 g's. Thus, it is clear that the firing of the Mark 1

pistons was marginal and apparently is confirmed by the fact that only two indented. If the acceleration of the pistons necessary to produce the observed indents is calculated, it is found that it is on the order of 70 g's. This figure is somewhat higher than the 40 or 50 g's mentioned but in the proper range. That two pistons passed the restraining spring but did not indent would indicate that they did not fire during re-entry (the scratch pattern on the anvil made by the two fired pistons during re-entry buffeting tend to confirm this supposition). It seems likely that at sometime during the pod's water entry and submersion they were forced out, perhaps by water slapping over the rear or by hydrostatic water pressure, less than a meter-high water column being sufficient.

Mark 2 Indenter. No meaningful indents were found on the anvil of this gage. In addition, one piston had not overcome the restraining spring, yet was not frozen or bound in its hole. Since the static release loading was high compared to the Mark 1 gage, about 150 g's, and the Mark 1 firing was only marginal at a telemetered re-entry deceleration of 40 g's, it is certain that the three passed pistons did not fire during re-entry. (It should be noted that the Mk 2 restraining springs were later changed to those identical with the Mk 1 springs for SF'.) Furthermore, had they fired then, indents similar to those of the Mark 1 anvil would have occurred (the restraining springs extract only a small fraction of the piston's kinetic energy). Hence, it is concluded that the pistons fired during water entry and submersion——a submersion depth of five feet would have provided the necessary hydrostatic pressure.

Conclusions. The information gathered from an analysis of the C3 instruments agrees with the temperature and acceleration history presented by the telemetry instrumentation of Reference 24. The various gages have established certain effects and/or background signals one can expect from the re-entry and water impact environments. That is, any Mark 1 pistons not fired by the X-ray impulse have a marginal chance of being fired during re-entry. Any Mark 2 pistons not fired by the X-ray impulse will not be fired during re-entry. Any pistons not fired by either effect will probably be pushed through during water entry and probably will not indent. Any temperature of 150°F or higher recorded by the calorimeter will not be the result of re-entry heating but rather of X-ray deposition and heating.

A.3 POD C1 INSTRUMENTS

Inverted re-entry and unretarded water impact resulted in substantial damage to all C1 instruments. The back plate was bent out, thus deforming some gages. The following descriptions are deliberately not extensive.

Fracture Gage. The entire lucite cylinder had been heated and softened from top to bottom as evidenced by its warped shape and the impressed grooves of every O-ring. A hole, approximately 3/64 inch deep was burned into the cylinder at the exposed end. A black greasy film covered the top.

Metallurgy Gage. The front face of this gage was warped from the deformation of the C1 back plate. The metallurgy sample was in essentially original condition except for a black greasy film.

R/V Gage. The Avcoat I sample partially ablated and was covered with a black greasy film. The foam backup melted.

Plated Hole. The carbon disks were apparently unaffected. However, the chrome plating had disappeared except for what appeared to be a few chips near the rear.

K-Edge. All the filters were burned out. The detector stacks were partially melted.

Carbon Calorimeter. Because the temperature crayons had been applied too generously, most had run out of their holes and into others, making analysis difficult. However, it was determined that the calorimeter reached a peak temperature of betwen 350°F and 660°F. This is consistent with a telemetered backplate temperature of over 400°F.

Mark 1 Indenter. All four pistons fired and indented with terminal velocities of about 400 cm/sec, which would imply a deceleration of 50 g's to account for the indent diameters. Also, the restraining springs permitted firing under a 50-g static load. The telemetered data indicated that, upon righting itself during re-entry, the pod experienced a peak deceleration of 40 g's. This figure agrees closely enough with the estimated 50-g piston acceleration to conclude that firing occurred during re-entry.

Mark 2 Indenter. All four pistons had fired and indented. However, in this case it is believed that firing did not occur during re-entry but rather upon water impact. The piston-restraining springs of the Mark 2 required a loading of about 150 g's to fire, considerably higher than the

40 to 50 g's estimated during re-entry. Also, the face of each piston had been partially blackened, probably by re-entry products, thus confirming that the pistons were in place during at least part of re-entry. That the pistons fired on water impact is the tentative conclusion. Since the parachutes failed to deploy, the pod struck the water at full terminal velocity. The impact deceleration could well have reached several hundred g's momentarily. And because of the 30° angle to horizontal of the pod, the observed shift in the whole indent pattern of 1/8 inch away from the true anvil center then becomes understandable. The indents measured required high piston velocities of about 800 cm/sec, or a pod deceleration of 195 g's. This figure is consistent with the water impact firing hypothesis suggested.

Conclusion. Pod C1 experienced severe thermal and deceleration loadings as evidenced by the condition of the X-ray instruments. The data extracted from these devices is consistent with that from the telemetry instruments. However, the information is not considered especially applicable to the analysis of gages from a properly functioning Star Fish pod.

APPENDIX B

LEAD ANVIL CALIBRATION

In order to reduce the raw impulse data obtained in the form of conical indents in a lead anvil, it is necessary to know the relation between the hole size and the piston energy that produced it. It should be mentioned that experience with similar arrangements has shown that over several decades of energy the hole volume is in fact just proportional to the kinetic energy of the piston. At very high energies, higher than those found in the Star Fish data however, the proportionality fails; see for example, Reference 3.

The calibration performed to establish the energy-hole volume relation was quite simple. Pistons similar to those used in the indenter gages were dropped from various heights into spare lead anvils which had been cast at the same time as those used in Star Fish. The pistons were made relatively stable aerodynamically with the addition of small very light foam tails. Just prior to impact, the piston was photographed stroboscopically so that, after certain corrections were applied, the velocity of impact could be calculated. Figure B. 1 illustrates the calibration setup. Since the mass of each piston was known, the kinetic energy could be calculated, and from each indent, one point on a KE vs. hole volume curve was obtained.

In truth, rather than dealing with the inconvenient quantity of hole volume, it was possible and preferable to measure only the hole diameter, or the minor axis of the surface ellipse in the case of tilted impacts. It may be shown that the hole volume for tilted impact is obtained if the minor axis of the surface ellipse is used in place of the diameter in the equation for the volume of a conical hole. Hence, the calibration curve was set up as KE vs. hole diameter or minor axis. The calibration curve resulting from almost three dozen piston drops is shown in Figure B. 2. Several comments are in order.

First, it is clear that over the energy range involved the KE $\propto$ (diameter)^3 relation holds. The piston energies did not go quite high enough into the 10^6 erg decade to cover all the Star Fish data, but the extrapolation is believed to be highly accurate. The reason is that in all other such calibration tests (for example, see Reference 3 again) the proportionality holds to almost the 10^8 erg decade. The higher energies

were not checked because higher piston drops were not practical (the highest velocity pistons fell from a three-story height). It would have been possible to increase the piston mass, but it was decided not to deviate from the original Star Fish piston mass by more than a factor of two. Consideration was also given to firing the pistons from an air gun arrangement, but preliminary experiments indicated that more effort would be required than was warranted.

It was of interest to permit the pistons to impact at various angles and observe how well the calibration held at extreme tilt angles on the order of 30°. Because the pistons fell unguided, they impacted randomly at various angles. Referring to Figure B. 2, it is clear that the deviations of the highly tilted indents from the drawn line are not more than the less tilted indents. This means simply that the hole volume is still proportional to the piston energy even at large impact angles.

The calibration curve of Figure B. 2 was used to reduce all the indenter gage data. It is interesting to note that the lead used in the Star Fish anvils was slightly harder than that used in the previous test operations. That is, to produce a given indent size, the piston energy required was higher. The necessity of anvil-piston calibration is thus demonstrated.

The tilt angle, θ, of each indent was measured in the following way (refer to the accompanying sketch). The length of the major axis, L, was measured. The distance, a, along the major axis to the projected hole botton was measured. It is a simple matter to prove the following relation:

$$\sin \theta = .866\ (1-2a/L)$$

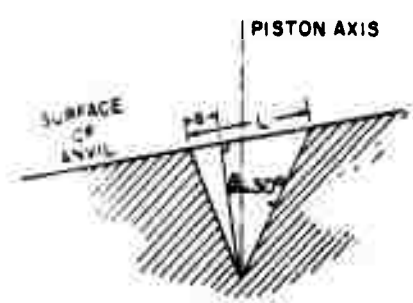

From this equation the tilt angle of each indent could be determined within an accuracy estimated at about $\pm 3^{\circ}$.

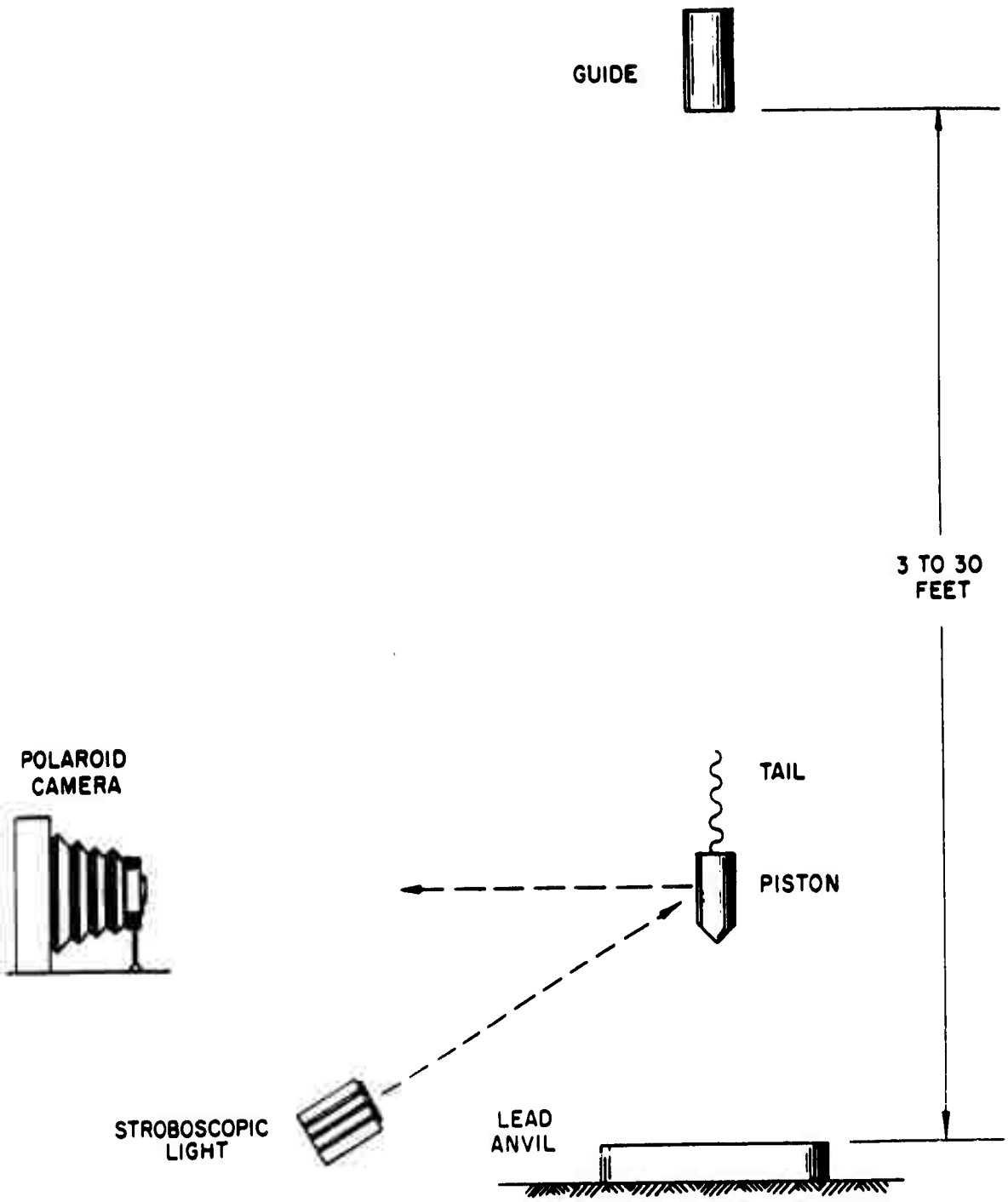

Figure B.1 Drop test setup.

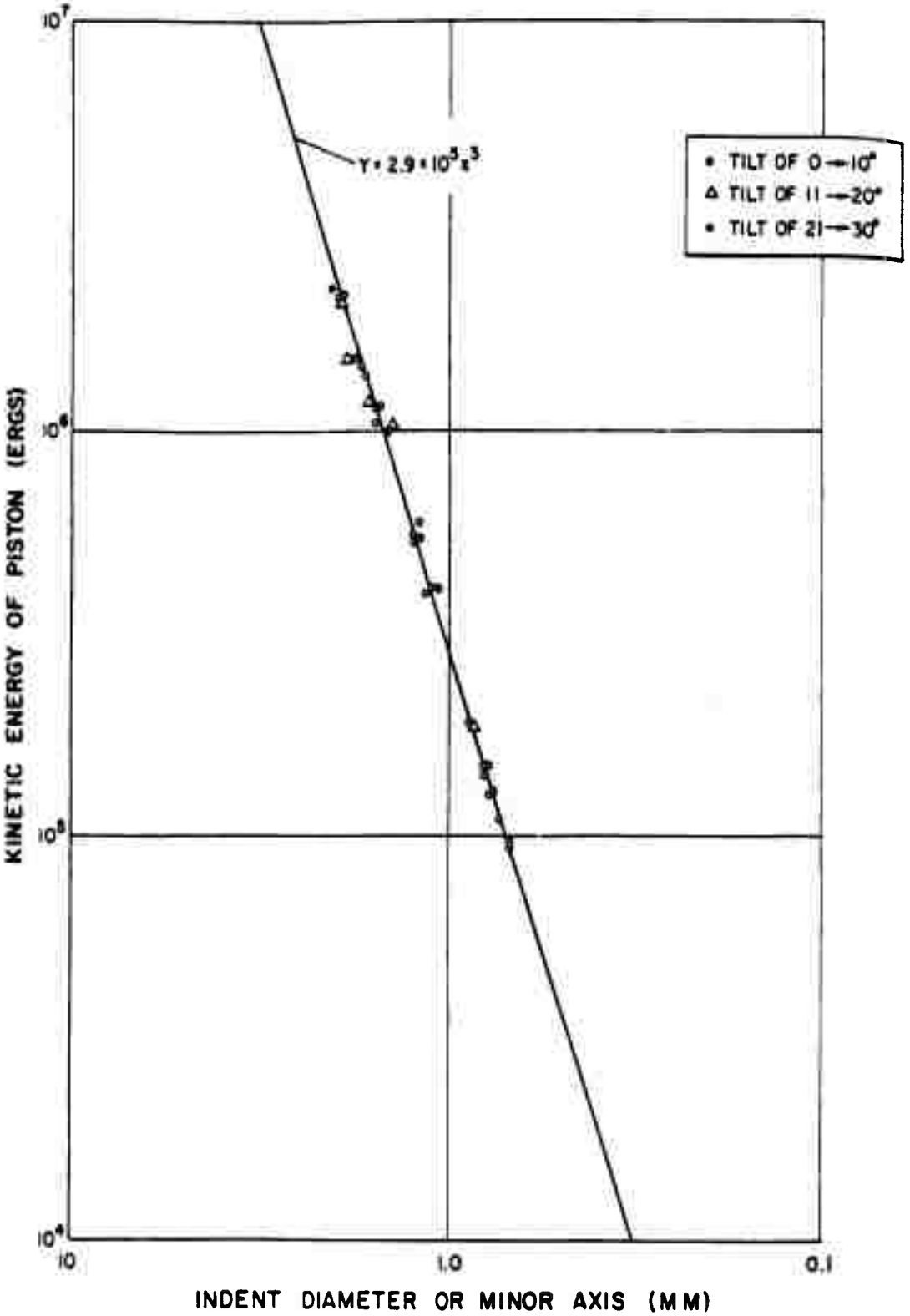

Figure B.2 Indent calibration curve for aluminum piston and lead anvil.

APPENDIX C

PISTON RESTRAINING SPRING CALIBRATION

The restraining springs pressing against the indenter pistons were necessary to ensure that prior to the X-ray-induced impulse the pistons remained in position. That is, the springs prevented the pistons from firing during handling or from lofting accelerations. The design of these springs was such that accelerations of up to about 40 g's would not fire the pistons. Missile accelerations prior to re-entry were below this value, and as a result only one piston in the Star Fish indenters was known to have fired prior to burst time.

However, it is obvious that the restraining springs absorbed part of the kinetic energy of the piston when it did fire. The velocity of the piston toward the anvil was less in every case than if the springs had been absent. Hence, the impulse recorded on the anvil is slightly less than that delivered to the piston. To correct the impulse data obtained from the anvil indents to the true impulse, the relation between the piston velocity before and after spring release is required. It should be noted that the piston is considered to have received a velocity instantaneously, i. e., in a time not comparable to the time of spring release. This assumption is probably accurate for the reason that, during the time to release, the blowoff pulse trapped within the piston made on the order of 100 internal reflections from each end. The irregularity of the piston combined with the effects of dispersion should result in a smooth flow of the entire piston at its final velocity well within the time to release.

The relation between the instantaneous initial piston velocity, v_o, and the velocity after release, v_r, will now be derived, subject to the assumption mentioned. The piston and two restraining springs constitute a familiar spring-mass arrangement within the limits of release displacement, see sketch.

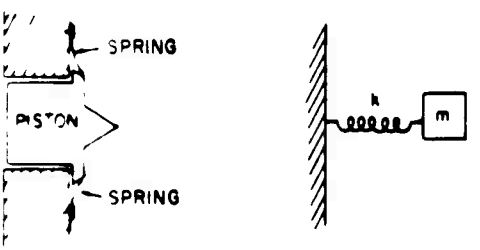

The motion of this system is described by the following equations:

$$m\ddot{x}(t) = -kgx(t)$$

$$\dot{x}(o) = v_o$$

$$x(o) = x_o$$

where:

m = piston mass (gm)
x(t) = displacement of piston at any time t (cm)
k = spring constant (gm/cm)
g = 980 cm/sec^2
v_o = theoretical initial piston velocity (cm/sec)
x_o = piston distance which spring is preloaded (cm)

The solution of the above equations is the familiar

$$x(t) = \frac{v_o}{\omega_o} \sin \omega_o t + x_o \cos \omega_o t \qquad (C.1)$$

where:

$$\omega_o = \sqrt{k/m}$$

If Equation C.1 is differentiated, squared, and added to $(\omega_o x)^2$ it can be shown that

$$\omega_o^2 x^2 + \dot{x}^2 = \omega_o^2 \left\{ \left(\frac{v_o}{\omega_o} \right)^2 + x_o^2 \right\} \qquad (C.2)$$

and by some further manipulation, the velocity of the mass at the instant of release is just

$$v_r = v_o \left\{ 1 - \frac{kg}{mv_o^2} \left(x_r^2 - v_o^2 \right) \right\}^{1/2} \qquad (C.3)$$

where: $v_r \equiv \dot{x}_r$ = the piston velocity at spring release (cm/sec)

x_r = displacement at which release occurs (cm)

The square root factor in Equation C.3 tells what fraction of the impulse delivered to the piston remains with the piston after having cleared the restraining springs. This factor must be applied to the measured impulse data to retrieve the correct impulse. Let us define

$$\beta = \left\{1 - \frac{kg}{mv_o^2}\left(x_r^2 - x_o^2\right)\right\}^{1/2} \qquad (C.4)$$

Now, the evaluation of β as a function of piston energy, $1/2\ mv_o^2$, requires the experimental determination of three parameters: spring constant, k; preloading displacement, x_o; and release displacement, x_r.

A series of measurements was made to determine these three parameters. Three unused SF' Mk 3 indenter cases were selected at random and loaded with Mk 3 pistons also chosen at random. The results from these Mk 3 cases can be applied to the other two types very easily as will be shown later; the only essential difference is the distance through which the pistons are preloaded, x_o.

As might be anticipated, the effective spring constant varied somewhat from piston to piston. In addition, small machining and assembly inaccuracies were reflected as significant variations in spring behavior because of the small area of contact between spring and piston. Nevertheless, because a number of pistons were studied, an average or typical spring constant could be deduced.

The procedure used was to load a given piston with successively greater weights and note the successive displacements from the initial position. The travel of a microscope focused on the piston surface was measured micrometrically for these data. The reproducibility of any given weight-displacement value was only fair, to within $\pm$ 2 mils or so, because of the spring-piston contact irregularities. Each datum point presented in Table C.1 represents the average of several determinations, and the displacements are uncertain to $\pm$ 2 mils. It is because of this uncertainty that nine different pistons in three different cases were tested.

In Figure C.1, the weight vs. displacement data are graphically displayed. The solid line running through the center of the data poir was found from a least squares calculation; the two dashed lines wer drawn by eye to show the limits within which most points fall. The zero displacement position on the abscissa is the rest position of the piston in the case, while the backward intercept of the solid line witl the abscissa shows the effective zero position if the springs were all to come to their nonstressed or zero position. The slope of the soli curve gives the spring constant of the average pair of springs and is

$$k = 6.3 \pm 1.0 \text{ lb/in}$$

or

$$k = (1.12 \pm .19) \times 10^{3} \text{ gm/cm}$$

Although the variation in k is not small, $\pm$ 16%, it can be shown that the resultant uncertainty in the piston velocity, v_r, is miniscule. For the range of piston energies being dealt with in Star Fish, the certainty in v_r from a 16% variation in k is less than 2% for piston velocities as low as 200 cm/sec, and is less than 1/2% for velocities of 500 cm/sec. Hence the spread in data in Figure C.1 is not important with regard to impulse data corrections, and the least square value for k can be used consistently.

In Table C.2 the data necessary for the determination of typical values for x_o and x_r are presented. The preloading displacement, x is simply the intercept value in Figure C.1 plus the distance beyond case that the piston end projects, or

$$x_o = 13 \times 10^{-3} + \text{projection} \quad \text{(inches)}$$

Since the Mk 1 and 2 pistons do not project, the values of x_o are:

Mk 1 ..... $x_o = 13 \times 10^{-3}$ inch
Mk 2 ..... $x_o = 13 \times 10^{-3}$ "
Mk 3 ..... $x_o = 24 \times 10^{-3}$ "

The average projection of the Mk 3 pistons, as given in Table C.2 is 11×10^{-3} inch.

In order to determine x_r, the release distance, the pistons were pushed inward until one spring was passed and then farther until the second spring was passed. The displacements were noted for each piston and tabulated in Table C.2. Because the piston cocked slightly after having passed the first spring, the distance measured to the passing of the second spring is believed to be greater than that which actually occurred in Star Fish. The average distance between passing both springs has been chosen as a reasonable compromise for x_r, or:

$$x_r = \frac{(0.043 + 0.013) + (0.071 + 0.013)}{2}$$

$$x_r = 0.070 \text{ inch}$$

It can be shown that, as before, variations or uncertainties in x_r are reflected into uncertainties in v_r much reduced for the piston energies being dealt with in Star Fish. With a 20% uncertainty in x_r, the resultant uncertainty in v_r is about 1 1/2% for piston velocities of 500 cm/sec. Thus, the compromise, or most likely value for x_r given above, is sufficiently accurate.

The three unknown parameters, k, x_r, and x_o having been determined, it is possible to evaluate the correction factor β from Equation C.4 in terms of different piston energies. This factor is presented in Figure C.2 as a function of $1/2\ mv_o^2$; Figure C.3 shows β as a function of $1/2\ mv_r^2$ and was determined from Figure C.2 and Equation C.3. It is obvious from these two figures that the effect of the restraining springs on the piston velocity was small in all cases except the very slowest pistons. For example, a Mk 3 piston given an initial velocity of 500 cm/sec was slowed only about 2% by the springs, the measured impulse deviating from the initial value by only 2%. In Figure C.4 the initial energy is related to the measured energy directly.

It is interesting to note that a minimum energy, and hence impulse, existed below which a piston would fail to pass the restraining springs. This energy is 1.53×10^4 ergs in the case of a Mk 3 indenter. This energy would correspond to a minimum impulse of $J_{min} = 2.1 \times 10^2$ taps. The minimum energy for a Mk 1 or 2 piston is 1.67×10^4 ergs.

TABLE C.1 WEIGHT VERSUS DEFLECTION DATA

Weights in grams; deflections in mils.

Case	Piston	Weights								
		38.7	52.0	56.2	63.3	69.5	80.8	91.9	105.2	116.5
010	3	2	-	8	-	13	18	21	-	-
051	1	3	-	9	-	-	13.5	18	-	25
051	2	3	-	10	-	-	12	19	30	31
051	3	-	5	-	-	12	-	20	-	26.5
051	4	4.5	-	-	11	-	-	23	-	-
007	1	1.5	-	-	7.5	-	-	20.5	25	-
007	2	3	-	4.5	-	-	10.5	15	-	27.5
007	3	C.5	-	-	6.5	-	11.5	-	-	21.5
007	4	-	5	-	-	8	-	19.5	-	22

TABLE C.2 PISTON TRAVEL DISTANCE TO FIRE

Case	Piston	Projection of Piston	Pass One Spring	Pass Second Spring
		inch	inch	inch
010	3	.017	-	.061
051	1	.012	.054	-
051	2	.011	.044	-
051	3	.010	.040	.075
051	4	.010	-	-
007	1	.009	.049	.069
007	2	.012	-	-
007	3	.010	.035	.076
007	4	.009	.034	.074
	Average:	.011	.043	.071

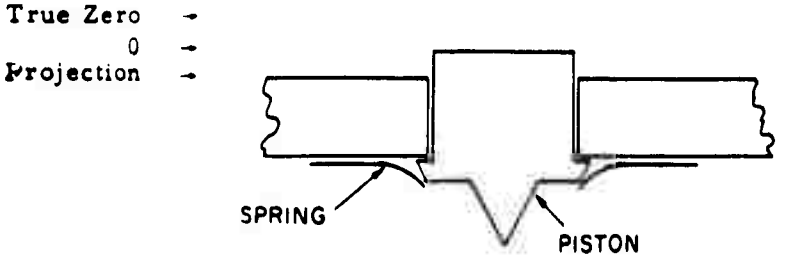

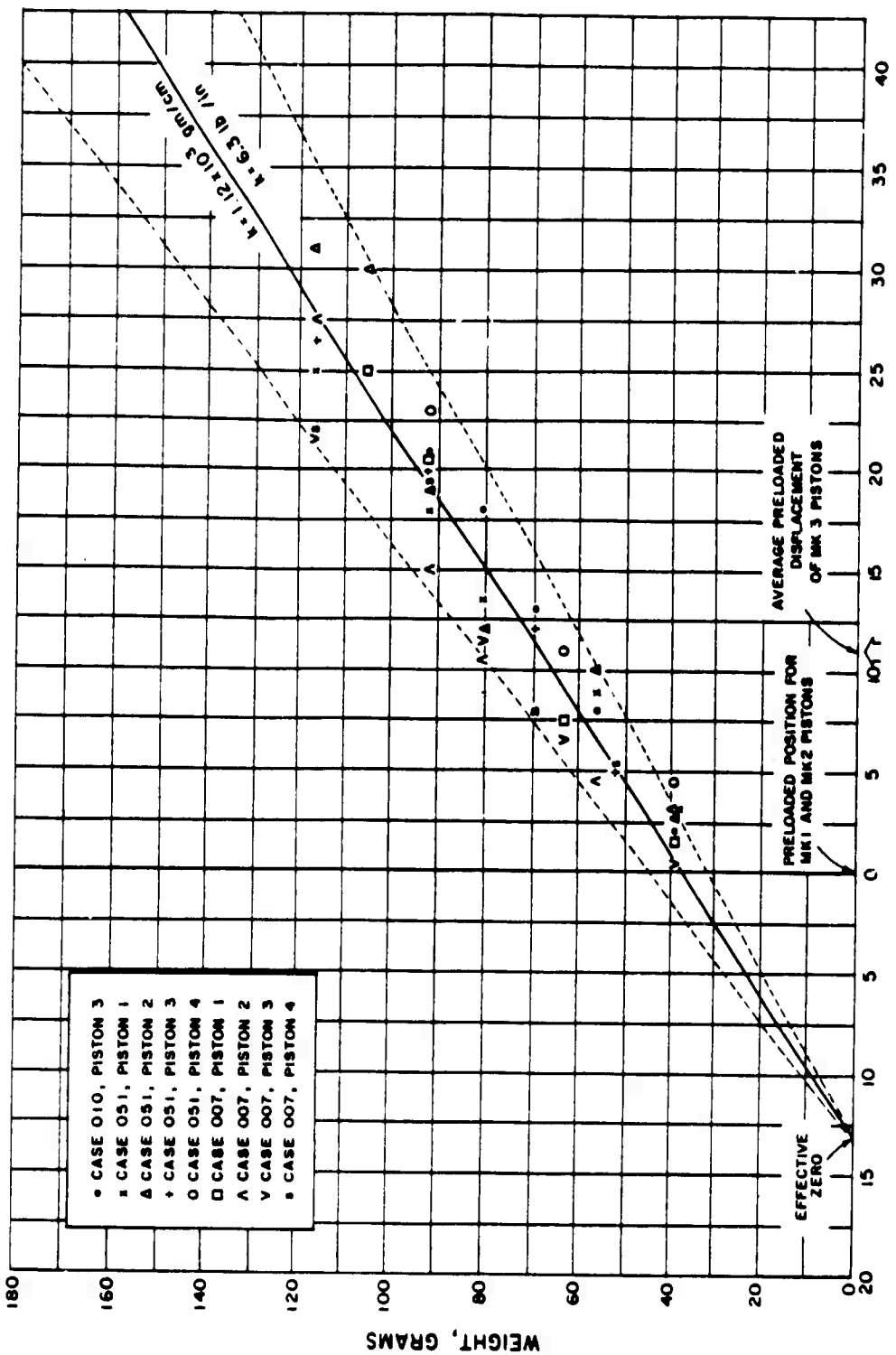

Figure C.1 Restraining spring deflection.

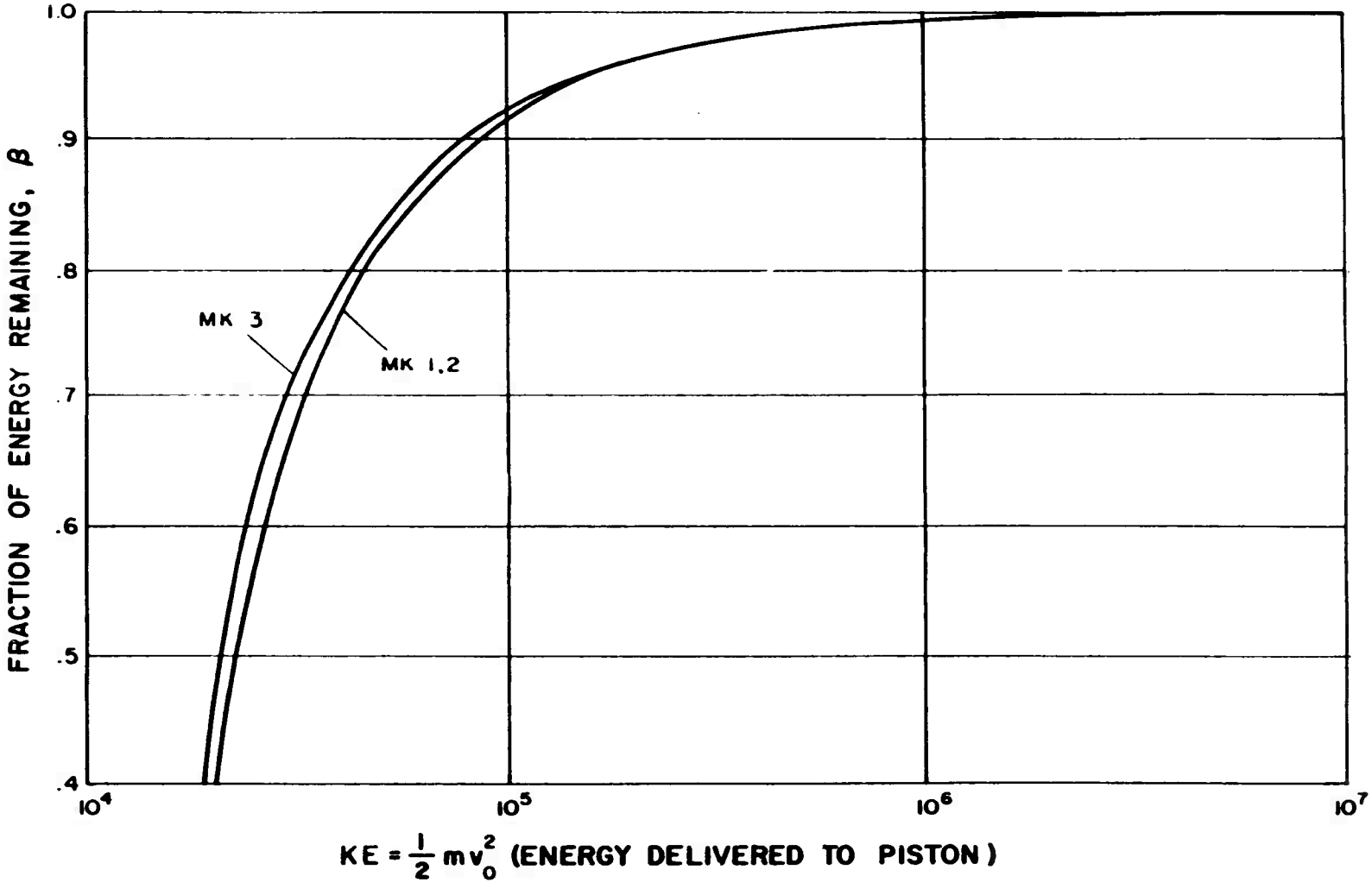

Figure C.2 Energy remaining in piston after spring deflection (energy delivered to piston).

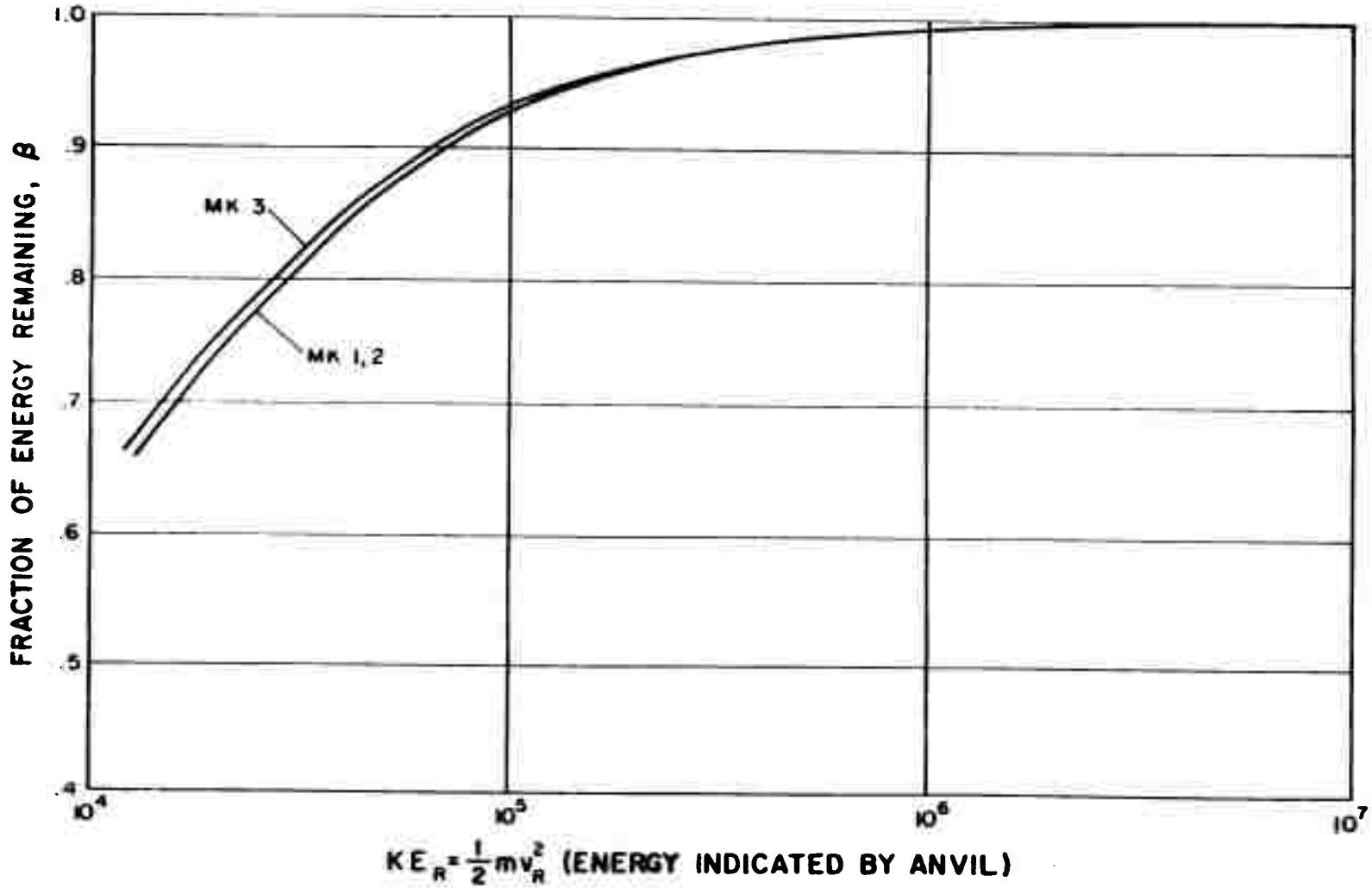

Figure C.3 Energy remaining in piston after spring deflection (energy indicated by anvil).

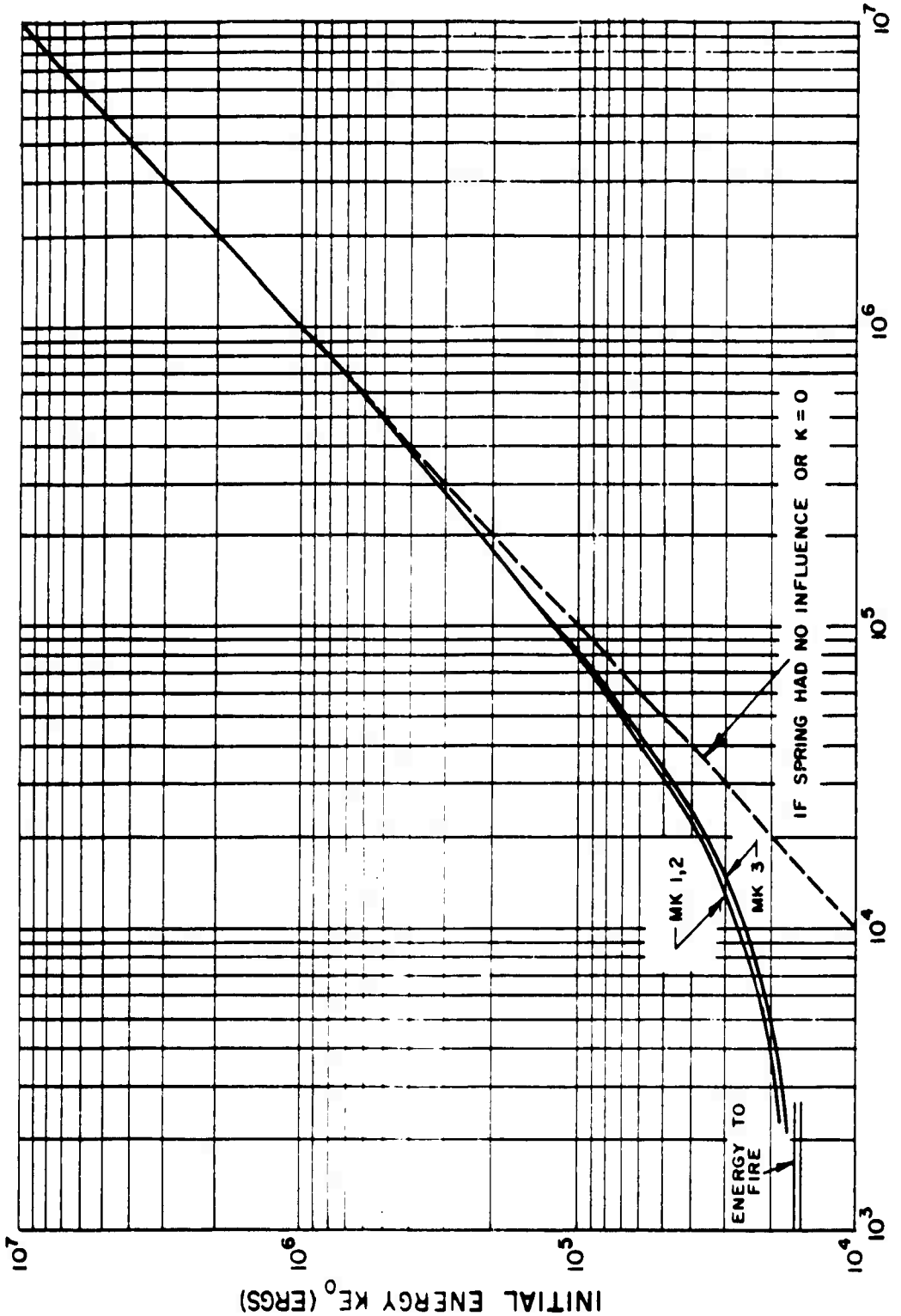

Figure C.4 Relation between anvil-indicated energy and initial energy.

APPENDIX D

RESUME OF THERMAL, PHYSICAL,AND X-RAY PARAMETERS

The data presented in this appendix represents those values used in various calculations performed during the Data Reduction Program.

Table D. 1 lists the densities, acoustic velocities, and melt energies for various materials. With regard to density, the measured values were generally close to those stated in the literature, but in certain instances the measured value was used. The X-ray coefficients for the materials which were pertinent to either the spectral gages or the spectral data reduction effort are presented in Figures D1→D3. The curve for CNP was computed on the basis of its composition as given in Reference 27.

TABLE D.1 THERMAL AND PHYSICAL DATA

Material	Energy to Melt [a]	Melt Temp.	Sound Velocity	Density	References
	cal/gm	°C	cm/sec	gm/cm^3	
Graphite (R/V Shield)	-	3650	-	1.78 [b]	26
Graphite, ATJ 5A0101 (Striker Plate)	-	3650	2.25×10^5 [c]	1.70 [b]	26
Beryllium	8.0×10^2	1284	12.8×10^5	1.84	20, 21, 26
Aluminum	2.3×10^2	660	5.2×10^5	2.7	21, 22, 26
Sulfur	0.35×10^2	120	-	1.95	26
Chrome	2.7×10^2	1550	-	7.14	21
Iron	2.3×10^2	1540	5.1×10^5	7.87	21, 22, 26
Gold	0.6×10^2	1063	2.0×10^5	19.3	21, 22, 26
Lead	1.7×10^2	327	1.2×10^5	11.34	21, 22, 26
Devcon (iron-epoxy composite)	-	-	-	2.21 [b]	-
Avcoat-2	-	-			
Polyethylene, CH_2	-	-			
C-124	-	-			
CNP	-	-			
GEFG	-	-			
Teflon	-	-	-		
Avcoite	-	-	-		
OTWR(U)	-	-	-		
Rad 58B	-	-	-		
TWNP	-	-	-		

[a] This includes not only the latent heat of melting but also the energy to raise the material to its melt temperature from 0°C.

[b] Measured at ARA.

[c] Calculated from data supplied by National Carbon Co.

[d] Based on data supplied by AFSWC.

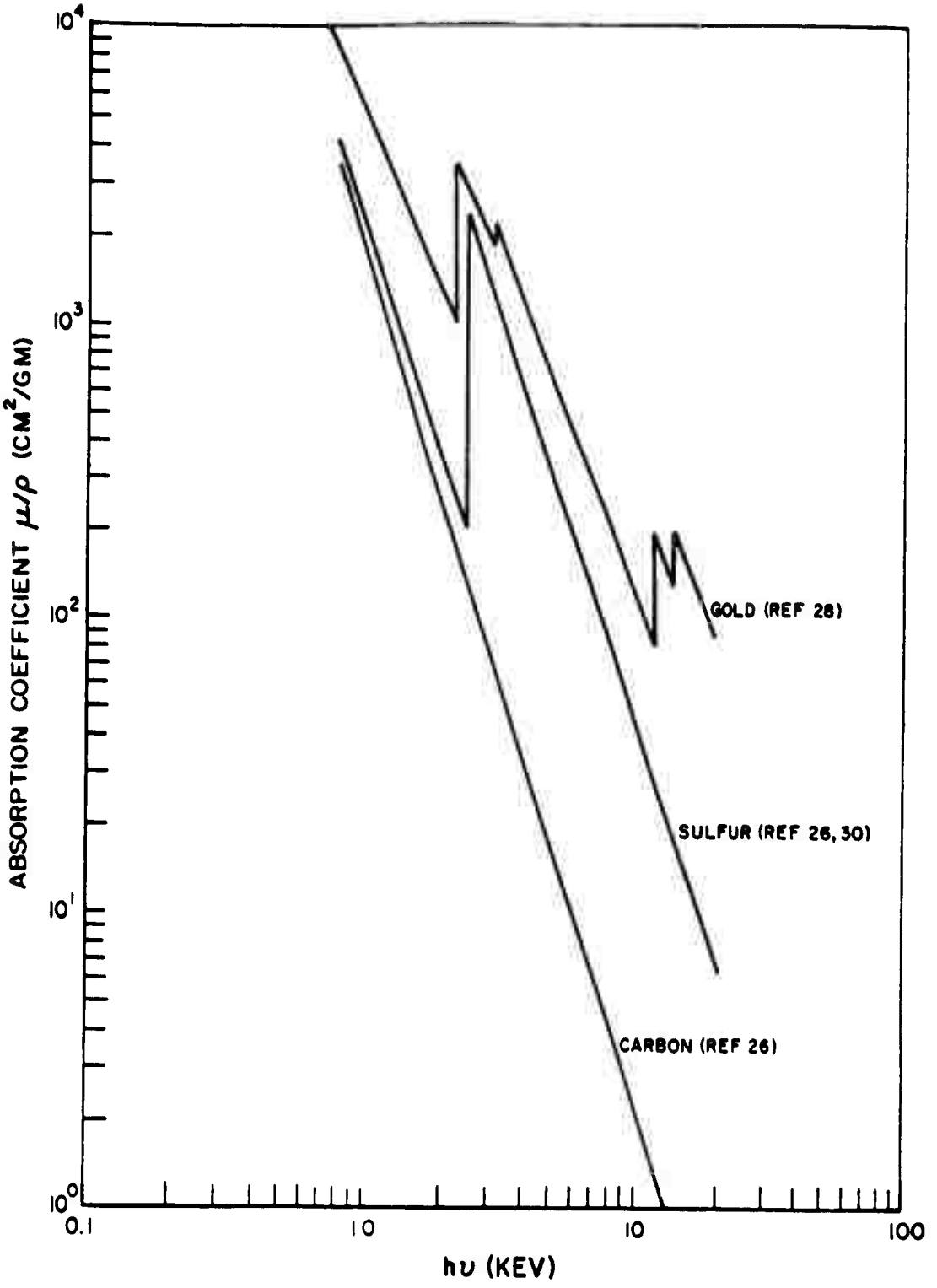

Figure D.1 X-ray absorption coefficients, Au, S, C.

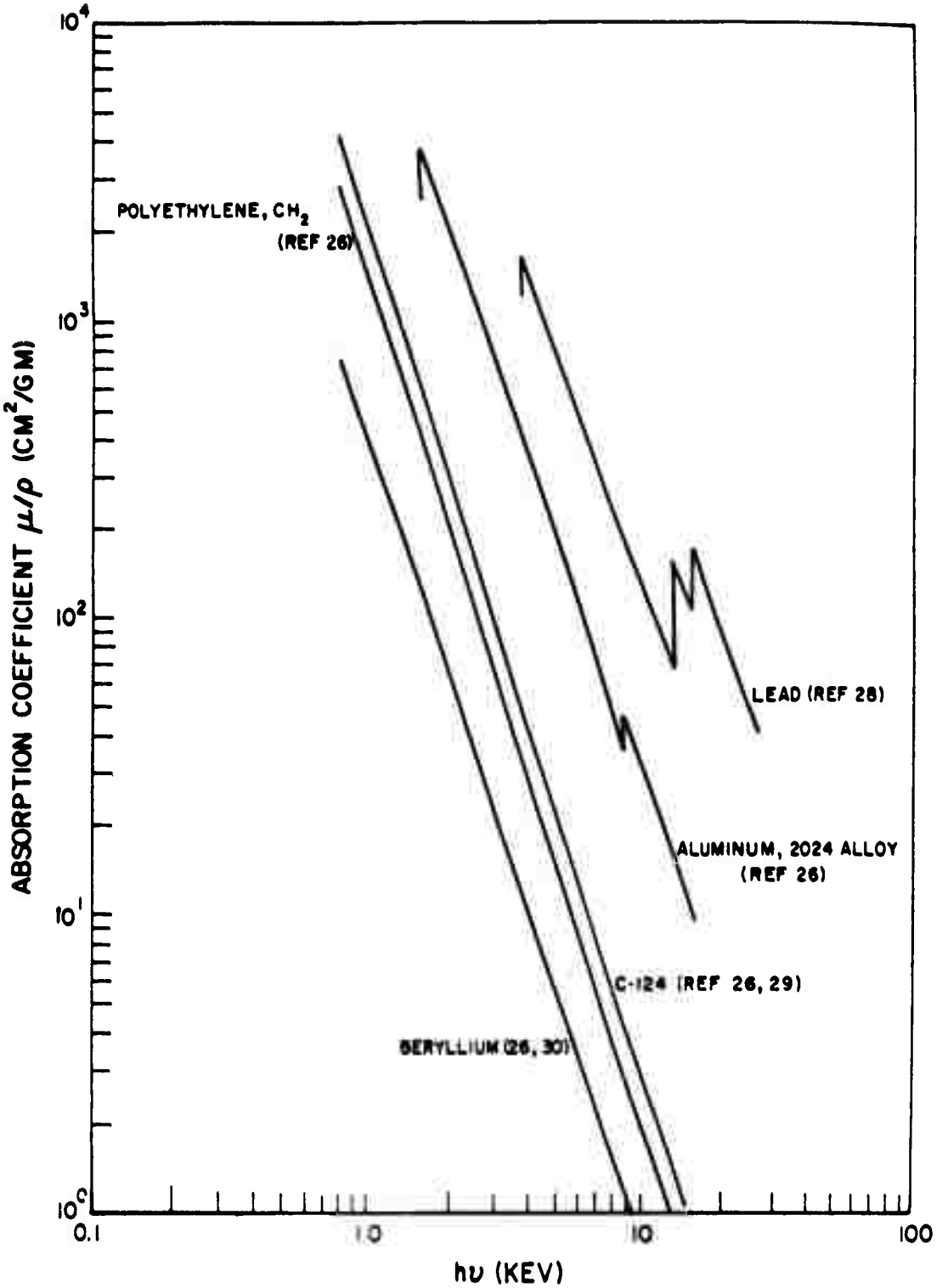

Figure D.2 X-ray absorption coefficients, Be, CH_2, C-124, Al, Pb.

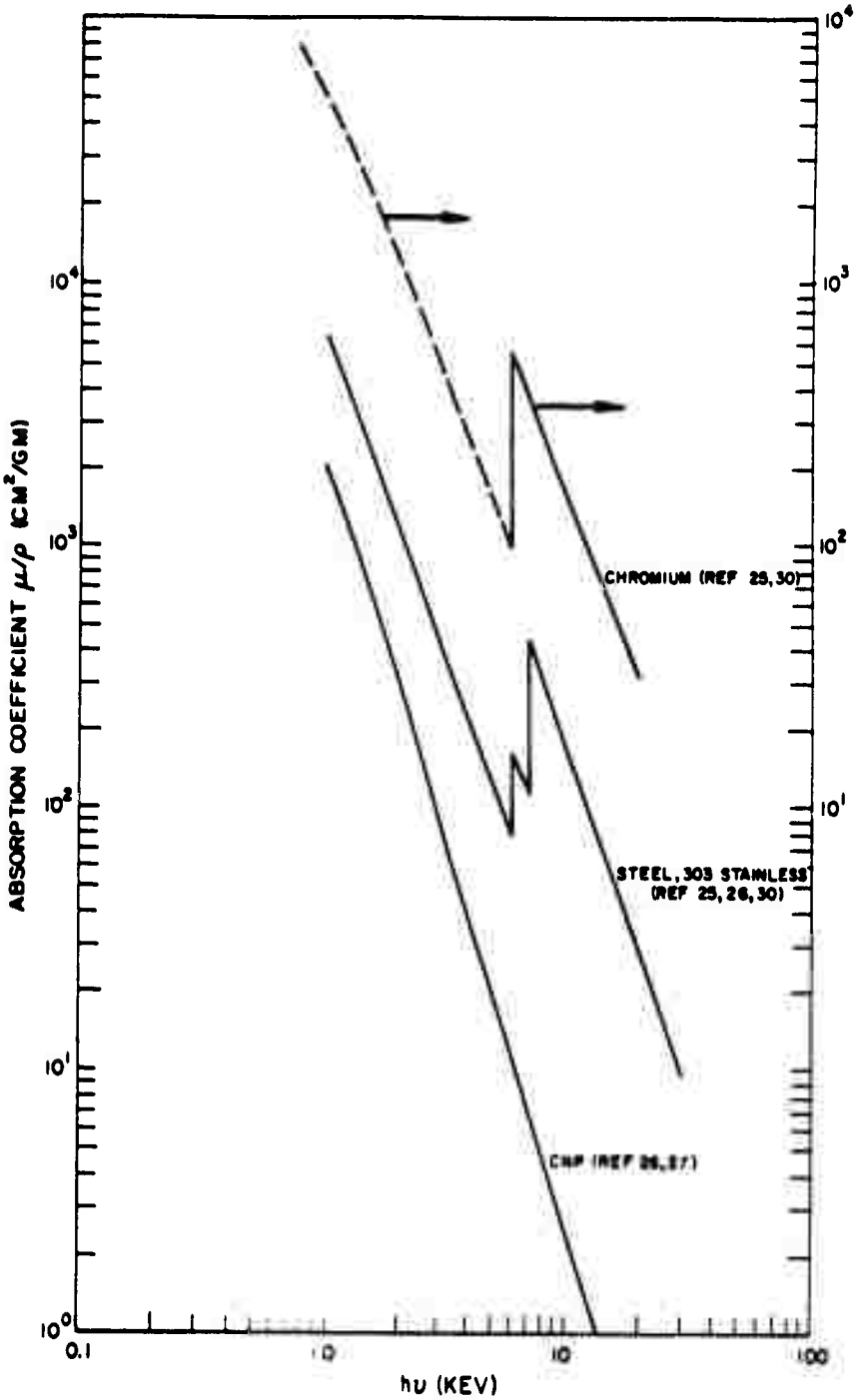

Figure D.3 X-ray absorption coefficients, Cnp, 303 steel, Cr.

REFERENCES

1. H.E. Stubbs and others; "Experiments on the Effect of High Altitude Nuclear Detonation"; ARA-689, 5 November 1959; Allied Research Associates, Inc., Boston, Massachusetts; Secret Restricted Data.

2. R.W. Collins, A.W. Winston, and W.P. Boquist; "Logan Event Data Reduction (U)"; WT-1792. June 1960; Allied Research Associates, Inc., Boston, Massachusetts; Secret Restricted Data.

3. P. Wing and others; "Final Report on Recoverable Instrument Design and Analysis for DASA Project 837"; AFSWC TR-60-49 (I), August 1960; Allied Research Associates, Inc., Boston, Massachusetts; Secret Restricted Data.

4. N. Harmon; "Final Design Report on Recoverable Instrumentation for DASA Program 800"; AFSWC TR-60-60, August 1960; American Science and Engineering, Cambridge, Massachusetts; Secret Restricted Data.

5. E. Perry; "Installation and Assembly of Catcher Support Hardware and Catchers DASA Project 854.1; LMSD 70327, 1 November 1960; Lockheed Missiles and Space Division, Sunnyvale, California; Unclassified.

6. W.P. Boquist; "Theory and Calculation of X-Ray Impulses"; ARA-QM-3051, 5 November 1958; Allied Research Associates, Inc., Boston, Massachusetts; Secret.

7. H.A. Bethe and W.L. Bade; "A Theory of the X-Ray Effect of High Altitude Nuclear Bursts and a Proposed Vehicle-Hardening Method"; RAD-TR-9(7)-60-2, April 1960; Avco Research and Development Division, Wilmington, Massachusetts; Secret Restricted Data.

8. W.L. Bade and others; "Analytic Theory of X-Ray Effects"; AFSWC TR-61-43, July 1961; Avco Research and Development Division, Wilmington, Massachusetts; Secret Restricted Data.

9. P. Swarztrauber; "SHARP Plotting Routine and X-Ray Deposition," Proc. AFSWC Hydrodynamics Conf.; AFSWC TR-60-12, March 1960, pp. 42-58; C.E. Ehrenfried; "Zoning Criteria," ibid., pp. 82-87; R.G. Allen; "Equation of State Sensitivity," ibid., pp. 88-90; Air Force Special Weapons Center, Kirtland Air Force Base, New Mexico; Secret Restricted Data.

10. W.A. Lokke; "The Radiated Flux and Debris Angular Distribution of Star Fish Prime (U)"; UCID-4551, January 1963; University of California, Lawrence Radiation Laboratory, Livermore, California; Secret Restricted Data.

11. N. Sissenwine and others; "Preliminary Note on the U.S. Standard Atmosphere, 1962"; Vol. 43, No. 7, July 1962; Bulletin of the American Meteorological Society; Unclassified.

12. M.S. Hider; "Description of Fish Bowl Metallurgy Experiment"; AFSWC Internal Memorandum, February 1962; Air Force Special Weapons Center, Kirtland Air Force Base, New Mexico; Unclassified.

13. H. Kolsky and A. Shearman; "Investigations of Fracture Produced by Transient Waves"; Research 2, 384; Unclassified.

14. L.E. Bailey and R.I. Miller; "Project 822: E (λ) Window: Design Specifications for a Passive Detector to Measure X-Ray Spectra"; SRIA-28, October 1960; Stanford Research Institute, Palo Alto, California; Secret.

15. "Radiography of Pyrographite"; Memorandum; 14 February 1962; Advanced Metals Research, Somerville, Massachusetts; Unclassified.

16. Commander, DASA, Sandia Base, New Mexico; "Final Data for Fish Bowl R/V Positions, Pod Postions, Pod Separation Distances"; TWX: cite 4-8-8368 (R 30/2225Z) 30 April 1963; Secret Restricted Data.

17. Commander, DASA, Sandia Base, New Mexico; "Best Estimates of Fish Bowl Yields"; TWX: cite 4-3-8161 (R 122-354Z) 12 April 1963; Secret Restricted Data.

18. Lt. Col. B.M. McCormak and Major J.E. Mock; "Operation Fish Bowl Technical Summary"; DASA Special Report 6, 19 November 1962; Defense Atomic Support Agency, Washington, D.C.; Secret Restricted Data.

19. Unpublished data supplied by Col. Irving Russell, Chief, Biophysics Branch, Air Force Special Weapons Center, Kirtland Air Force Base, New Mexico.

20. D.E. Gray; "American Institute of Physics Handbook"; First Edition 1957; McGraw-Hill Book Company, Inc., New York, New York.

21. C.A. Hampel; "Rare Metals Handbook"; First Edition 1954; Reinhold Publishing Corporation, New York, New York.

22. H.F. Olson; "Elements of Acoustical Engineering"; Second Edition 1947; D. Van Nostrand Company, Inc., Princeton, New Jersey.

23. Capt. Marvin Atkins and Capt. Claude M. Gillespie; "Reentry Vehicle Composites (U)"; POR-1853, Project 834, Operation Nougat, Shot Marshmallow, May 1963; Air Force Special Weapons Center, Kirtland Air Force Base, New Mexico; Secret Restricted Data.

24. "Test Evaluation Report, DASA Piggy Back Pods C-1, C-2, C-3"; AE 62-0557, 21 May 1962; General Dynamics/Astronautics, San Diego, California; Confidential.

25. J.I. Hopkins; "Low Energy X-Ray Attenuation Measurements for Elements of Low Atomic Number"; J. of Applied Physics, February 1959, Vol. 30, No. 2, pp. 185-187; Unclassified.

26. "Handbook of Chemistry and Physics"; 41st Edition 1959-1960; Chemical Rubber Publishing Company, Cleveland, Ohio.

27. "Theoretical Calculations of Shock Propagation in Ablative Materials"; AFSWC TDR 61-63, March 1962; McAllister and Associates, Albuquerque, New Mexico; Secret Restricted Data.

28. F.R. Gilmore; "Graphs of X-Ray Absorption Coefficients for Fourteen Substances"; RM-2367-AEC, April 1959; The RAND Corporation, Santa Monica, California; Unclassified.

29. Private communications from Captain C.M. Gillespie, Air Force Special Weapons Center, Kirtland Air Force Base, Albuquerque, New Mexico.

30. B.L. Henke and others; "Semi-Emperical Determination of Mass Absorption Coefficients for the 5 to 50 Angstrom X-Ray Region"; J. of Applied Physics, January 1957, Vol. 28, No. 1.

31. F.C. Gilbert, C.R. Curry, and F.D. Seward; "LRL High-Altitude Diagnostic Experiments and Star Fish Results (U)"; UCRL 7151, December 1962; University of California, Lawrence Radiation Laboratory, Livermore, California; Secret Restricted Data.